

**Residual Oil Monitoring in
pressurised Air with SnO₂-based
Gas Sensors**

**Restölüberwachung in Druckluft
mit SnO₂-basierten Gassensoren**

DISSERTATION

**der Fakultät für Chemie und Pharmazie
der Eberhard-Karls-Universität Tübingen
zur Erlangung des Grades eines Doktors
der Naturwissenschaften**

2004

**vorgelegt von
NIKOS PAPAMICHAIL**

Tag der mündlichen Prüfung: 28.1.2004

Dekan: Professor Dr. H. Probst

1. Berichterstatter: Privatdozent Dr. U. Weimar

2. Berichterstatter: Professor Dr. G. Gauglitz

1	Introduction	1
1.1	Motivation for the development of a residual oil monitor	1
1.2	State of the art in residual oil monitoring	3
1.3	Alternative solutions.....	4
1.3.1	The saturation problem and the aerosol vaporisation.....	5
1.3.2	The choice of the sensor	8
1.3.3	Real life measurements.....	9
2	Experimental set up.....	11
2.1	Compressor.....	11
2.2	Metal oxide sensors	13
2.2.1	Preparation and description of the sensors	13
2.2.2	Housing and connection of the sensors	15
2.2.3	Operation temperature of the sensors	17
2.2.4	Sensing mechanism of metal oxide sensors for hydrocarbons .	17
2.3	Flame Ionisation Detector	22
2.3.1	Description of the used FID instruments.....	23
2.3.2	Conversion of FID reading	24
2.3.3	FID-related problems when measuring oil vapours	25
2.4	Vaporisation by expansion via capillary.....	30
2.4.1	Characterisation of the capillary expansion process.....	30
2.4.2	Vapour pressure over aerosols.....	31

2.5	Gas mixing system	34
3	Experimental results and discussion.....	36
3.1	Exploratory measurements	36
3.1.1	Headspace GC/MS.....	36
3.1.2	Results with gas mixing system.....	38
3.2	First compressor set up	41
3.2.1	Set up	41
3.2.2	Measurements at different sampling points.....	45
3.2.3	Results.....	49
3.3	Second compressor set up	50
3.3.1	Set up	50
3.3.2	Long term measurements.....	52
3.3.2.1	<i>Measurements with daily occurrences.....</i>	<i>54</i>
3.3.2.2	<i>Measurements with short term changes</i>	<i>58</i>
3.3.2.3	<i>Seasonal effects.....</i>	<i>62</i>
3.3.3	Behaviour at high humidity	64
3.3.3.1	<i>Description of water spikes</i>	<i>65</i>
3.3.3.2	<i>Thermodynamic explanation</i>	<i>67</i>
3.3.3.3	<i>Measures against water spikes</i>	<i>70</i>
3.3.4	Results.....	71
3.4	Third compressor set up	72
3.4.1	Set up for dosing of oil & gravimetric referencing	72

3.4.2	Measurements with dosing of oil.....	76
3.4.3	Results of measurements with dosing of oil.....	83
3.4.4	Measurements with gravimetric referencing	84
3.4.5	Results of gravimetric referencing.....	92
4	Conclusion.....	94
4.1	Proof of Feasibility	94
4.1.1	Vaporisation via capillary expansion.....	94
4.1.2	Sensor sensitivity	95
4.1.3	Cross sensitivities in real life measurements.....	95
4.2	Other findings.....	96
4.2.1	Measurement of oil vapours with FID.....	96
4.2.2	Real life set up with compressor.....	96
4.3	Outlook.....	97
4.3.1	Proposed steps of further development and investigation	97
4.3.2	Will the residual oil indicator be established?.....	97
5	References	100
6	Publications.....	103
7	Acknowledgements.....	105

Symbols and units:

cm^3	cubic centimetre
c_{aer}	aerosol contamination
$^{\circ}\text{C}$	degree centigrade
γ	surface tension
Δm	mass difference
Δp	pressure difference
F	flow rate
g	gram
k	Boltzmann constant
l	litre
l_{cap}	capillary length
$m_{\text{liq}}^{\text{nor}}(\text{oil})$	mass of liquid oil in case of normal oil contamination
$m_{\text{liq}}^{\text{inc}}(\text{oil})$	mass of liquid oil in case of increased oil contamination
m^3	cubic meter
mg	milligram
mm	millimetre
min	minute
ml	millilitre
mN	millinewton
μm	micrometer
η	dynamic viscosity
N_L	Avogadro's constant ($6.0 \cdot 10^{23}$ parts per mol)
p_{amb}	ambient pressure
p^{aer}	vapour pressure over aerosol droplet
p_{comp}	pressure of the air after compression in the compressor
$p^{\text{inc}}(\text{oil})$	partial pressure of oil in case of increased oil contamination
$p^{\text{nor}}(\text{oil})$	partial pressure of oil in case of normal oil contamination
p^{pla}	vapour pressure over a planar surface
$p_{\text{sat}}(\text{oil})$	saturation vapour pressure of oil
p_{tot}	total pressure
r_A	radius of the aerosol droplet
r_{cr}	critical radius
R	ideal gas constant
R_0^{heat}	heater resistance at ambient temperature

R_h^{heat}	heater resistance when heated
R_0	sensor baseline resistance
R_{Exp}	sensor resistance at exposure to analyte
R_t	retention time
S	sensor signal
S_{Hum}	sensor signal due to humidity changes
S_{Oil}	sensor signal due to changes of oil content
S_{rat}	saturation ratio
S_{Tot}	total sensor signal
t	time
t_R	residence time
T	temperature
T_o	ambient temperature
T_h	sensor temperature
V	volume
V_C	inner volume of the capillary
V_F	flow volume
V_M	molar volume
$V_{\ddot{O}}$	oxygen vacancy with a charge of +2
%	per cent
'	inch

List of abbreviations:

A/D	analogue / digital
amu	atomic mass unit
DSMS	dynamic sampling mass spectrometer
FID	flame ionisation detector
GC	gas chromatography
GC/MS	gas chromatography coupled with mass spectrometry
IPC	Institute of Physical Chemistry
MFC	mass flow controller
MID	multiple ion detection
MOX	metal oxide
PCB	printed circuit board
pH	potentia hydrogenii
ppb	parts per billion
ppm	parts per million
QIC	quick inlet capillary
RGA	residual gas analyser
r. h.	relative humidity
V2A	stainless steel alloy

1 Introduction

1.1 Motivation for the development of a residual oil monitor

Pressurised air is one of the most versatile products and it is used in most industrial sectors with wide and sometimes unexpected applications in many fields of production and services. It is used as a reactant and as an oxygen supplier, as a carrier of energy or as a tool to clean or to cool, it moves bulk cargo and it opens bags by blowing in. All pressurised air is produced by compressors and the most common compressors, such as classical reciprocating compressors or screw-type compressors, need oil as lubricant, as a sealant and, even more important, as cooling medium. The oil is in direct contact with the air and so a contamination with oil takes place. The low partial pressures of the compressor oils prevent a high degree of vaporisation, but due to turbulences and mechanical stress the oil forms dramatic amounts of aerosols that heavily contaminate the pressurised air. The magnitude of contamination is unacceptable even in terms of loss of oil for the compressor.

In order to produce clean air and to leave most of the oil inside the system, compressors are equipped with an oil separator. The oil separator, as shown in **Figure 1**, is a filter based on the effect of coalescence. It is coupled with a backflow possibility to reinject the oil into the system. After the air leaves the compressor it runs through a subsequent filtering line, adapted to the respective application in order to reach the required purity.

The oil separator is, of course, an element with a limited lifetime that has to be replaced before expiration. Its lifetime is specified by the producer of the oil separator, who has to ensure the effectiveness of the product for that period. This value is the result of elaborate investigations, which, therefore, cannot be carried out very often. In order to investigate the lifetime of the oil separator and to monitor the decrease of its functionality, the oil aerosol content can be

measured repeatedly until the limit is reached. Due to the cost, this is only done by the manufacturers of filters or compressors for research, development and random sampling testing, but not at the customer for regular surveillance.

Of course, the investigated lifetimes show statistical variation, even for the same type of oil separator, and in addition to this, the lifetime will be influenced by the operating conditions at the respective application. So, the producer defines a (minimum) lifetime, that gives a maximum of security, but this implies the exchange of the oil separator before the real end of its lifetime. An individual indication of the filter status could prevent that, but the investigation, as performed up to now, is a discontinuous, expensive and time consuming method, not at all appropriate for the monitoring of the oil content at the numerous sites where compressors produce pressurised air.

The danger of an excessive oil content in the pressurised air is the possibility of contaminating the tubing system that delivers the air from the central compressor to the points of use. It can be very extensive and, so, the cleaning of such a system can be very costly. To be on the safe side, the oil separator tends to be exchanged more often than really necessary, which affects not only the costs for the element and the needed manpower but also availability of pressurised air during replacement. If it would be possible to continuously monitor the real state of the oil separator and to exchange it just in time, important resources could be saved.

Furthermore, a possibility for the online monitoring of the oil content would solve, or at least diminish the severe problem of the breakthrough of the oil separator. A breakthrough of the oil separator represents the worst case in handling of pressurised air from compressors: it means a sudden and massive increase of oil content that will contaminate the tubing system very fast and probably widely, because it may not be immediately noticed. In these cases, the cleaning of the tubing system is very costly and in addition, the unavailability of pressurised air during cleaning may cause production downtimes.

1.2 State of the art in residual oil monitoring

The measurements of oil aerosol content of pressurised air, as performed for example by the manufacturers of filters and oil separators, are gravimetric ones: for a defined time, the air from the outlet of the compressor is channelled through a so-called “absolute filter”, followed by a flow meter. Absolute filters, as shown in **Figure 1** (right side) also work by the principle of coalescence, they remove 99.9 % of the oil aerosols [Gil00], which is collected in the filter material. The filter is weighted before and after exposure, so the amount of oil can easily be calculated. Water, also collected, is removed by drying the filter before weighting.



Figure 1: Pictures of new filters: oil separator (left) and absolute filter (right)

The weight of the aerosols, the time of exposure and the volume flow enable the calculation of the mean of the oil aerosol content during exposure. Consequently, the method is unable to monitor changes with time constants smaller than the usual time of exposure. The low contamination of the air determines a high throughput in order to reach a reliable increase in mass. This results in exposure times in the range of hours.

Additionally to the need for long exposure, the method is costly and labour intensive. The absolute filter is a one-way product (after the measurement it is contaminated with oil) and all working steps are usually performed by human operators.

Despite these disadvantages, the absolute filter is the state of the art in the investigation of the residual oil content, applied for example in currently developed test benches for the newest field of oil aerosol filtration, the removal of oil aerosols in blow-by gases from car crankcases: the blow-by gas is injected in the air intake of the motor and therefore must not be oily [Man03].

1.3 Alternative solutions

The monitoring of the residual oil content in pressurised air is complicated because, as a classical aerosol, the oil is dispersed in air and shows colloidal behaviour. The system is neither homogeneous, nor heterogeneous in the meaning of physical chemistry and therefore it cannot be measured and specified like a classical one-, or two-phase system. There are methods and instruments for the quantification of the number and/or the size of the particles like Mobility Particle Spectroscopy [Dah01], Differential particle Sizer System [Fis83], Condensation Particle Sizer [Aga80] or Laser dispersion [Nob96], and attempts to investigate the composition of the particles via coupling to Mass Spectroscopy [Nob96]. Another approach uses Infrared Spectroscopy for the overall quantification of gaseous and aerosol compounds [Bre97]. A solution presented in a patent of 1987 – specifically dedicated to the problem of residual oil monitoring in pressurised air - works via deposition of aerosols in an electric field on a pellistor, followed by a heat-up in order to burn the oil. In the end the heat of combustion is measured. These elaborate methods illustrate the difficulties of a direct quantification of aerosol content and why adequate aerosol sensors are not available up to now and in the foreseeable future.

As a consequence, the solution described here follows a completely different approach: if it is possible to vaporise the oil aerosols, the concentration of gaseous oil will represent the oil aerosol content and with adequate gas sensors it will be possible to monitor the oil content in the gas phase. The expected concentration of gaseous oil is not very high, but if the change of the sensor response due to the change of the concentration of the oil vapours is high enough to be detected out of the noise, a completely new and promising concept of residual oil monitoring in pressurised air will be enabled.

The development of this concept must deal with three challenges that have to be met in order to prove the overall feasibility:

- The vaporisation has to be sufficient enough to produce the necessary amount of analyte to be detected by the gas sensor and to prevent the gas sensor from poisoning by residual aerosol.
- A gas sensor that shows a response towards the oil vapours has to be found; it has to be sensitive to the oil vapours in the concentration range delivered by the vaporisation process and it has to be selective enough not to respond towards other analytes. On the other hand, it must not be specific or too selective, because the vapours may differ from oil to oil and in dependency of the age of the oil.
- The sensor must not be influenced very much by cross interferences that will occur when operated in a real life environment: a compressor takes in air from the ambient that is subject to alterations in dependency of e. g. the season or the time of day.

1.3.1 The saturation problem and the aerosol vaporisation

The oil separator inside a compressor is a cylindrical filter, flown through from inside to outside. It works by coalescence and it is able to remove the biggest part of the aerosols of the air. The contamination of the air before the oil separator can be estimated to a value of some hundreds mg per m³; after a properly working oil separator, the value is below 3 mg/m³. In parallel to this

aerosol loading, there usually is a wallflow of oil of changing extent, originating from the aerosol deposition. This means that even in case of a working oil separator the pressurised air ($p_{1,tot} = p_{comp} = 7$ bar overpressure) is in permanent and direct contact to a certain amount of liquid oil $m_{liq}^{nor}(oil)$. Consequently, the oil vaporises until its partial pressure $p^{nor}(oil)$ reaches its saturation vapour pressure $p_{sat}(oil)$, which depends on the oil and the temperature inside the system. In case the liquid oil does not run out and the two phase system reaches equilibrium, the partial pressure of oil stays constant independently from the amount of liquid (illustrated in **Figure 2**):

$$p^{nor}(oil) = p^{inc}(oil) = p_{sat}(oil) \quad \text{when}$$

$$m_{liq}^{nor}(oil) \neq 0 < m_{liq}^{inc}(oil)$$

An increased amount of liquid oil, $m_{liq}^{inc}(oil)$, will not influence the partial pressure of the oil under these conditions and so the increase will not be detectable with gas sensors. This effect is more probable at high total pressure (p_{tot}), low saturation vapour pressure (p_{sat}) or low temperature.

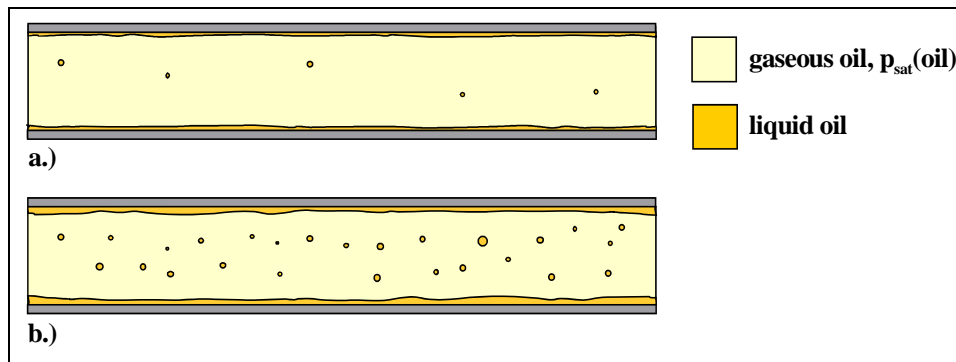


Figure 2: Schematic of the oil contamination of a tube downstream a compressor with a.) a properly working oil separator and b.) over aged oil separator with significantly reduced functionality.

Things change when the pressure inside the system decreases, for example when the oil/aerosol mixture is expanded to ambient pressure ($p_{2,tot} = p_{amb} \approx 1$ bar): the saturation vapour pressure is constant, but the total

pressure (p_{tot}) decreases when the volume increases. The partial pressure of the oil is accordingly decreasing, inducing further vaporisation of oil in order to reach the saturation vapour pressure. In case the liquid phase runs out, the saturation vapour pressure cannot be obtained, resulting in a lower partial pressure of oil compared with the case of a residual liquid phase of oil, where the saturation vapour pressure is obtained.

$$p^{nor}(oil) < p^{inc}(oil) \leq p_{sat}(oil) \quad \text{when}$$

$$m_{liq}^{inc}(oil) \geq m_{liq}^{nor}(oil) = 0$$

This means that by sufficiently expanding the sample the difference in aerosol content can be monitored with appropriate gas sensors, even though the description given here is oversimplified, especially concerning the following two points:

- Compressor oils are multi component liquids with differing saturation vapour pressures, including ionic components which will not vaporise under the conditions discussed in this thesis. This means that there will be residual aerosol (even after expansion) and that the different components will contribute in different extent to the change in gas composition, as detected by the gas sensor(s).
- The assumption that the system reaches equilibrium might not be true. If the period between the air-to-oil contact and the expansion is too short, kinetic reasons may lead to $p^{nor}(oil) = p^{inc}(oil) < p_{sat}(oil)$. One has to keep in mind that the higher surface in case of increased aerosol content can have an effect only between the oil separator and expansion and not between compressing unit and oil separator (which is the bigger part). Also, the residence time of the air in the compressor is, anyway, low. Therefore, the difference in partial pressure after expansion could also be kinetically caused due to the increased aerosol surface in case of increased aerosol content.

It was not the aim of this work to investigate these points in detail, the efforts to analyse the composition of aerosols, described in 1.3 prove the complexity of this challenge, even without the obstacle of time dependency.

For various reasons, the first choice was to perform the expansion with a capillary: it is a passive and simple device, well known and available in different materials and sizes. The expansion is controllable concerning throughput time and volume by adaptation of length, diameter and number of the capillaries, the large outer surface provides an isotherm process control at ambient temperature or heated. It also leads to a continuous flow, it is unaffected by wallflow and the only critical point may be the blocking of the capillary.

1.3.2 The choice of the sensor

There are different types of compressor oils, synthetic ones, like polyalphaolefins or diesters, and mineral ones. All of them are on hydrocarbon basis; oils on silicon basis are not used for this purpose. Hydrocarbons are well known to be good target molecules for semiconducting metal oxide based gas sensors (MOX sensors). In fact, the use of metal oxides as gas sensors was first developed and introduced for the monitoring of combustible hydrocarbon gases and for a long time this was the main market where MOX sensors came to application. Nowadays, they are also established for online monitoring in other applications, taking advantage of the possibility to change the properties by the use of different metal oxides, various dopants and sophisticated processing or operation techniques. They are selective towards classes of analytes, which generally is a disadvantage; in this case, where one can expect different alkanes (for example in dependency of the type or the age of the oil) it may contribute to the robustness of the correlation between oil content and sensor response.

As a rough estimation, the concentration of hydrocarbons, resulting from the vaporisation of some mg oil per m³ will be in the range of low ppm to high

ppb, depending on the vaporised compounds of the oil. It is known, that the sensitivity of semiconducting metal oxide sensors towards hydrocarbons can be high enough to match this, so three SnO₂-based thick film sensors, differing in doping and preparation, were chosen to be tested for this application. All of them were produced at the Institute of Physical and Theoretical Chemistry at the University of Tuebingen and optimised towards the selective detection of hydrocarbons in the low contamination range.

1.3.3 Real life measurements

When working with sensors, one of the most important issues is cross sensitivity. Due to the sensing principle, this notably affects metal oxide gas sensors, especially in case of measurements performed in real life conditions. In order to prove the real life feasibility, it was necessary to keep as close as possible to the real life conditions of the application. In the present case, the real life conditions are mainly represented by the use of ambient air as a carrier gas, but also by the chosen experimental set up.

The response of a MOX sensor is always related to the gas composition as a whole, which may be rather complex. Of course, the sensitivity can be optimised towards a target gas or classes of them, but the sensitivity towards possibly interfering analytes cannot be completely eliminated. Furthermore, it is known that, for example, humidity has a considerable effect, not only as an analyte, causing a sensor response but also as the precursor of surface species influencing the sensor response towards the analyte. This means that it is desirable to monitor not only the target compound(s) with a reference device, but also all other relevant compounds and parameters, which could influence the measurement, in order to prove that the sensor response is caused with the parameter of interest, and to reveal measurement artefacts.

Assuming a dependency on interfering parameters, it will be important to investigate the extent of its influence in order to prove the overall feasibility of the concept because cross sensitivities and artefacts can cover or spoil the

response towards increased oil content. This surely can happen on short-term-, but also on long-term-basis, for example because ambient air underlies both daily changes as well as seasonal ones. The sensor response can also be influenced by the aging of the oil in the compressor, which also represents a real life effect.

So, besides performing reference measurements in parallel to the sensor measurements, an empirical approach was also followed: the experimental set up was operated and monitored for a long enough period to provide conditions of the real life conditions.

2 Experimental set up

The experimental set up, as it was used for the measurements described in this work has undergone several modifications and conversions in order to be able to measure under different scenarios or in an optimised manner enabled by newly gained knowledge. Most of the main components were kept throughout the two years measurement time, but the alignment, the connections and the operating conditions changed. All important components are subsequently described here in individual chapters. The different, specific set ups, used in the respective subchapters of 3 (Experimental results and discussion) are separately characterised there.

2.1 Compressor

All real life measurements were performed at a used screw-type compressor (Kaeser SM11). Screw-type compressors are the most common ones because of their high performance: they can deliver up to 15 bar (liquid injected, single stage) and 150 m³/min. The Kaeser SM11 produces ~ 1 m³/min at an overpressure of 6.5-7.5 bar. The overpressure of ~ 7 bar was chosen because a lot of applications (tools, etc.) run at this pressure and therefore it is a very common setting. The compressor was operated with compressor oil type “*Kaeser Sigma Fluid plus*”. At the beginning it was already slightly used during the investigations it was necessary to refill substantial amounts of new oil due to the loss when measuring high oil concentrations and malfunctions. So, the compressor generally ran a mixture of new and used oil.

The compressor and the rest of the set up was placed in a room located at the tenth floor of the institute; in the room a window (~ 0.8 m x 1.2 m) was always completely opened, except for some very cold days in winter when it was tilted.

The exhaust was directed to the outside, some meters away from the window, so the air intake of the compressor was always supplied with fresh air from the

outside and no accumulation of oil contamination could take place in the air in the room. Unfortunately all the jalousies on the building are remotely controlled and therefore automatically closed and opened in the summer; that lead to a measurable increase of the temperature in the room due to the hindered access of air, because the exhaust air that was pumped to the outside could not effectively remove the heat, produced by the compressor.

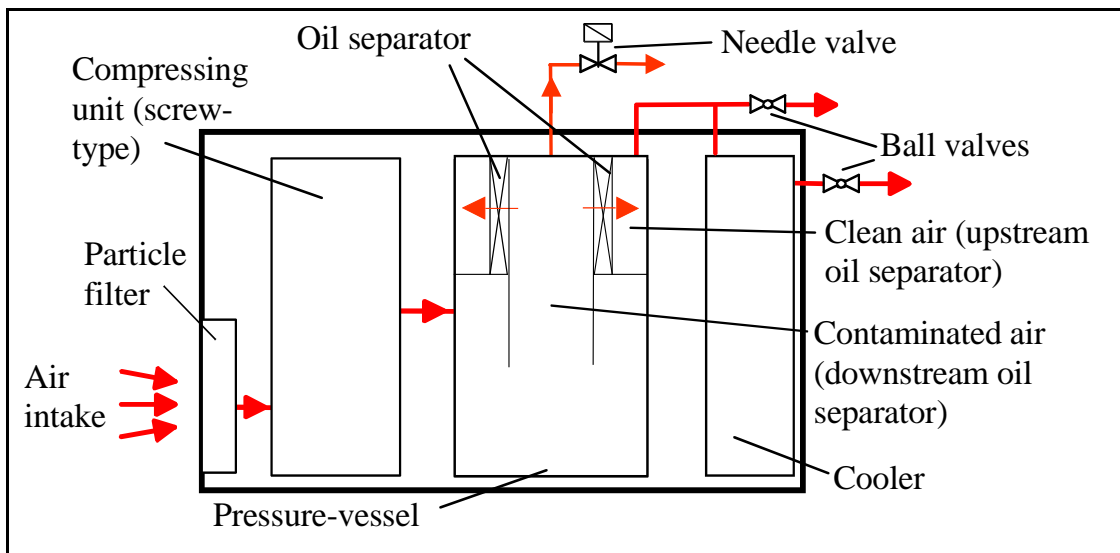


Figure 3: Schematic of the modified compressor: contaminated air can be sampled from an additional drain upstream the oil separator; a second additional drain was mounted between the pressure-vessel and the cooler. The oil separator is shown cross-section-like in order to illustrate the flow from inside to the outside.

For the measurements, the compressor was modified in two points, as shown in **Figure 3**:

- A drain for extremely contaminated air from upstream the oil separator was installed. This air can be added to filtered, uncontaminated air in order to simulate the increase of oil content, normally caused by aging or breakthrough. A ¼' hose was used, equipped with a needle valve to enable a continuous dosing. In the subsequent line the air could be injected where it is required. The pressure drop at the bypassed oil separator ensured a

higher pressure of the injected air, in comparison to the air that was filtered by the oil separator.

- The connection between the pressure-vessel (including the oil separator) and the cooler, which was in ½'-size and originally had been kept inside the compressor, was passed outside and equipped with a drain (also ½'), that could be opened by a ball valve. This made possible to investigate the main air stream without the influence of the cooler by opening this valve and closing the second ball valve, mounted downstream the cooler, at the regular outlet of the compressor (see **Figure 3**). With the second valve opened, it was also possible to use this as a drain for small sample volumes.

2.2 Metal oxide sensors

2.2.1 Preparation and description of the sensors

For the measurements of the vapours originating from the vaporisation of oil aerosols, three different SnO₂-based thick film sensors were used, in the following named as S 1, S 2 and S 3. The preparation of the sensors was performed according to the process flow shown in the schedule of **Figure 4**.

The hydrated tin dioxide (SnO₂ + y H₂O) was precipitated with ammonia from an aqueous solution of SnCl₄ and the residual ammonia and chlorine were removed by washing with water. In case of gel impregnation (Sensors S 2 and S 3), the chloride of the dopant (PdCl₄) was added to the gel, 2 % (of weight of the SnO₂) in case of sensor S 2 and 0.2 % in case of sensor 3.

As it can be seen in **Figure 4**, all three materials were dried afterwards, then ground, heated up to remove the residual water (calcination) and ground again. The powder impregnation of the material used for sensor S 1, was performed at this point: the powder, resulting from grinding the second time, was thoroughly mixed with PdCl₄ and water, followed by heating it up in

order to remove water and residual chlorine.

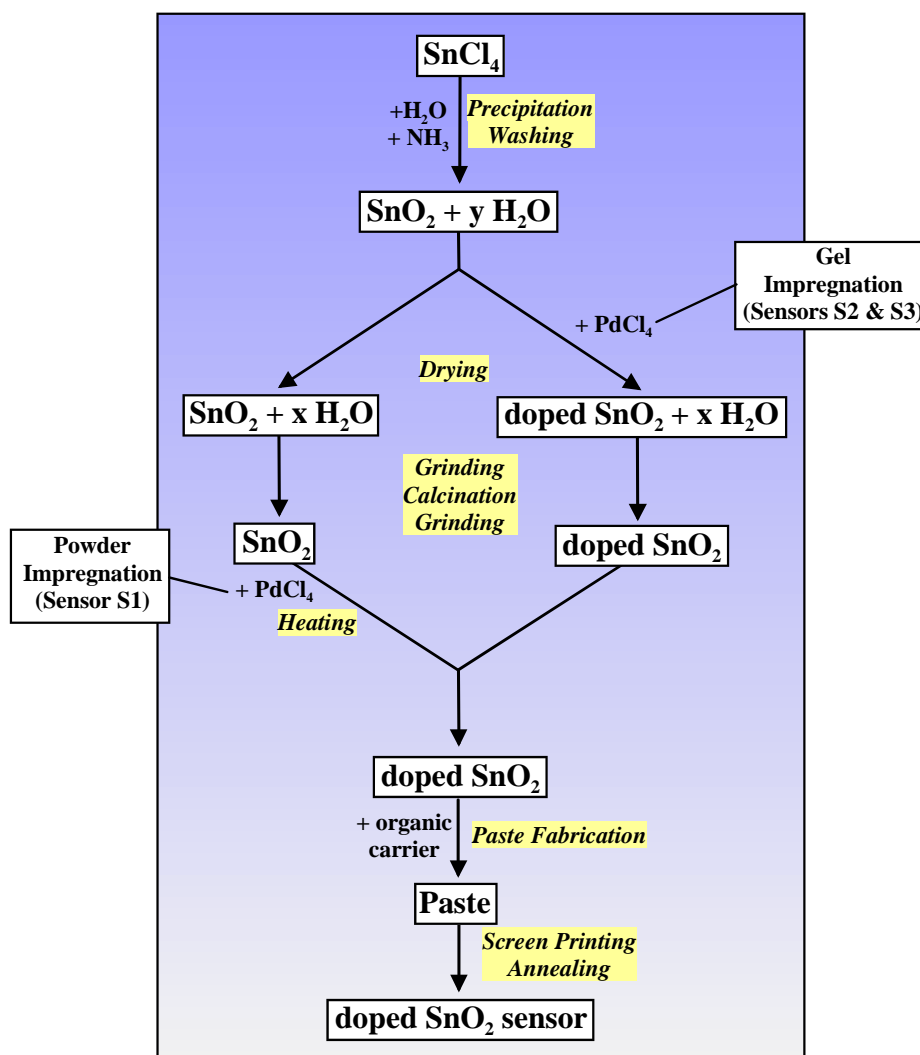


Figure 4: Flow chart of the preparation of the three SnO₂ thick film sensors used in this work. The difference in performance is due to the different methods of doping, (gel impregnation or powder impregnation) and the extent of doping.

The resulting powder was treated in the same way for all three sensors. It was mixed with an organic carrier in order to obtain a paste that could be deposited by screen printing. The sensing layers were printed on an alumina substrates (thickness 0.7 mm), equipped with a platinum heater on the back side and interdigital gold electrodes on the front side. The final step was the annealing of the paste on the substrate in order to remove the organic carrier and to mechanically stabilise the sensing layer. **Figure 5** shows a cross section of the

characteristic sensor components.

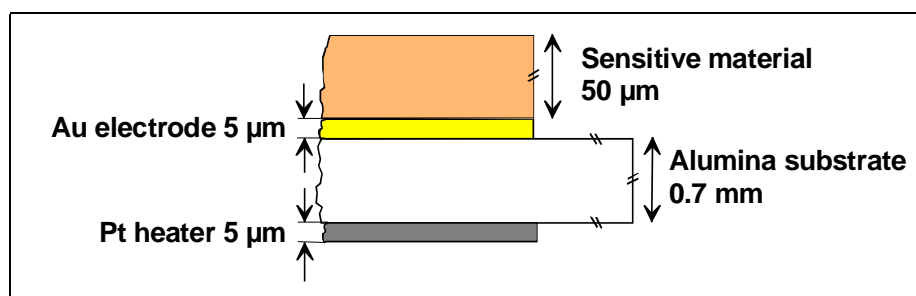


Figure 5: Cross section of the sensor, used for the measurements. The three sensors differ in characteristics of the sensitive material, caused by different dopings.

For all three sensors SnCl_4 from the same batch was utilised as raw material, and apart from the differing impregnation methods the preparation route was the same for the three sensors. Also the sensor fabrication was the same for all of the three sensors, which indicates that the different sensitivities and selectivities, as described later, must have their origin in the impregnation method and the extent of doping.

2.2.2 Housing and connection of the sensors

The alumina substrate with the sensing layer was fixed in the housing by the bonding wires to the four connectors of the socket, as shown in **Figure 6**, left side.

Every sensor sockets was plugged in a measurement holder (parts in contact with sample gas were mainly out of Teflon), which allowed a gas tight feedthrough of the electric connections (**Figure 6**, right side). The cubic Teflon measurement chamber (**Figure 7**), usually equipped with three measurement holders (each with socket and sensor), had an inner volume of approximately 30 cm^3 , the connection to the gas flow was located on two opposite corners.

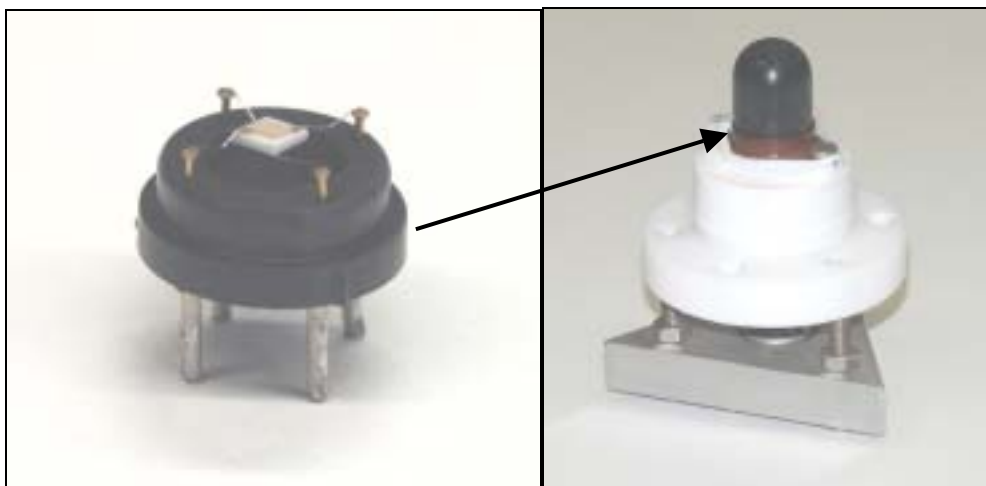


Figure 6: Pictures of one sensors and its socket (black, left side) and a Teflon measurement holders (left side), equipped with sensor and socket (black, with black cap on sensor socket).

The heaters of the sensors were supplied in parallel by a potentiostatic voltage source (Voltcraft 2256). The readout was realised by a VOCMeter Vario (AppliedSensor), based on a potentiostatic measurement principle.

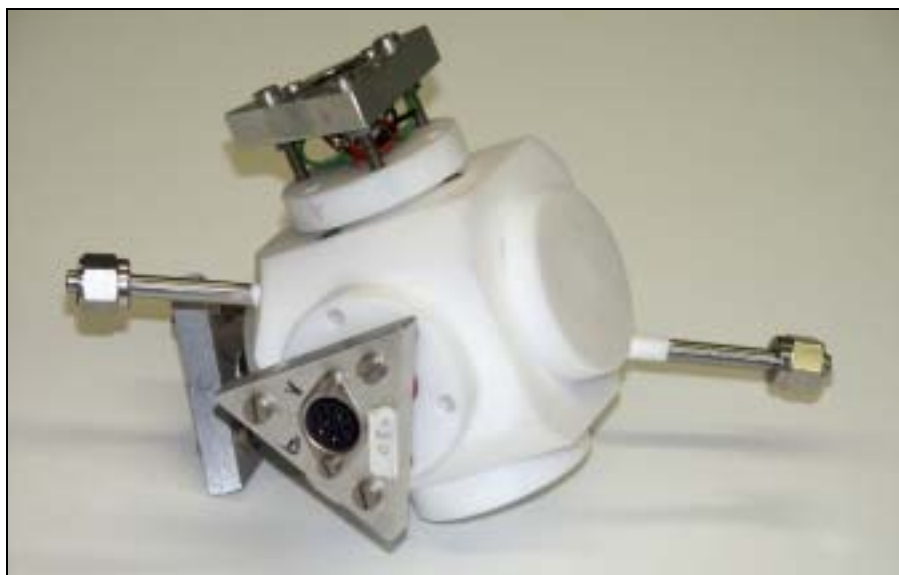


Figure 7: Cubic Teflon measurement chamber, equipped with three measurement holders.

2.2.3 Operation temperature of the sensors

The operating temperature of the sensors was calculated on the basis of the resistance of the heater and a calibration curve, given by [Bar00],

$$R_h = R_0 \left(1 + 3.66 \times 10^{-4} (T_h - T_0) - 7.23 \times 10^{-7} (T_h - T_0)^2 \right)$$

with: R_h^{heat} = resistance when heated,

R_0^{heat} = resistance at ambient temperature

T_h = sensor temperature

T_0 = ambient temperature

The calibration was obtained by measurements of the heater resistances of the sensors at different temperatures, when heated in an oven. The resistance when actively heated was calculated from simultaneous measurements of voltage and current of the sensor heater. In order to obtain more exact results, the resistance of the measurement holders including wires were subtracted from the results for the sensor resistances. The operating temperatures of the sensors were estimated to:

S 1: 283°C

S 2: 280°C

S 3: 278°C

2.2.4 Sensing mechanism of metal oxide sensors for hydrocarbons

Hydrocarbons are the oldest analytes of interest for the mass application of gas sensors based on the metal oxide semiconductors, and SnO₂ is the material which has been in use for this purpose for the longest time. This is why it represents the prototype material for numerous investigation of the mechanisms that cause the change of conductivity of the metal oxide. A

comprehensive summary of the current status of knowledge, including further references, is given in [Wei02].

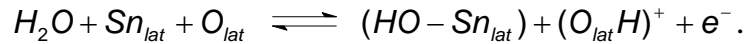
The MOX-based sensing of hydrocarbons chemically results in a combustion of the hydrocarbons [Sch02], id est a heterogeneously catalysed reaction at the surface of SnO₂. The complete reaction path is not known and important preconditions, which influence the surface condition and therefore the sensor performance, like the interaction of the sensor surface with water are not completely clear.

The state of the SnO₂ surface is dependent on the ambient gas; in the given application it has by ~ 20 % O₂ and contains H₂O and / or oil vapour in varying quantities. Ambient oxygen is adsorbed on the SnO₂ surface; at ~ 300 °C the dominant species are ionosorbed O⁻ and O²⁻. The negative charge is provided by free charge carriers, electrons, originating from the conduction band of SnO₂, so the counter charge is delocalised in the depletion layer: id est the surface layer of the SnO₂ grain, which is influenced by alterations of the surface states. The ionosorption leads to a surface band bending which works against further ionosorption and results in an equilibrium state with an O⁻ coverage in the range of 10⁻³ – 10⁻⁵ of a monolayer (Weisz Limitation). It has to be stressed that the ionosorption is strongly facilitated by lattice defects the like vacancies and so the O⁻ formation is localised there.

The band bending is macroscopically observable in a change of resistance; in case of the n-type semiconductor SnO₂ the resistance increases in comparison to the situation without ambient oxygen.

The interaction with water leads to a decrease of the resistance according to an opposite but comparable charge transfer mechanism, although the reaction mechanism is not yet fully clear. [Hei88] proposes two different mechanisms of H₂O adsorption:

- a homolytic dissociation of H₂O on the surface and a reaction with lattice Sn and a lattice O according to



In this case the hydrogen and the lattice oxygen form a “rooted” hydroxyl group which acts as an electron donor to the conduction band; the following equation takes the charge of the lattice oxygen into account



On the contrary to the rooted hydroxyl group, the hydroxyl group coupled to the Sn is called isolated hydroxyl group and it is assumed that it rather changes the oxidation state of the Sn ion than it contributes to the conduction process.

- The second mechanism proposes a heterolytic dissociation and a proton transfer to a lattice oxygen. This rooted hydroxyl group changes into an isolated hydroxyl group by forming a bond to a Sn nearby and an oxygen vacancy $V_{\ddot{O}}$ with a formal charge of +2. This model contributes two electrons to the conduction band according to



Both mechanisms explain the decrease of the resistance with the formation of a rooted or an isolated hydroxyl group out of a O^{2-} of the lattice. In both cases it is assumed that the bonding to the Sn does not contribute to the concentration of free charge carriers, which implies that not all the surface tin atoms are in oxidation state +4 because otherwise the formation of the Sn-OH bond would need an electron from the conduction band. This assumption is reasonable because tin has two stable oxidation states, +2 and +4, and the most stable surface of tin dioxide, (110), can easily be conditioned to show atoms with both oxidation states. Furthermore it is known that defects like vacancies are an essential factor for the performance of SnO₂ gas sensors and it probably is not realistic to base a mechanism on the situation on a perfect

surface. [Emi01] and [Har03] proved the formation of rooted and isolated hydroxyl group on the SnO₂ surface in the presence of water, so the final result is clear even if the exact mechanism still gives room for speculation.

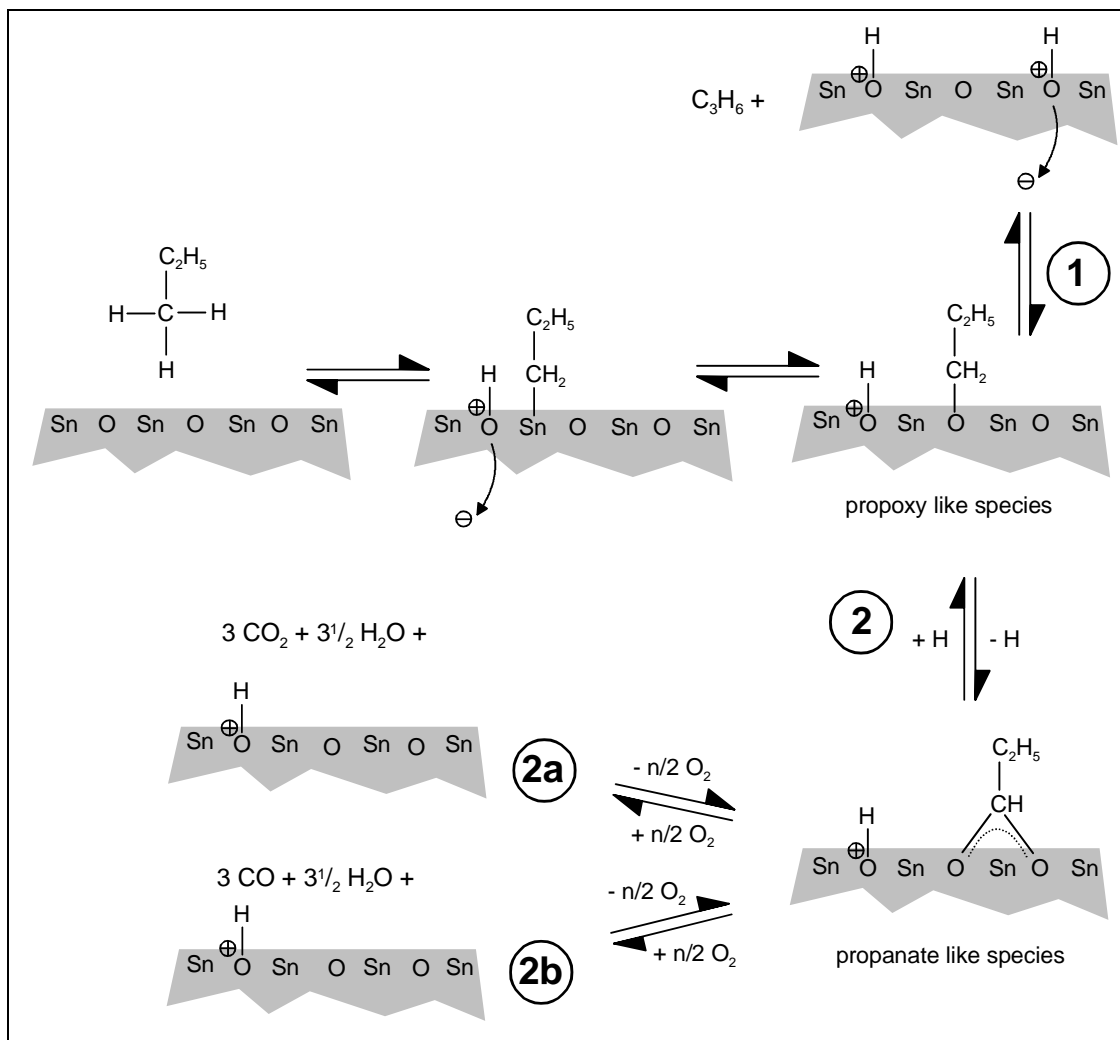


Figure 8: Mechanism of the reaction of propane on the heated SnO₂ surface as far as known, focused on the oxidation of carbon. For the sake of simplification, all oxygen is shown as lattice oxygen, details are given in the text.

The well known cross sensitivity between water and hydrocarbons (lower sensor signal towards e. g. Methane with increasing humidity [Wei02]) implies a competition for adsorption sites respectively a comparable starting mechanism, and the abstraction of a hydrogen / proton is also the most logical

starting point for the heterogeneously catalysed combustion of hydrocarbons. It is assumed that, analogue to the water dissociation, the carbon fragment is adsorbed at first at a tin atom and then transferred to an oxygen atom. It is not known which oxygen species plays an essential role for this step, even if it is known that ionosorbed oxygen is more reactive. **Figure 8** shows the steps of the oxidation of hydrocarbons (exemplified by propane) which are known: [Hei88] found an intermediate propoxy like species and a subsequent propanate like species by means of reactive sputtering in vacuum and mass spectrometric detection.

The propanate like species proves that not all oxygens for the combustion can be ionosorbed ones because two neighbouring ionosorbed oxygens are very improbable due to the Weisz limitation. It has to be stressed, that even if the propane in **Figure 8** is bonded to lattice oxygen, this is only done in order to simplify the diagram; it is not known which oxygen species plays which role.

Combustion measurements with exceeding oxygen (carrier gas: synthetic air; 1 bar) showed that in this condition H_2O and CO_2 are the only oxidation products detectable with mass spectrometry and IR [Sch02]. This proves that the complex is bonded to the surface throughout the whole reaction channel and under this conditions reaction path 2a in **Figure 8** is the only relevant one. The complete oxidation of the hydrocarbon is not time limited and proves that the oxygen originates from the ambient gas and in equilibrium condition the oxygen is continuously re-supplied to the lattice, respectively to the surface. **Figure 8** takes this into account, reaction path 2a and 2b include the oxygen balance ($\pm n/2 \text{O}_2$) and end up in a SnO_2 surface without oxygen vacancies. Reaction paths 1 and 2b cannot be observed under atmospheric conditions. The (rooted) hydroxyl groups, shown at the end of all three paths are in equilibrium with hydroxyl groups due to water adsorption.

Due to the proposed elementary steps of this sensing principle and the signal transduction from the surface reaction to a change of band structure and consequential, to a change of resistance, as described in detail in [Wei02], the

dependency of the sensor resistance from the concentration of analyte is logarithmic and the resistance change is dependent on the baseline value. In order to have a more transferable parameter for the characterisation of sensor performance, the sensor signal S is defined as

$$S = R_0 / R_{Ex} \quad \text{with}$$

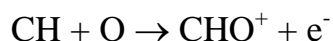
R_0 = baseline resistance, and

R_{Ex} = resistance at exposure to analyte

2.3 Flame Ionisation Detector

A Flame Ionisation Detector (FID) is a measurement device which is specific towards hydrocarbons, with a measurement principle, based on the combustion of hydrocarbons in a hydrogen flame [Ott00], [Cam01].

In the burning chamber of an FID, a flame of highly pure hydrogen in hydrocarbon-free air is burned under controlled conditions (flow rates, pressure, temperature) in an electrostatic field, which has a typical gradient of some hundred Volts over the burning chamber in parallel to the flow. In the inner part of the reducing hydrogen flame (pyrolysis zone), the C-C bonds are reduced to C-H. In the outer part of the flame (oxidation zone) where sufficient oxygen is present, C-H is oxidised according to



forming an intermediate cation and an electron. The nozzle, injecting the mixture of hydrogen and the sample gas in the burning chamber, is kept at negative potential, and so the electrons are accelerated to a ring-shaped collector anode and produce the signal current. Due to the measurement principle, the signal current is largely proportional to the number of carbon atoms of the measured hydrocarbon. The signal is also dependent on the species of hydrocarbon because hetero substituted carbon atoms contribute

less or not at all to the signal current. This circumstance is represented by a response factor, which is also dependent on the FID, as it is influenced for example by the burner geometry and the operation mode.

It is clear that H₂O or other molecules that can not be further oxidised by a flame do not change the (ionic) current and, therefore, do not show a signal in an FID. Other gases like CO or NO, that can undergo oxidation do not contribute to the signal current due to a different reaction path. This indicates that the FID seemed to be a reasonable reference method for the monitoring of oil vapours, as it reacts very sensitively towards the expected target analytes and not at all towards the expected main interfering compound, which is water. The only cross sensitivity is towards the background hydrocarbon content of ambient air, which is known to be 1-2 mg/m³.

Besides this, the FID is an online with short response time; it is much more flexible in comparison to the discontinuous gravimetric method and therefore it was chosen as the main reference analytics for this work.

2.3.1 Description of the used FID instruments

During the investigations, two different FID models, of the same manufacturer, have been used: at the beginning a Testa „2001 T“ and later a modified Testa „1230 Modul“. They mainly differ in the intake rates, which are 750 ml/min („2001 T“) and 18 ml/min („1230 Modul“). The detector itself, the sample feeding and the operating temperatures are the same, so the transferability of the results is ensured.

A 3 µm particle filter out of sintered metal was mounted upstream the burning chamber; the filter and the burning chamber were heated to 300 °C. For both FIDs, the sampling was actively done by a pump downstream the burning chamber with an intake rate of ~ 18ml/min (to the burning chamber!). The „2001 T“ was equipped with a split upstream the sintered filter and an additional pump in order to obtain the intake of 750 ml/min. This is done to guarantee a reasonable throughput and therefore a fast response time when

working with long sample paths and large tubings in case of more typical, industrial applications.

Due to the active intake the FIDs had to be mounted with an open split; the connection to the ambient was equipped with a long tube in order to prevent back diffusion.

2.3.2 Conversion of FID reading

Both FIDs delivered a readout in “ppm propane”, which is very common because propane is the most usual calibration gas for FIDs. In order to convert it into the unit of interest, mg oil per m³, the following considerations have been made:

$$\begin{aligned}
 1 \text{ ppm propane} &= 1 \text{ molecule C}_3\text{H}_8 \text{ per } 1,000,000 \text{ molecules air} \\
 &\approx 3 \text{ (CH}_2\text{) per } 1,000,000 \text{ molecules air} \\
 &= \frac{42 \text{ g mol}^{-1}}{6 \cdot 10^{23} \text{ mol}^{-1}} \text{ (CH}_2\text{) per } 1,000,000 \text{ molecules air}
 \end{aligned}$$

with Avogadro’s constant $N_L = 6.0 \cdot 10^{23} \text{ mol}^{-1}$

$$\begin{aligned}
 &= \frac{42 \text{ g mol}^{-1}}{6 \cdot 10^{23} \text{ mol}^{-1}} \text{ (CH}_2\text{) per } \frac{1000000}{6 \cdot 10^{23} \text{ mol}^{-1}} \text{ air} \\
 &= 42 \text{ g (CH}_2\text{) per } 1.000.000 \text{ mol air}
 \end{aligned}$$

with a molar gas volume of $V_M = 22.4 \text{ l / mol}$

$$\begin{aligned}
 &= 42 \text{ g (CH}_2\text{) per } 22.4 \cdot 10^6 \text{ l} \\
 &= 1.875 \text{ mg (CH}_2\text{) per } 1000 \text{ l} \\
 &\sim 1.875 \text{ mg/m}^3
 \end{aligned}$$

This means, with the two assumptions

- The response factor for the oil vapours is ~ 1 , which a reasonable assumption: non functionalised alkanes (C₂-C₈) and also toluene and benzene have response factors between 1 and 1.04 [Tes00].

- The structure of the oil is $(\text{CH}_2)_n$, which is not true, but the longer the alkane chains becomes, the smaller the error will grow (Hexane: 2.4 %, Heptane: 2.0 %, ...).

that the FID readout of 1 ppm propane corresponds to an oil vapour concentration of $\sim 1.9 \text{ mg/m}^3$. It should be stressed that this value includes oil vapours originating from the capillary vaporisation as well as vapours from the vaporisation of aerosols at the heated, sintered filter of the FID (see 2.3.1), but not the oil aerosols that reach the burning chamber. They, probably, will only partly be oxidised and differently behave when burning in the electric field.

2.3.3 FID-related problems when measuring oil vapours

The sample feedings of the two FIDs had to be realised in two different ways, due to their strongly different intake rates. The feeding of the Testa „2001 T“ could not be realised in a comparable manner to the sensors' one: the sample feeding for the sensors was done with a capillary, in order to vaporise the aerosols as widely as possible while expansion. The flow through a capillary is depending on the pressure difference between the endings, its length and its inner diameter. All of these parameters, could not be changed too much: the pressure was determined by the application (see 2), the capillary parameters affect the dwell time of the aerosol in the capillary and therefore probably also the vaporisation. As demonstrated in 2.4.1, one capillary, as it was used for most of the measurements, delivered a flow of $\sim 25 \text{ ml/min}$. For this reason, the only possibility to identically feed the Testa „2001 T“, with its intake rate of 750 ml/min , would have been a parallel combination of approximately 30 capillaries. This seemed to be unrealistic, so for the Testa „2001 T“ another approach was chosen; **Figure 9** shows a schematic of it: a slightly opened needle valve restricted the flow from the seven bar overpressure region to the ambient to roughly 800 ml/min and an open split between the needle valve and the FID prevented the exposure to overpressure to the FID.

The expansion at the valve was not slow and isothermal like in the case of a capillary, so most of the aerosols reached the FID. Instead, a heated filter of sintered glass (~200 °C) and heated filter out of sintered V2A steel (pore size 3 µm, 300 °C) were used to block or vaporise most of the aerosols.

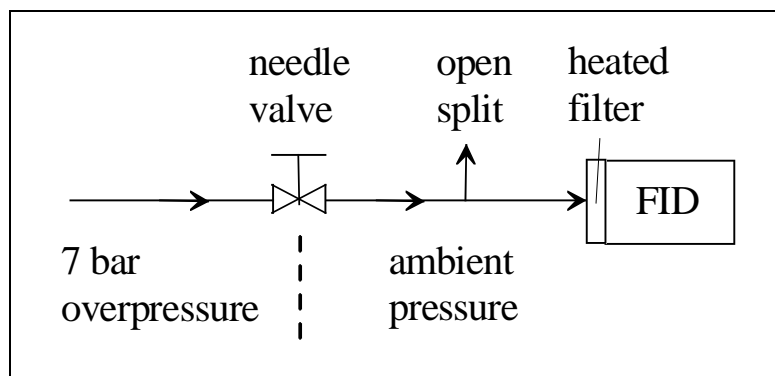


Figure 9: *Sample feeding as used for the Testa „2001 T“, in order to produce a flow of 750 ml/min sample gas.*

The measurement results were encouraging: an addition of contaminated air to the sampled air reproducibly lead to an increase of the FID reading, which was in accordance to the sensor results. The extent of dosing of contaminated air correlated both with the sensor signal and the FID readout, even though there was no proportionality due to the dosing principle. Originally, the Testa „1230 Modul“ is the 19‘-rack version of the Testa „2001 T“ differing only in details, for us, it was modified to the smallest possible intake rate, namely ~18 ml/min. This was done in order to use the capillary expansion also for the sample feeding of the FID and therefore to make the reference measurements more comparable to the sensor measurements. The results of both FIDs did not differ much and in this work measurements with both FIDs are shown. In the description of the respective set up it will be made clear which one was in use.

It has to be mentioned that the „2001 T“ was in use for nine months, including measurements with dosing of highly contaminated air, before it was replaced by the „1230 Modul“ which, after less than one month, showed a malfunction

that was due to the fact that the pressure in the burning chamber was too low. The flow through the burning chamber is restricted by the sintered metal filter and a capillary between this filter and the burning chamber. The respective pump, located downstream the burning chamber, is controlled in relation to the low pressure inside the burning chamber. The reason for the defect of too low pressure in the burning chamber was a clogging of this capillary. The repair service found some tiny, dark, coal-like incrustation in the capillary. After returning, the „1230 Modul“ was operated for another two month without any trouble until, at the very end of the measurements, the same malfunction reappeared. Together with the lack of sensitivity, as discussed in the following, this strongly indicates that especially the Testa FID „1230 Modul“ and, in spite of the trouble-free running of the Testa FID „2001 T“ for nine months, in general FIDs are not appropriate for this application.

At the end of the measurements a comparison with the existing state of the art was needed and reference measurements with parallel investigation of the oil content with MOX sensors, FID and absolute filters were performed. The results (see also 3.4.4) were surprising: a discrepancy of a factor ~ 300 between FID ($\sim 0.49 \text{ mg/m}^3$, calculated from ppm Propane readout) and absolute filters (139 mg/m^3) showed that the FID misses the main part of the analyte. In principle there are four possible reasons for this mismatch, probably concurrently present:

1. A lack of sensitivity towards the vaporised oil compounds
2. Only a small part of the aerosols is vaporised and therefore detected by the FID
3. Residual aerosols disturb the detection and lower the FID response
4. The biggest part of the aerosols is vaporised, but it does not reach the burning chamber, due to sorption, deposition and/or decomposition

The malfunction described above may contribute to the estimation for the

respective impact of these four possible explanations, especially in the case of „1230 Modul“ it appeared twice and for the „2001 T“ never, in spite of the longer runtime: in principle, there is no reason why both FID differently coped with the same situation because the affected component (the capillary inside the FID) of the devices was identical for both FIDs. This was in contradiction to the components upstream, which were different, especially the sample feeding:

Assuming a substantially higher degree of vaporisation via capillary in comparison to the expansion via needle valve, more oil aerosols reach the „2001 T“ (needle expansion), but they are blocked by the filter. In case of capillary expansion more aerosols are vaporised and so more oil vapours can reach the critical part of the „1230 Modul“ (the capillary downstream the filter) and causes the defects.

It was not the aim of this work to find a complete explanation for that, so no additional investigations were performed. Nevertheless, some conclusions and proposals can be made on the basis of the results, obtained during the investigations presented in this work, helping to judge upon possible reasons presented above:

Concerning point 1.:

The vaporisation delivers gaseous analytes, appropriate for the FID. The measurements described in 3.1.1 identified only some of the analytes, like Cyclohexane, but proved all of them to be hydrocarbons, which are the original target gases for an FID.

Concerning point 2.:

The sensors respond very sensitively (sensor signal: ~ 4) to exposure in the range of 30 mg/m³, which corresponds to the carbon content of 16 ppm Propane concerning the FID. In contradiction to the FID response, which is

nearly proportional to the carbon content (for $C_2 - C_8$, [Tes00]), the MOX sensors will show less response per carbon atom with increasing molecule size, according to the reaction path given in 2.2.4, and therefore the corresponding amount of Propane will actually be lower. This means, either the main part of the oil reaches the sensor and causes a response, or the sensors show an amazing sensitivity with a limit of detection in the lower ppb range, which is likely to be too optimistic.

Furthermore the vaporisation degree must be rather high, otherwise the sensing layers would have been poisoned and the surface inside the measurement chamber would show a deposition of oil after more than 18 months of operation including the exposure to high oil content.

Concerning point 3.:

If the aerosols would have reached the burning chamber, they surely would have caused a defect of this extremely sensitive component, or, at least, they would have been noticed when opening the burning chamber while repairing the breakdown.

Accordingly, the most probable explanation is that most of the aerosols are vaporised but a noticeable part of the oil vapours react at the filter of sintered V2A steel. They are oxidised, perhaps not only to CO_2 but also to other species with low response factors and other decomposition products that may form the incrustation. The surface of V2A steel is covered by Cr_2O_3 and mixed crystals based on chromium (III) oxide are also discussed as a sensor material based on the same principle like SnO_2 , resulting in the combustion of the analyte [Roe95], [Woe01], [Wil99]. According to [Ulr03] it was already observed that sometimes small concentrations (low ppm range) of bigger molecules ($> C_6$) were not detected by the FID. The sintered material with its large surface, the surface composition and the temperature of $300\text{ }^\circ\text{C}$ may enable a respective reaction.

2.4 Vaporisation by expansion via capillary

2.4.1 Characterisation of the capillary expansion process

For the slow, isothermal expansion of the pressurised air a standard stainless steel capillary with an inner diameter of 180 μm was used. Assuming a laminar behaviour the law of Hagen-Poiseuille [Kuc84]

$$V_F = \frac{\pi \Delta p t r^4}{8\eta l} \quad \text{with}$$

V_F = flow volume

Δp = pressure difference

t = time

r = radius

η = dynamic viscosity and

l_{cap} = length of the capillary

can be applied. It can be seen that the flow rate F

$$F = V_F / t = \frac{\pi \Delta p r^4}{8\eta l}$$

is proportional to the length of the capillary and to the pressure difference. Most of the measurements have been performed with capillaries lengths of five meters, resulting in a flow of ~ 50 ml/min. The orienting measurements, with the first compressor set up (3.2), were performed with a ten meter capillary and delivered ~ 26 ml/min.

The residence time, t_R , of the air in the capillary, which is one part of the response time of the overall system, can be calculated by

$$t_R = \frac{V_C f_p}{F} = \frac{\pi r^2 l}{F} \quad \text{with}$$

V_C = inner volume of the capillary and

f_p = pressure correction factor

The formula is based on the fact that the flow rate is correlated with the inner volume of the capillary by the residence time: it is the time which is needed to exchange the complete quantity of air in the capillary. The inner volume of the capillary can be easily calculated and the quantity of air is measured anyway downstream the capillary. The measurement is at ambient pressure and the pressure in the capillary is higher, accordingly a pressure correction factor has to be introduced. For a pressure difference of 7 bar, the average pressure in the capillary is 3.5 bar, assuming a linear pressure drop. In case of the five meter capillary and a flow rate of 50 ml/min this results in

$$t_R = \frac{\pi (90 \cdot 10^{-4})^2 \cdot 500 \cdot 3.5}{50} \frac{\text{cm}^2 \text{ cm min}}{\text{cm}^3}$$

$$t_R = 8.9 \cdot 10^{-3} \text{ min or } 0.53 \text{ s}$$

The residence time of the sampled air in the capillary is about half a second and therefore the influence on the overall response time will be negligible.

2.4.2 Vapour pressure over aerosols

The vaporisation of the aerosols by a slow, isothermal expansion of the pressurised air takes advantage from the Kelvin effect: the vapour pressure over aerosols is different from the vapour pressure over classical liquids. It is given by [Goe96] or [Atk01]

$$\ln \left(\frac{p_{aer}}{p_{pla}} \right) = \frac{2 \gamma V_m}{R T r_A} \quad \text{with}$$

p^{pla} = vapour pressure over a planar surface

p^{aer} = vapour pressure over aerosol droplet

r_A	= radius of the aerosol droplet
γ	= surface tension
V_m	= molar volume of the oil
R	= gas constant and
T	= temperature.

Or, rearranged, by:

$$p_{aer} = p_{pla} e^{\left(\frac{2\gamma V_m}{RT r_A}\right)}$$

This means that the pressure is dependent on the size of the aerosol droplet and therefore the size determines whether the aerosol droplet will grow or vaporise even in a saturated atmosphere. The critical radius r_{cr} is given by

$$r_{cr} = \frac{2\gamma V}{k T \ln(S_{rat})} \quad [\text{Mue01}] \text{ with}$$

V = volume of the droplet

S = saturation ratio, defined as the ratio of partial pressure of analyte X, $p(X)$ and its saturation vapour pressure, $p_{sat}(X)$, and

k = Boltzmann constant.

As shown in 1.3.1, the expansion decreases the partial pressure $p(\text{Oil})$; therefore, the saturation ratio decreases and the critical ratio increases; most aerosols tend to vaporise, or, taking into account the chemical inhomogeneity of the oil, some components will increasingly vaporise, others less prone to vaporisation will also start to vaporise.

This qualitative considerations may explain the increased vaporisation due to

the expansion, but a quantitative statement would be more useful. The surface tension of an used compressor oil of the type Kaeser Sigma plus was found to be 30.65 mN/m at $T = 19.5\text{ }^{\circ}\text{C}$; one has to remember that the results of both equations are dependent on the size of the aerosol droplet. Unfortunately, no specific information about oil aerosols could be found, so an aerosol diameter from 10^{-9} to 10^{-5} m had to be assumed, which is a range of four orders of magnitude. In the case of the critical radius this range increases to twelve orders of magnitude because the volume is used. The calculation of the critical radius additionally suffers from the lack of exact figures for the saturation vapour pressure of the oil and therefore no significant calculation is possible.

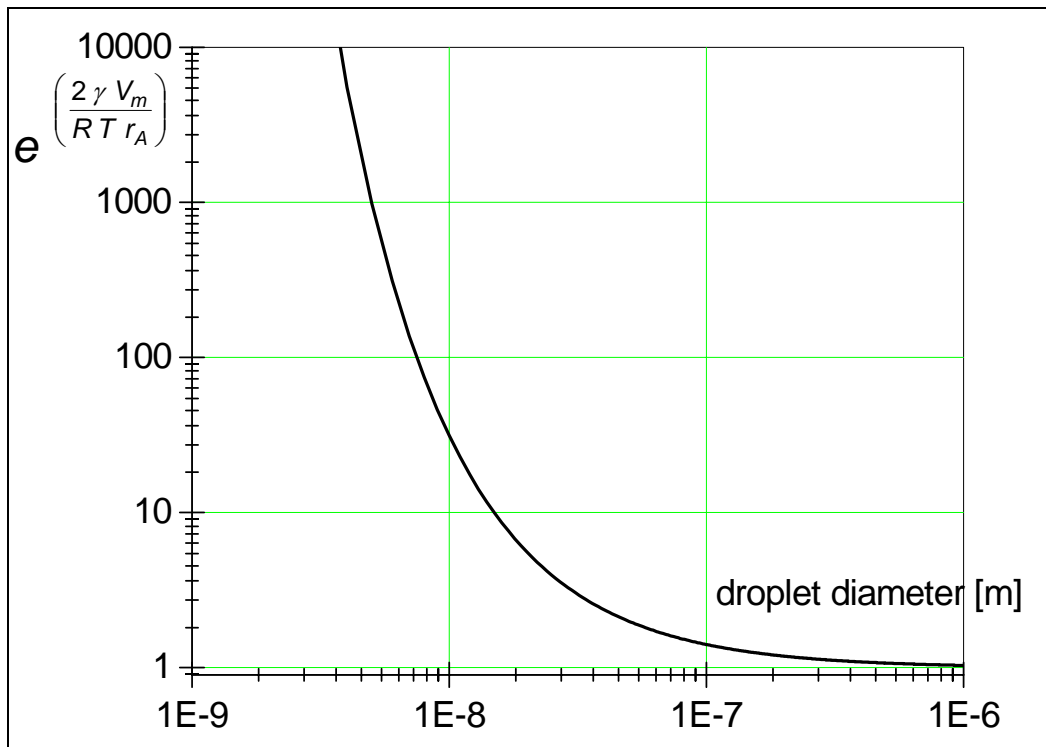


Figure 10: Graph of the exponential factor $e^{\left(\frac{2\gamma V_m}{RT r_A}\right)}$ in dependency of the aerosol diameter $d = 2 r_A$.

In case of the vapour pressure over aerosols, the exponential factor depends, among other parameters, on the molar volume of the oil, V_m . It is given by the molar volume M_m divided by the density, σ , for new *Kaeser Sigma fluid plus* they are:

$$M_m = 590 \text{ g/mol and [Zei03]}$$

$$\sigma = 843 \text{ kg/m}^3 \text{ [Kae96]}$$

For a temperature of 25 °C, the exponential function is $e^{\left(\frac{-3.447 \cdot 10^{-8}}{r_A}\right)}$, with r_A in meter, **Figure 10** visualises this dependency. It is obvious that the Kelvin effect does not affect aerosols with a diameter of more than 10^{-7} m, corresponding to 0.1 μm , and starts to have a dramatic influence on droplets of 10^{-8} m, (0.01 μm).

2.5 Gas mixing system

The orienting measurements in 3.1.2 were performed in a gas mixing system as it is shown in the schematic of **Figure 11**.

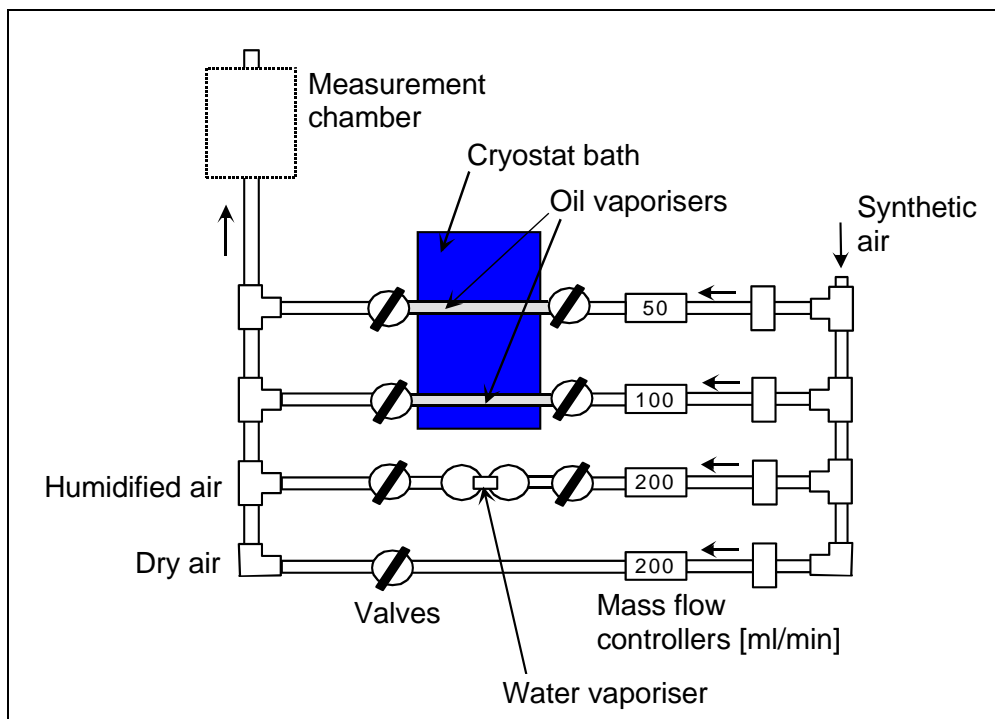


Figure 11: Gas mixing system as it was used for the measurements presented in 3.1.2.

The synthetic air was delivered by a zero-air-generator (Residual humidity: ~500 ppm H_2O , residual hydrocarbons: equivalent < 0.1 ppm CH_4). The

vaporisers were u-shaped glass tubes filled with chromosorb®; the respective liquid (oil or water) was adsorbed by the chromosorb®. Due to the high surface of this heterogeneous packing, the air blown through the vaporiser gets saturated with the analyte, according to the respective saturation vapour pressure. The saturation vapour pressure is temperature dependent and so the vaporisers are immersed in a thermostatised bath of a cryostat in order to vaporise the liquid under clearly defined and reproducible conditions. Furthermore this allows to vaporise the liquid at different temperatures and therefore with different saturation vapour pressures.

The mass flow controllers (MFC) and the valves were controlled by a home made software program (Poseidon), which ensured a consistent total flow and closed the valves upstream and downstream the vaporisers in case they were not in use (This was done in order to prevent uncontrolled diffusion). The gas mixing system enabled the mixing of user-defined gas samples and kept track of the four flow rates. In this way possible errors can be identified.

3 Experimental results and discussion

3.1 Exploratory measurements

3.1.1 Headspace GC/MS

To identify the volatile components, some Headspace GC/MS analysis was performed. 10 ml of compressor oil were filled into a 20 ml headspace vial; the vials were equilibrated for 60 min at 85°C in the headspace sampler. After equilibration 3 ml of the headspace were injected to the GC column (HP VOC). The MS was adjusted to detect only masses above 33 amu in order to exclude the background of water, nitrogen and oxygen.

Five different oils were investigated, three new ones (BP B35 Breox, Universal Lubricants Panolin and Ingersoll Rand Ultracoolant) and two used ones (Kaeser Sigma plus and Shell Comptella S46). The results are shown in **Table 1**. The figures in the columns 3-7 show the percentage of peak area of the complete chromatogram. Sums less than 100 can be found due to very small peaks which are not listed here or peaks which doubtlessly are not correlated with the headspace of oil (column bleeding...).

The first column shows the compounds proposed by the HP Chemstation software but they should not be taken for granted as most of the qualifiers are not high enough: the concentrations in the headspaces generally were rather low and resulted in mass spectra with fragmentation patterns that did not allow a reliable structure identification. Nevertheless, the fragments that can be found are characteristic and allow to identify the original hydrocarbons. Even if the exact hydrocarbon species can not be identified, these results clearly demonstrate that there is an appreciable headspace and that the headspace components are, at least, mainly hydrocarbons. This was an important precondition for the use of metal oxide gas sensors.

Possible Compound	Rt [min]	BP B35 Breox [%]	Ingersoll R. [%]	U. L. Panol. [%]	Shell C. S46 [%]	Kaeser S. F. + [%]
2-Methyl-hexane	12.79					5.24
1-Bromo-3,4-dimethyl-	12.96					2.20
3-Methylhexane	13.17				5.08	7.43
Methylcyclohexane	15.30				8.66	9.62
1,2,3-Trimethyl-	15.78					2.36
2-Methylheptane	16.47				10.82	6.97
3-Methylheptane	16.76				8.50	6.05
1,3-Dimethylcyclohexane	17.27				14.30	11.53
Dimethyl-1,4-dioxane	17.45		4.98			
1,1,-bis (dodecycoxy)hexadecane	17.63		4.01		6.88	
cis-1,2-Dimethylcyclohexane	18.01					2.38
4,5-Dihydro-3,4,5-Tyrazol	18.23				4.36	
trans-1,3-Dimethyl-	18.23					3.32
4,4-Dimethyl-heptane	18.39					1.34
2-Methyldecane	18.57					1.12
2,5-Dimethylheptane	18.82				5.18	3.25
1,3,5-Triethyl-cyclohexane	19.04				5.03	3.02
Ethylcyclohexane	19.20				12.56	7.70
1-(2-Propenyloxy)-2-	19.49	43.68	50.20			1.36
2-Methyloctane	19.71	6.06	27.02		14.83	8.45
3-Methyloctane	19.95				3.80	2.19
n-Butylether	20.34	2.83				
trans-1-Ethyl-4-methylcyclohexane	20.86					1.17
1-Butoxy-2-propanol	22.27	9.03				
o-Decyl-hydroxylamine	23.58			0.56		
Undecane	26.13			1.39		
Triethylphosphate	27.10	23.61	4.03	98.05		
1-[1-Methyl-prop-2-en]2-propanol	27.80	13.29	9.62			

Table 1: Results of the Headspace GC/MS analysis of three new and two used compressor oils. The figures given in the columns of the five oils represent the percentage of peak area of the respective chromatogram.

Although different types of oil have been investigated (Mineral oil,

Polyalphaolefin, Pentaerythrit-tetra-fatty acid) another tendency is clearly seen: new oils do not show as much different components as the used ones and the evaporated components have a higher mass and a longer retention time (second column in **Table 1**). The vanishing of these components (present in new oils, but not in used ones) can be explained by a depletion of additives or production residues; the appearance of different, smaller compounds in used oils probably is an effect of degradation. Both effects are also observed by [Lev01], although [Lev01] investigates the aging of engine oils and therefore the results are not fully comparable.

Kaeser Sigma Fluid plus, the oil which was in use in the compressor during the investigations presented in this work is a Polyalphaolefin, a macromolecule originating from the polymerisation of aliphatic long chain hydrocarbons with terminal double bonds. The educts are usually produced by polymerisation of ethylene. After the polymerisation, the product gets hydrogenated in order to saturate residual double bonds. The polymer does not contain hetero atoms and shows a defined distribution of molecular masses which typically is in the range of some thousand amu. Due to their defined structure Polyalphaolefins are very stable towards oxidation [Mob99]. This may explain why the vapours of *Kaeser Sigma Fluid plus* listed in **Table 1** show mainly hydrocarbons and not the products of oxidative degradation like [Lev01].

3.1.2 Results with gas mixing system

Before the measurements at the real life set up have been made, investigations at a gas mixing system as described in 2.5 had been performed with a Residual Gas Analyser (RGA), as a analytical instrument and with the sensors that were intended for the real life measurements. A RGA is a rugged, easy to handle quadrupole mass spectrometer with less sensitivity than a classical mass spectrometer but a flexible probe feeding possibility: it is usually used in industry for process control. The Hiden DSMS RGA 301 was equipped with a

Quick Inlet Capillary (QIC) and was fed by the gas mixing system via open split with 50 % synthetic air and 50 % synthetic air that had flown through a vaporiser at room temperature filled with used *Kaeser Sigma Fluid plus*.

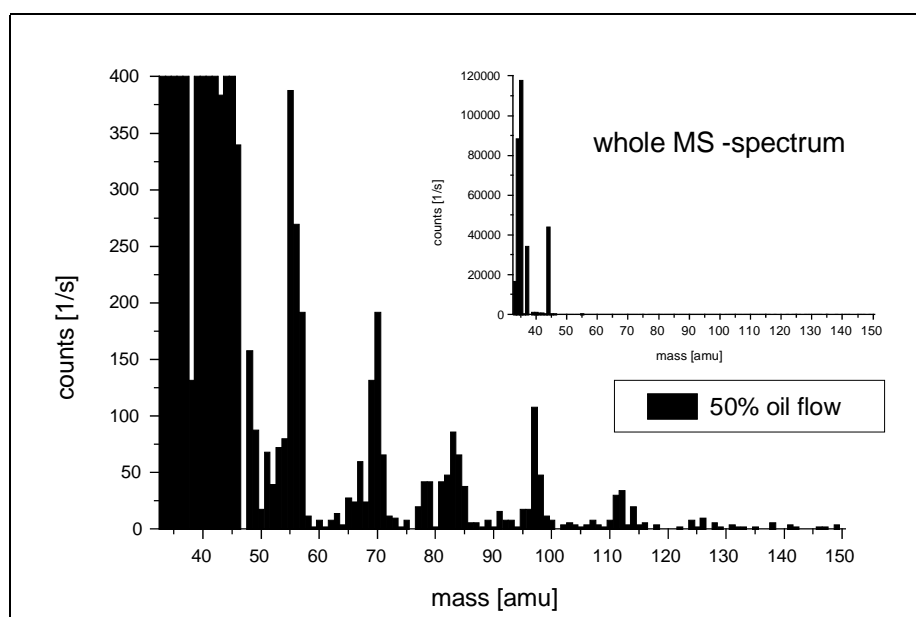


Figure 12: Difference mass spectrum of 50 % air through a vaporiser filled with used compressor oil at room temperature, residual: synthetic air.

Figure 12 shows the difference spectrum resulting from the subtraction of the spectrum of 100 % synthetic air from the spectrum with 50 % contaminated air.

The intensity is low but the typical wave-like pattern of hydrocarbons is clear to be seen. Often these waves, with a wavelength of 14 amu, are related to the (undesirable) presence of oil originating from the vacuum pumps. This is not the case here, as it could be proven by an MID scan. An MID scan (Multiple Ion Detection) is the time dependent visualisation of selected mass per charge ratios. **Figure 13** explicitly shows that the exposure to 50 % air from the oil vaporiser reversibly increases the hydrocarbon content. This proves that the main part of the hydrocarbons originates from the sampled gas and not from the vacuum pumps.

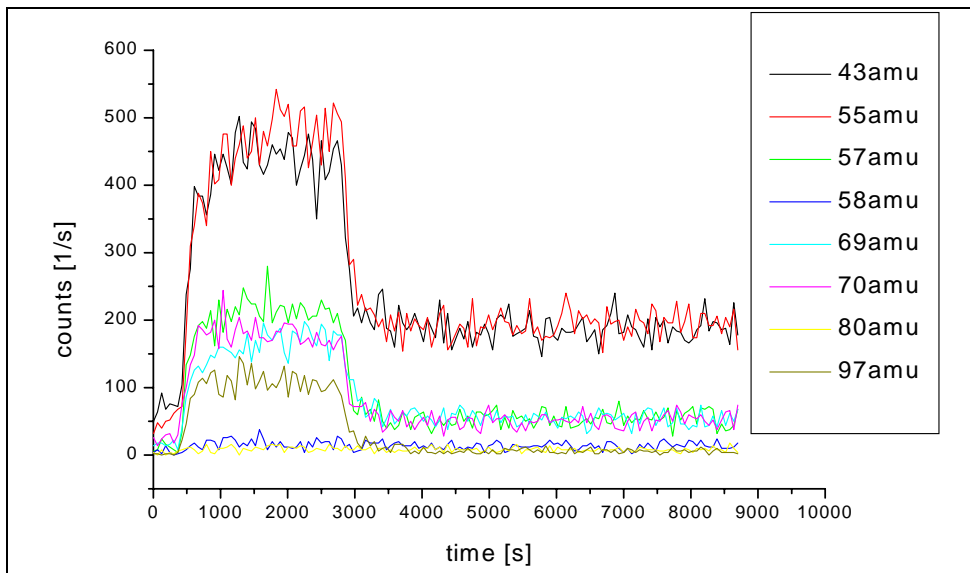


Figure 13: *Transient response of the RGA when exposed to 50 % air through an oil filled vaporiser at room temperature for 45 minutes. Balance and purging: synthetic air.*

The sensors, the sensor chamber and the devices for operation, as described in 2.2.2 and as used for the measurements at the real life set up, have also been installed at the outlet of the gas mixing system and exposed to mixtures of dry synthetic air and dry (synthetic) air saturated with oil vapour by flowing through a vaporiser filled with used *Kaeser Sigma Fluid plus* at room temperature.

Figure 14 shows the resistances of all three sensors when exposed to different proportions of contaminated air. The sensors react in a reversible way and the response is clearly correlated with the proportion of air going through the oil filled vaporiser. These measurements proved that MOX sensors can detect the compounds vaporised out of compressor oil and even a rather low proportion of three percent of contaminated air cause a response. The second precondition for the prove of feasibility as explained in 1.3 is met, as far as vapours from the gas mixing system are concerned.

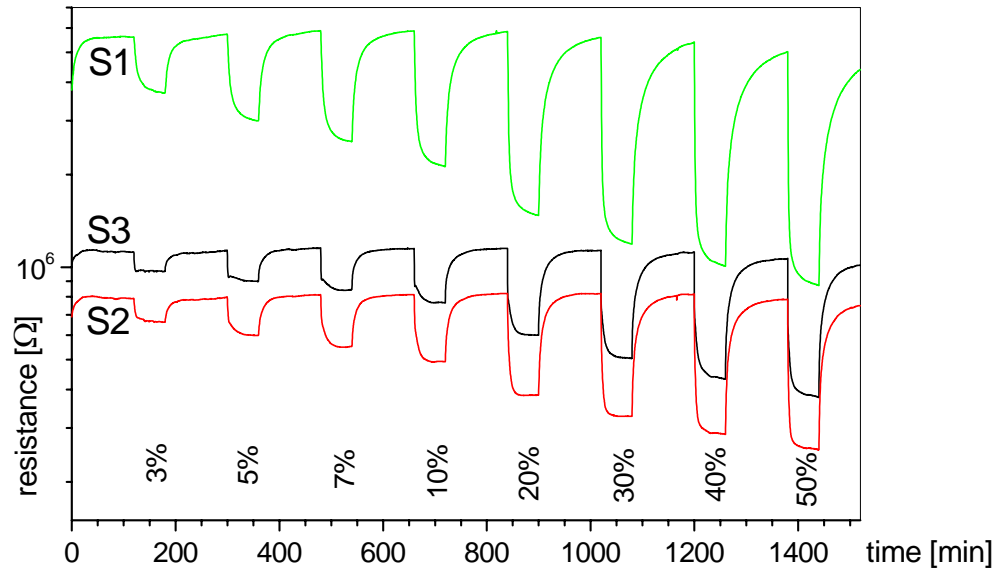


Figure 14: Sensor response towards exposure to increasing amounts of oil vapours in dry air, produced via vaporiser in a gas mixing system.

The powder impregnated sensor material of sensor S 1 shows the best sensitivity, the gel impregnated sensing layers of sensor S 2 and S 3 show a faster response to exposure to oil vapour and a faster recovery.

3.2 First compressor set up

3.2.1 Set up

In order to investigate the degree of contamination at the different points in a typical filtering line and the respective sensor response, four stub lines equipped with ball valves were mounted in a filtering line that contained a fine filter, a dryer and a charcoal filter.

Figure 15 show the alignment subsequent the outlet of the compressor, the illustration of the compressor is simplified in comparison to the schematic in **Figure 3** by showing only the lines in use at these measurements: only the regular compressor outlet, for air filtered by the oil separator, has been used.

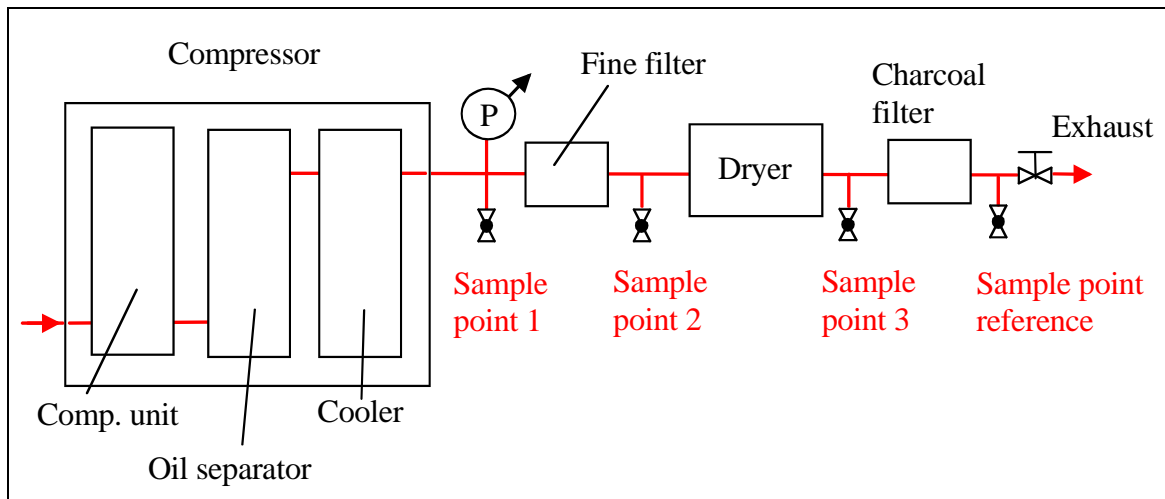


Figure 15: Schematic of the location of the sampling points within the filtering line for the measurements at different sampling points (3.2).

The expected contaminations at the different sampling points were [Man00]:

Sample point	Oil aerosol content	Oil vapour	Humidity
1	3-30 mg/m ³	+	≤ ambient*
2	0.1-3 mg/m ³	+	≤ ambient*
3	0.01-0.1 mg/m ³	+	
reference	0.003-0.01 mg/m ³	-	

Table 2: Contaminations at the different sample points as shown in **Figure 15** according to [Man00] (*Details concerning humidity limitation are explained in 3.3.3).

The exact values for oil aerosol is dependent on the conditions of the oil separator and filters, but it can be seen that all devices contribute to the aerosol filtering process:

- Between sample points 1 and 2 the fine filter does some additional filtering, also based on the coalescence principle like the oil separator, but designed for less contamination and higher purity.
- The dryer is equipped with an internal fine filter downstream the drying unit in order to eliminate residual particles of the drying medium; of course, it also filters aerosols.
- The charcoal filter removes most of the gaseous oil by adsorption (but also aerosols).

The charcoal filter is the final point of this typical filtering cascade, which is very common for a lot of applications. The air from sample point “reference” was regarded as clean and therefore used like synthetic air in classical laboratory set up for purging and for the baseline signal.

Figure 16 shows the assembly of measurement devices and the corresponding sample feedings, supplied by the different sampling points. The sample feeding for the MOX sensors was equipped with two capillaries with a length of ten meters and both of them have continuously been flown through: the fitting of the capillary, which was currently not feeding the sensor chamber was slightly opened directly upstream at the three-way-valve supplying the measurement chamber (**Figure 16**) and the other subsequent devices. This was done in order to provide equilibrium conditions concerning the expansion process and to avoid artefacts, for example by pressure charges when changing the sample point. The exact measurement procedure is explained below. The Testa „2001 T“ FID was operated and fed as depicted in detail in **Figure 9**.

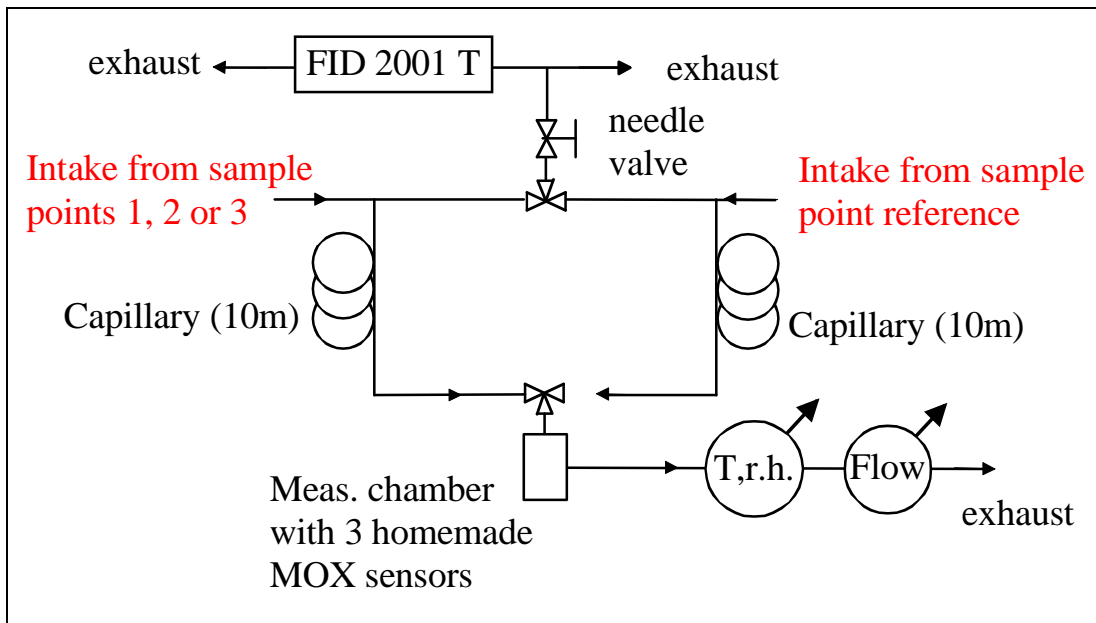


Figure 16: Assembly of the measurement devices and sample feedings of the measurements at different sampling points (3.2). Both capillaries have been continuously flown through.

The baseline, monitored for example in the beginning of every measurement, was recorded when air from sample point “reference” supplied both the FID and the sensor measurement chamber (and, of course, the devices downstream this line). In this period, the capillary from sample point 1, 2 or 3 was loosened at the low pressure end (at the three-way-valve) in order to enable a continuous flow in spite of the “closed” three-way-valve. When measuring air from sample point 1, 2 or 3, the capillary from sample point 1, 2 or 3 was mounted properly and the capillary from sample point reference was loosened. This means, the procedure of switching, for example, from “reference” (baseline measurement) to 1, 2 or 3 (exposure to air with higher oil and / or water content) was:

- Tightening of the capillary from sample point 1, 2 or 3 at the three-way-valve
- Switching of both three-way-valves (to sensor measurement chamber etc. and to FID)

- Loosening of the capillary from sample point “reference” at the three-way-valve

For switching back from sample point 1, 2 or 3 to sample point “reference”, all three actions had to be undone in reverse chronological order.

3.2.2 Measurements at different sampling points

Measurements of air from sample points 1, 2 or 3 were performed, all of them using air from sample point “reference” for the baseline. The measurements (typical results are given in **Figure 17** to **Figure 19**) showed some fluctuations of pressure, flow and FID reading which should be explained:

The dryer, included in the respective set up, as shown in **Figure 15** works in a discontinuous operation mode. Every two minutes it switches between two dehumidifying cartridges. A small part of the dry air obtained by using one cartridge is used to regenerate the other. 20 seconds before the next switch the flow through the regenerated cartridge stops. This stop of the additional drain leads to an increase in pressure in the system, which leads to the upward spikes every two minutes in the pressure graphs **Figure 17** to **Figure 19**. The downward spikes appearing every four minutes, are caused by the automatic venting of the built-in fine filter. Both types of changes in pressure can be observed in all conditions (reference and contaminated air) and directly affect the flow through the capillary, according to the correlation given in 2.4.1.

The correlated influence on the FID signals observed in **Figure 17** to **Figure 19** is also a negligible artefact: it is caused by the intake of ambient air due to reverse flow through the open split (shown in **Figure 9**). The periodical pressure drop, caused by the dryer, leads to a small decrease in flow through the needle valve, which intermediately falls below the intake rate of the FID. So, the FID takes in air from the ambient and, due to the continuous spoilage of the room air by the compressor, the ambient air is more contaminated than the outside air after one passage through the compressor. Consequently, the FID shows an upward spike, correlated with the pressure drop caused by the

dryer.

The appreciable increase in flow during exposure to sample gas from sample points 1 to 3 is caused by the higher pressure at these sample points in comparison to the sample point “reference”. This is due to the pressure drop at the filter elements between sample point “reference” and sample point 1 to 3. It may be useful to stress that this temporary pressure increase cannot be observed in the pressure graph, as the pressure gauge was all the time integrated direct after the compressor (see **Figure 15**) and therefore it was not exposed to different pressures.

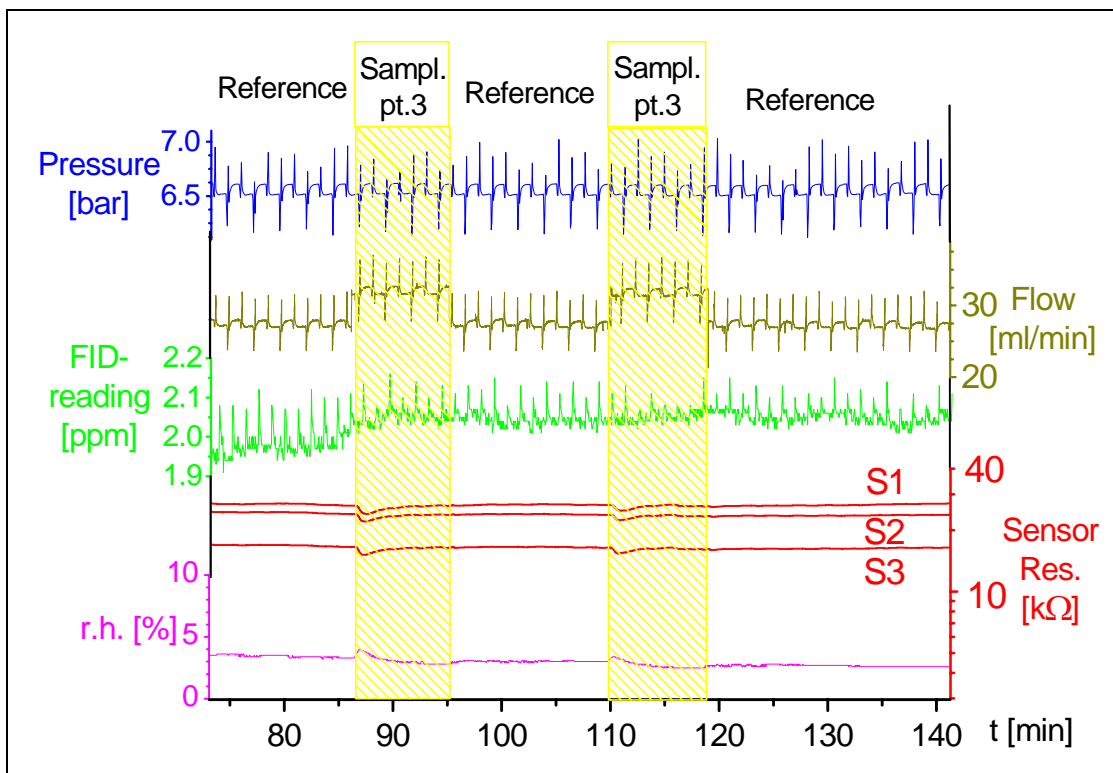


Figure 17: *Graphs resulting from a measurement with switching between sample point reference and sample point three (see **Figure 15**), characterised by a charcoal filter in between. An interpretation is given in the text.*

Figure 17 shows graphs from a measurement with switching between “reference” air and air from sample point 3. As it can be seen, the humidity and the hydrocarbon content according to the FID stayed constant, only the

flow through the capillary and the subsequent devices was increased from ~ 26 ml/min to ~ 32 ml/min. This corresponds to a relative increase of $\sim 15\%$ but **Figure 17** clearly shows that this does not relevantly influence the sensor response.

Due to the operation mode including opening of the fittings the switching causes a short increase of humidity and therefore a sensor response. This artefact was eliminated in the measurements with dosing of oil (3.4.2).

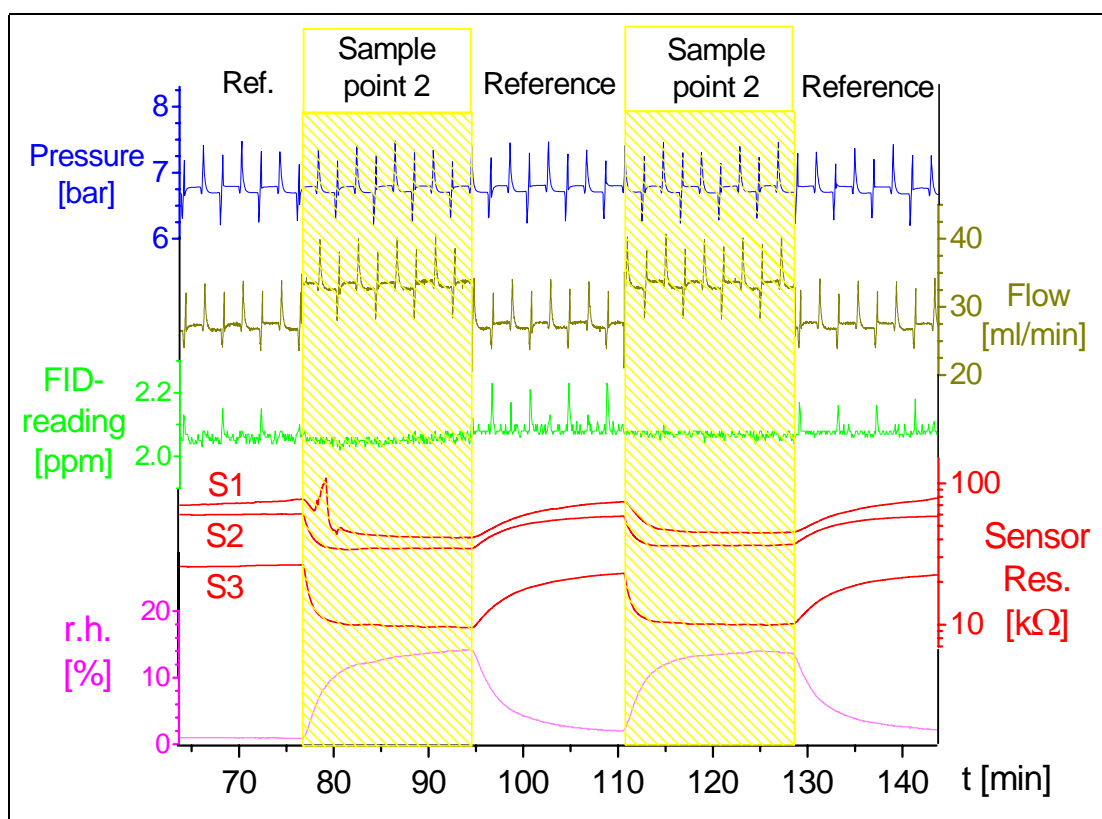


Figure 18: *Graphs resulting from a measurement with switching between sample point reference and sample point two (see **Figure 15**), characterised by a dryer and a charcoal filter in between. An interpretation is given in the text.*

Figure 18 shows typical results of a measurement with switching between “reference” air and air from sample point 2, which have a dryer and a charcoal filter in between. Again, the flow through the capillary increases but here, also the humidity shows a substantial increase from 1 % r. h. to 14 % r. h., due to

the effect of the dryer. The FID signal stayed constant but the spikes caused by the reverse intake of air disappear while exposure to air from sample point 2. This is a consequence of the accidentally higher working pressure of the compressor in comparison to the measurements shown in **Figure 17** and **Figure 19**. The difference is small, but enough to prevent the intake of ambient air while sampling from sample point 2.

The hydrocarbon content, according to the FID, stays constant, so the change of the sensor resistance is correlated to the humidity change alone. Subsequent measurements revealed a substantial limitation of the FID, restricting this statement. They are discussed below (3.4.5) and not taken into account in this chapter.

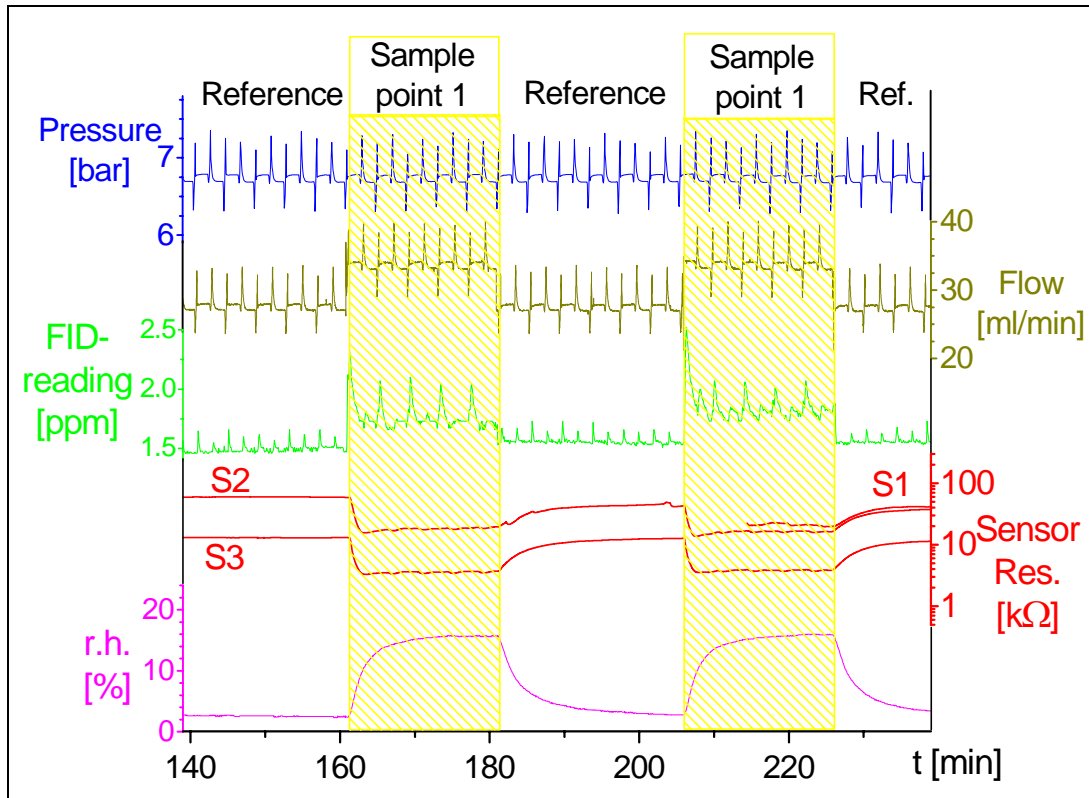


Figure 19: Graphs resulting from a measurement with switching between sample point reference and sample point one (see **Figure 15**), characterised by a fine filter, a dryer and a charcoal filter in between. An interpretation is given in the text.

The graphs given in **Figure 19** show the effects of switching between “reference” air and contaminated air from sample point 1; the effects observable here, add up the contributions of a fine filter, a dryer and a charcoal filter. Again, the flow increases due to higher pressure and the humidity also increases due to the dryer. But, in opposition to **Figure 17** and **Figure 18**, the FID shows a significantly higher (mean) value.

According to the FID, the air from sample point 1 contains more hydrocarbons than the reference air. Consequently, the sensor response is correlated with the increase both of humidity and hydrocarbon content, even if the hydrocarbon content is not monitored correctly by the FID (see 2.3.3). The resistance of sensor S 1 is not completely shown in **Figure 19**, due to temporary problem with the electrical connection.

3.2.3 Results

The measurements at different sample points provided some insights and also some preliminary conclusions, to be verified with measurements to come:

- The sensor resistance is not strongly dependent on the flow rate through the measurement chamber. A change of 15 % of flow did not determine an effect. This is an important finding for the development of a residual oil indicator, because compressors usually work within an appreciable pressure frame and therefore an useful sensor must be able to cope with changing flows due to the changing pressure.
- As expected, humidity causes a sensor response: the resistance clearly decreases with increasing humidity,. Numerical values for the sensor signal determined by the humidity change, S_{Hum} , are given in the second row of **Table 3**.
- The sensors also show a response to the parallel increase of humidity and hydrocarbon content, as monitored by the FID. **Table 3** lists the respective sensor signals S_{Tot} . Assuming an additive behaviour of the changes of sensor responses, the sensor signal due to the increase of oil content, S_{Oil} ,

can be calculated to S_{Tot} / S_{Hum} , which is also given in **Table 3**. It is obvious that the sensors S 2 and S 3 are generally more sensitive, both to humidity and oil content, but especially the sensitivity towards oil is, by far, better. The impregnation method seems to play a substantial role for the sensor performance which is not surprising as it has already been reported that the paste preparation directly and strongly influences the morphology and the distribution of the dopant [Kap01]. The gel impregnation seems to be much more appropriate for this application: it strongly increases the sensitivity towards hydrocarbons and this benefit probably outweighs the cross sensitivity towards humidity, which is also increased.

Changing analyte(s)		S 1	S 2	S 3
Δ Humidity: ~ 14 % (Figure 18)	S_{Hum}	1.7	2.6	1.8
Δ Humidity: ~ 14 % + Δ Hydrocarbon content: ~ 0.2 ppm FID-reading (Figure 19)	S_{Tot}	2.1	8.3	4.6
$S_{Oil} = S_{Tot} / S_{Hum}$	S_{Oil}	1.2	3.2	2.6

Table 3: *Sensor signals and correlated changes of humidity and hydrocarbon content as reported by reference analytics.*

3.3 Second compressor set up

3.3.1 Set up

One main issue for the real life application of non-specific chemical sensors, such as MOX sensors, is cross sensitivity. The most practical way to estimate its impact is the empirical approach: to investigate the concentrations of possible interferences and its influence on the sensor resistance by measuring these parameters within a representative time frame. In order to obtain reliable

long term data the set up was simplified in comparison to the set up presented in Figure 15 and Figure 16 by leaving out what was not needed for these measurements. The resulting, set up is shown in Figure 20.

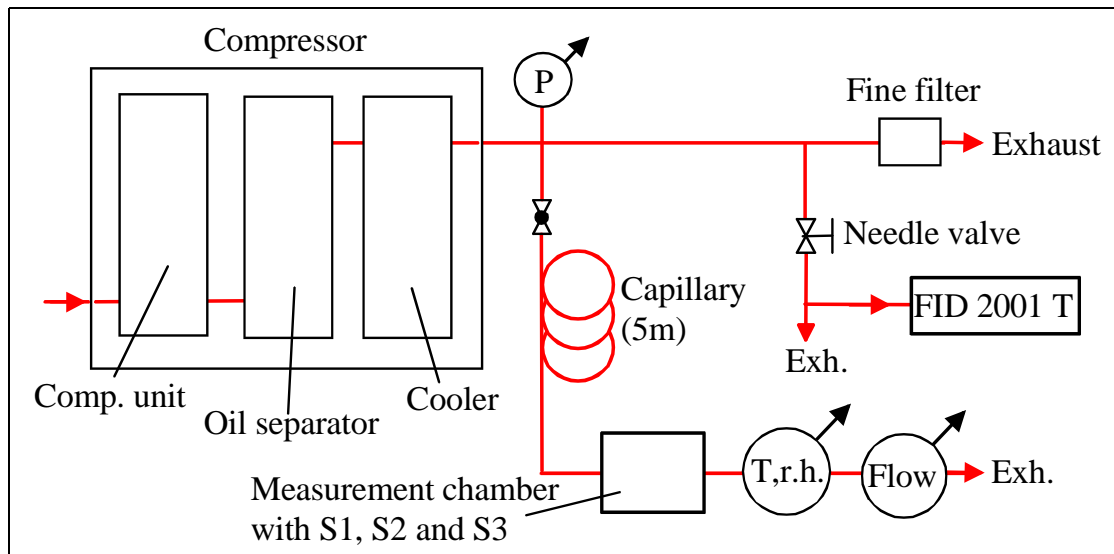


Figure 20: Schematic of the second compressor set up, as used for the long term measurements.

It is characterised by the following properties:

- The most appropriate sample point for these measurements was directly after the (regular) outlet of the compressor, so no additional device could influence the parameters of interest.
- In principle, the filters and the dryer as shown in **Figure 15** are not needed; for environmental reasons a fine filter was mounted in the main exhaust line.
- The capillary was shortened to five meters after intermediate measurements showed no appreciable difference between results with ten meters capillary and five meters capillary. As expected, the flow was roughly doubled, but this did not have any measurable effects on both the vaporisation process and the sensor performance.
- Again the Testa „2001 T“ FID with the large intake rate of 750 ml/min was utilised and fed via needle valve and open split, as explained in detail

in 2.3.3. At the end of the measurements, it was exchanged by the Testa FID „1230 Modul“. Due to the smaller intake rate of ~ 18 ml/min it was possible to feed it via capillary, in order to obtain more comparable results. The resulting schematic is shown in **Figure 21**.

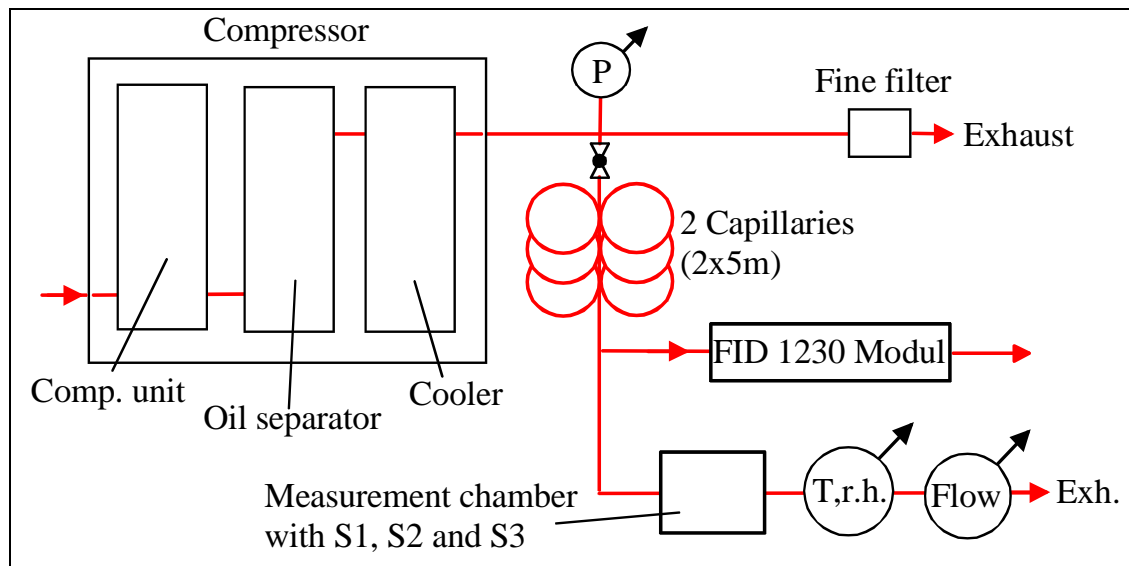


Figure 21: Schematic of the modified set up, as used at the end of the long term measurements, including the Testa FID „1230 Modul“ with an intake rate of ~ 18 ml/min.

3.3.2 Long term measurements

The long term baseline measurements have been performed for more than six months, from the middle of November „2001 T“o the end of May 2002. This period covered autumn, winter and spring, including very cold days and some very hot days with the corresponding effects, e. g. substantial changes of ambient humidity.

In order to investigate also the effects of long term operation of the sensors in this environment and to measure under equilibrium conditions, the compressor and the whole system run nearly without any interrupts. Two longer breaks of several days were made due to vacations, another one because of the effects of high humidity; some short breaks were necessary for minor modifications at the system or power breakdowns.

It was also tried not to disturb the system or fake the results by intermediate measurements with increased oil content. Unfortunately this could not be set aside completely due to time reasons; later on it turned out not to have a too dramatic effect.

As it can be seen in **Figure 20**, five different measurement devices were implemented in the set up: four commercial ones and the ipc MOX sensors, which led to unforeseen problems concerning the overall measurement stability and data collection. Probably due to the harsh environment in the compressor room or due to a lack of suitability, the measurement devices regularly suffered from errors and breakdowns. The humid and oily room air, temperatures of more than 40 °C, constant vibrations and regular runtimes to the upper limit determines malfunctions for every device. This resulted in a decreased of the number successful measurements with parallel monitoring of all parameters. Fortunately, as already stated in 3.2.3, not all devices proved to be of importance: the flow is mainly determined by the pressure inside the system, furthermore, as it was proven, moderate flow changes did not play an important role and therefore flow and pressure did not have to be monitored for all measurements.

The data logging turned out to be another handicap, as none of the devices could be continuously operated due to the software limitations. It was necessary to regularly synchronise and restart the different devices and computers, so it is not possible here to present a continuous data set.

Other measurements suffered from artefacts, some of them could be cleared and will be explained in the following, others were not reproducible and therefore still give room for speculation.

As already stated in 3.3.1, the long term baseline measurements represent an empirical approach, which, in contrary to the classical experimental one, did not allow to create isolated, determined conditions with a possibility to vary one single parameter and observe its influence. Therefore this chapter presents

observations that were made in a complex system and interpretations of effects and relations that regularly appeared and implied a causality. The observations had to rely on conditions and circumstances that could not be influenced or even repeated.

In the following, the different observations are presented, grouped in terms of the time scale of the effects.

3.3.2.1 Measurements with daily occurrences

Some measurements showed daily modulations of most of the parameters, appearing, while others proved to be completely unaffected. This implies an influence by the ambient, as such changes were not recorded without changes of ambient parameters. Both types are presented here:

- Measurements without significant changes of the ambient parameters, often recorded on colder days, as presented in **Figure 22**. This is the way the measurements were expected to be.
- Measurements with typical changes, often changes of several parameters with a reasonable indication for a causal relation, an example is shown in **Figure 23**. These measurements increasingly appeared as warmer the days were.

Both measurements started at about 11:30 and lasted 13 hours, so the temperature maximum after ~ 6.5 hours took place at about 18:00. The set up was located in a room with large windows looking westward and directly exposed to the sun; this fact explains the late point in time of the temperature maximum. As already mentioned in the introduction of 2, the sun-blind was automatically operated, this resulting on the one hand in protection from direct sunlight, but on the other hand in hindering the exchange of air with the outside. However, the measurement shown in **Figure 23** reports a clear temperature increase, correlated with a decrease of pressure and an increase of hydrocarbon content, as monitored by the FID. The sensors respond with a

parallel decrease of resistance and after the maximum all parameters behave vice versa. This was regularly observed and manifests a causal relation. It should be kept in mind that the temperature was measured downstream the capillary and the sensor chamber: the air flow of ~ 50 ml/min through the this part of the set up did not affect the temperature of the components. So the temperature shown in **Figure 23** represents the room temperature as balanced between dissipation of heat from the compressor to the outside and external heating by the sun, and not a change internally caused by the system.

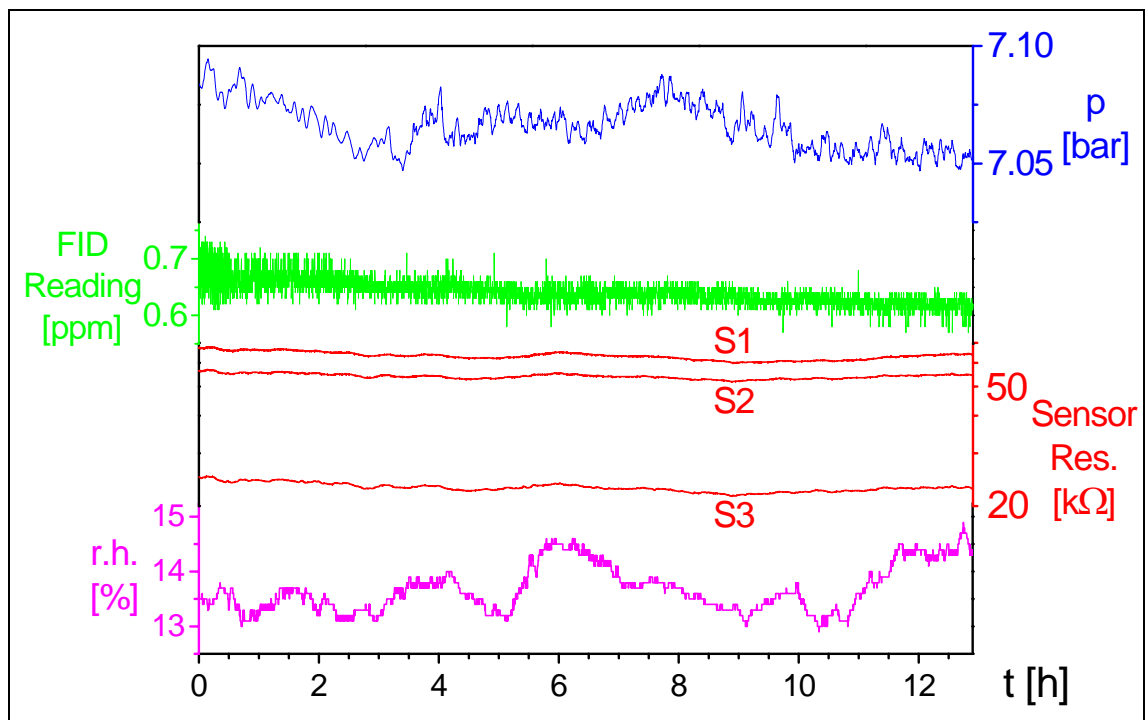


Figure 22: Typical graphs of a measurement on a cold day with stable values for all observed parameters. The change of humidity does not affect the sensor response. The temperature (not shown) stays constant.

As it can be seen in **Figure 23** the relative humidity stays rather constant but it is clear that in this case the absolute humidity goes in parallel with temperature. This means that there was an increase of humidity in the first part of the measurement, the dew point changed from -2 °C to $+5$ °C, which is not surprising as the vapour pressure is dependent on the temperature and the

temperature change, as displayed in **Figure 23**, reflects a temperature change of the ambient.

The reasons for the changes of pressure inside the system and of FID reading are less clear; the most reasonable assumption is a decrease of compressor performance due to higher temperature: the air taken-in is warmer, less dense and the compressor may not be able to compensate this. Consequently the pressure in the system is lower and the therefore more oil aerosol can already vaporise in the high pressure region upstream the capillary.

This explanation is also consistent with the observation when the compressor was turned off for some seconds and restarted before the pressure inside completely went down to ambient pressure: the resistance dramatically decreased and needed a long time for recovery, a behaviour one typically would expect for exposure to high oil vapour content.

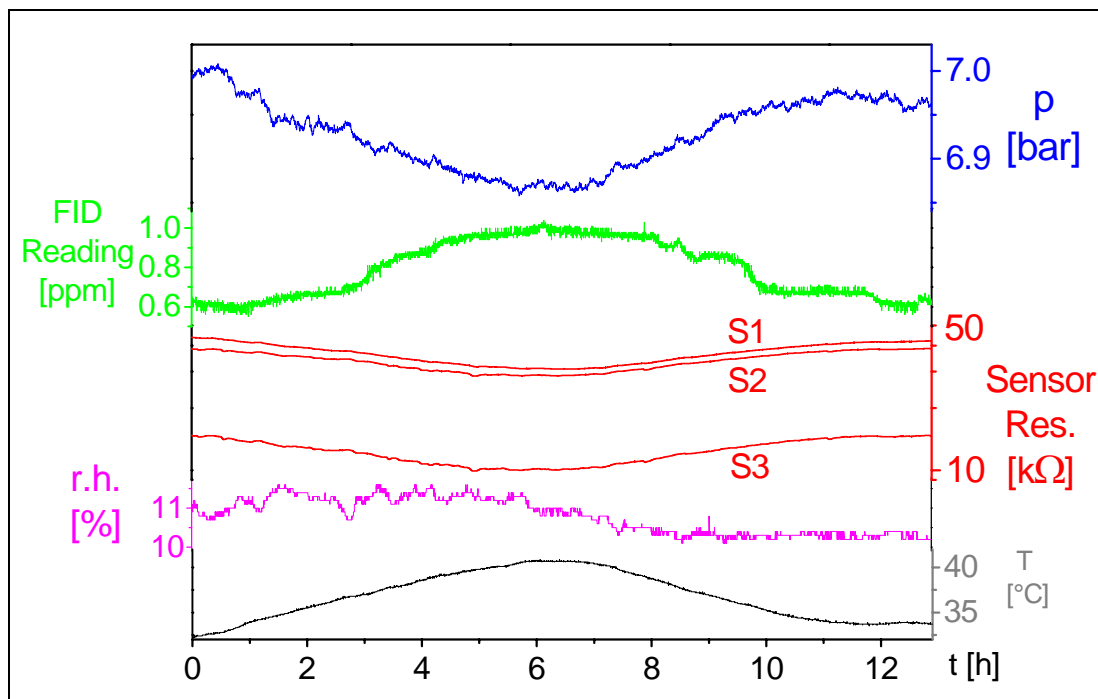


Figure 23: Graphs of the measurements obtained on a warm day. The increase of temperature, given in the graph at the bottom is likely to be the reason for the change of the other parameters.

Unfortunately the temperature effects on absolute humidity and pressure

mostly go in parallel and the FID does not provide reliable and accurate data, comparable to the sensor results, especially due to its different expansion process and the problems described in 2.3.3. Furthermore, it was not possible to determine the ambient conditions of the measurements and so a structured and systematic investigation of the influence of single parameters could not be made; nevertheless, the measurements that could be performed indicate that the impact of humidity is more important than the effect via system pressure.

Measurements, performed later in the year, with even higher temperature and absolute humidity, revealed another effect on the measurements, we called “water spikes”. This effect is described and discussed separately in 3.3.3, due to its impact on the sensors and its direct consequence on the construction of a residual oil indicator.

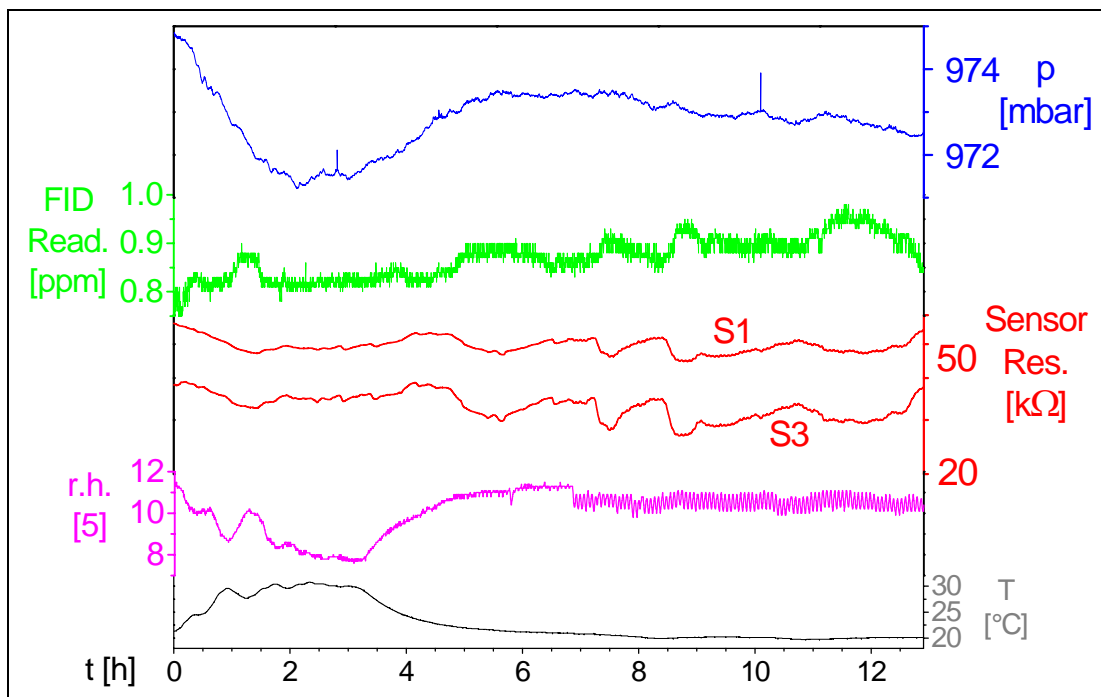


Figure 24: *Graphs of a measurement with monitoring of the ambient pressure. In the second half of the measurement, the humidity signal is corrupted because of coupling. Sensor S 2 was not measured. The sensor resistance is mainly correlated with the hydrocarbon content.*

In addition, some measurements have been performed with the monitoring of the ambient pressure in the room instead of the pressure inside the system. The results are visualised in **Figure 24**. No correlation between ambient pressure and sensor resistance is observed, the only correlation observed is a reciprocal one with the ambient temperature. It is very rough but it is present in all measurements with monitoring of ambient pressure. The similarity with the result for relative humidity is a consequence of the temperature change; absolute humidity (not shown) is not correlated at all. The main influence of the sensor resistance in **Figure 24** is obviously the hydrocarbon content, as monitored by the FID.

3.3.2.2 Measurements with short term changes

Figure 25 shows the same “daily” effects of temperature, pressure, FID reading and sensor resistance as **Figure 23**, just shifted in time due to the later beginning of the measurement, at about 15:30. In opposition to the measurement shown there (**Figure 23**), where humidity and FID reading, the two main triggers for a sensor response continuously change in parallel, **Figure 25** shows several short term increases of hydrocarbon content and a correlated sensor response. Humidity stays constant within these periods and can be excluded as the origin of these sensor response.

It is not clear why the hydrocarbon content changes, but in spite of the different expansion processes, the change is recorded both by the FID and the sensors. It should be stressed that the peaks from both devices even show the same peak shape, which excludes an artefact caused by a trigger like a short disturbance. These kind of correlated peaks were observed regularly and they represent another indication that the sensors really monitor the hydrocarbon content in pressurised air.

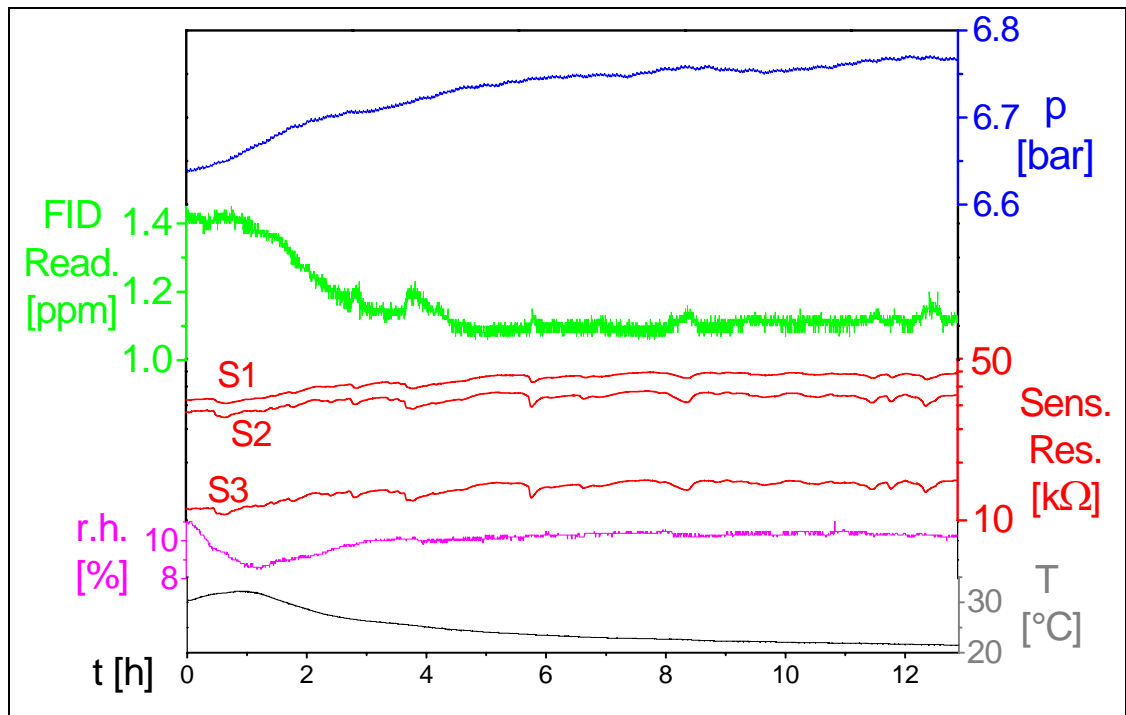


Figure 25: Graphs of a measurement with changes of hydrocarbon content and correlated sensor response. Humidity stays constant within the time frame of the peaks of interest.

Figure 26 shows graphs of another typical measurement result: according to the FID, the hydrocarbon content remains constant, even though the pressure inside the system changes in a range comparable to the measurement shown in **Figure 23**. Here it goes in parallel with correlated changes of humidity and sensor resistance. Temperature stays constant, so the change of humidity (recorded in the measured gas, not in the ambient) is probably caused by the pressure changes, according to the effects described in detail in 3.3.3.2; this results in an inversely proportional relation of pressure and humidity. The changing humidity causes a sensor response, even if both are rather small. The sensor resistance is linearly displayed in **Figure 26**, in order to facilitate the visibility of the effect.

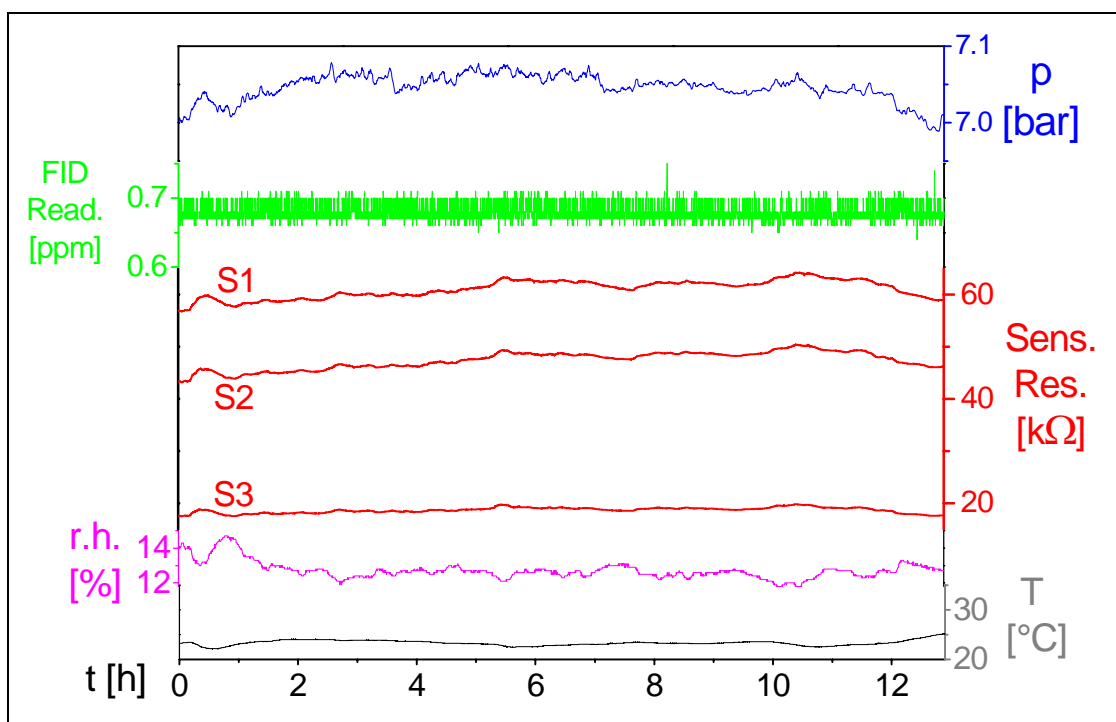


Figure 26: Graphs of a measurement with constant FID reading but correlated changes of pressure, humidity and sensor resistance. In contrary to most other figures the sensor resistance is displayed linear.

The sensor effects shown in **Figure 23** to **Figure 26** correlate with changes of parameters that were monitored in parallel with reference analytics, some (preliminary) explanations or assumptions have been given. It has to be stressed that not all observed sensor effects of comparable magnitude go in parallel with changes of humidity or FID reading. The graphs given in **Figure 27** demonstrate this: at the end of the measurement, the sensor resistance and the FID readout clearly correlate, but the peak at the beginning is only monitored by the FID. In contrary to changes of humidity, which are generally also displayed in the sensor resistance to a certain extent, changes of hydrocarbon content according to the FID are not always reflected by a sensor response.

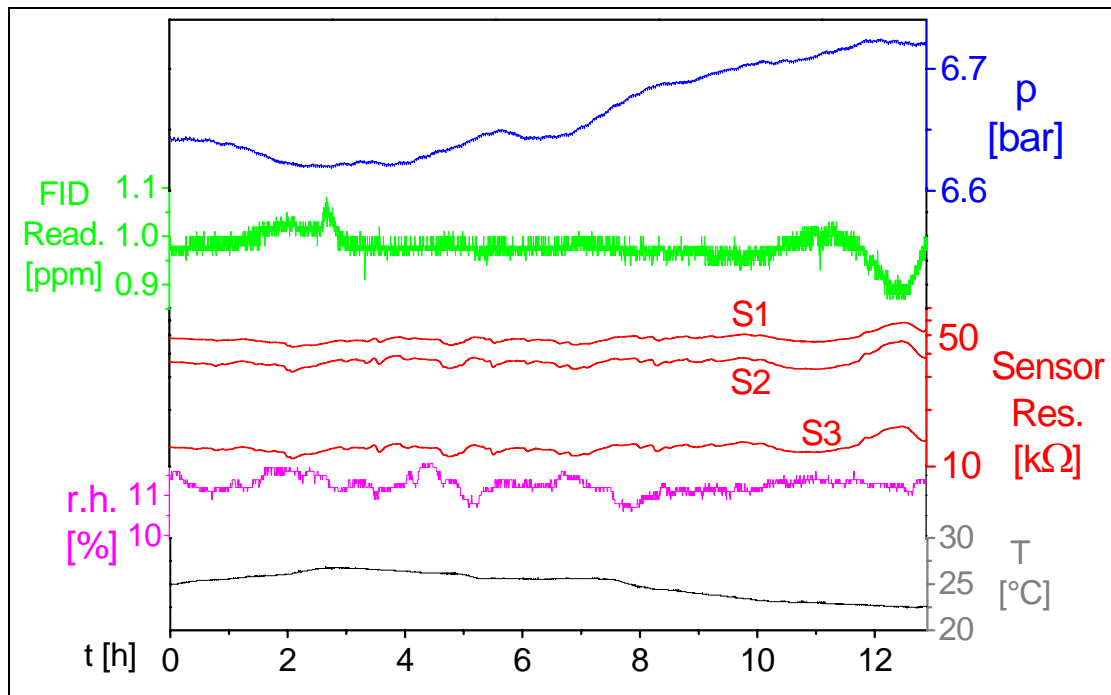


Figure 27: Results of a measurement with non-correlated effects of sensors and FID. A discussion is given in the text.

Other measurements show the opposite: changes of sensor resistance which are neither paralleled by changes of hydrocarbon content according to the FID, nor by changes of humidity. This discrepancy is very probably caused by hydrocarbons, not by humidity, because:

- As it is given in the description of the system (**Figure 20**), MOX sensor measurement chamber and humidity meter are in the same line of sample gas; and the sensitivity to humidity of both devices is doubtless.
- The sensors and the FID use different sample feeding lines and expansion processes, which may lead to differing results.

So, assuming that humidity changes are reliably recorded in parallel by both humidity meter and MOX sensors, this means in reverse, that MOX sensor signals without humidity meter signals are caused by hydrocarbon, even if there is no corresponding FID signal; this is in accordance with the observation of FDI signals without corresponding MOX sensor signal. But this means furthermore, that the hydrocarbons, responsible for both types of

peaks recorded not in parallel, origin from the compressor, because changes of hydrocarbon content of the ambient air should similarly affect both measurement devices (MOX sensors and FID).

3.3.2.3 Seasonal effects

As it can be seen in **Figure 23** - **Figure 26**, the sensor resistances and the relevantly influencing parameters underlie substantial changes on day term or shorter. This complicates the investigation of seasonal effects, because they are overlapping with these shorter term effects. Some of the dependencies could be explained and humidity and hydrocarbon content turned out to be the factors, which mainly affect the sensor resistance. It was probable that they also dominate the long term effects, but it was necessary to verify that and to find out the maxima. Furthermore, it was unclear whether the FID would represent the sensor-relevant hydrocarbons correctly on a longer term, as they may change their composition within the year.

The long term evaluation and its visualisation are complicated by the lack of continuous data and the time dependent disturbances and responses, as shown in the previous two chapters, correlated or not. In order to evaluate representative data, only measurements that had reached equilibrium conditions were taken into account. For most of the measurements that reached equilibrium conditions, this was the case at the end of the 13 hours measurement period. The data of the utilisable measurements are displayed in **Figure 28**; every measurement provided one humidity value, one FID value and three sensor values. In case of problems related to data acquisition or instrumental errors, single values of some measurement have been left out. The rather long break in April 2002 was due to a problem with humidity (described in detail in 3.3.3) and a reconstruction including the Testa FID „1230 Modul“, as shown in **Figure 21**.

In **Figure 28**, the humidity is displayed in ppm H₂O, because the absolute value provides comparability. From the beginning until the middle of March,

the humidity changes only within a small frame of 2200 – 4400 ppm H₂O: the compressor takes in air from the ambient and the ambient humidity is limited by the ambient temperature. As soon as the ambient temperature rises, the absolute ambient humidity dramatically increases.

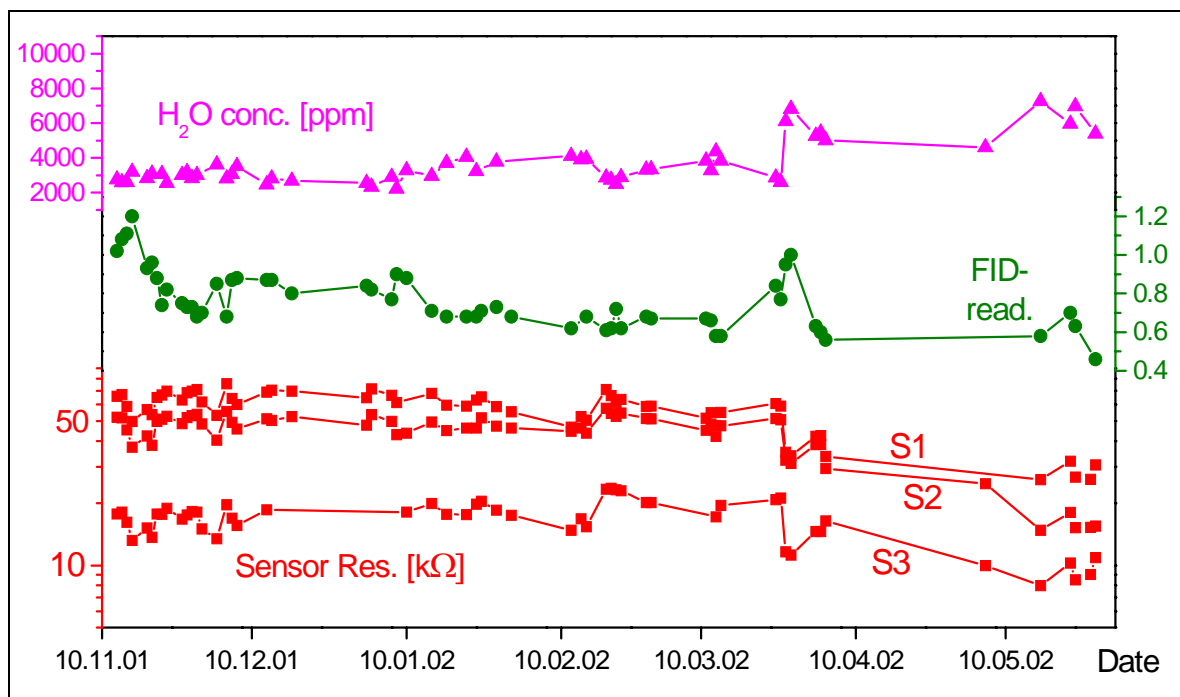


Figure 28: Results of the long term baseline evaluation.

In **Figure 28** no water concentration above ~ 7000 ppm can be found, due to the fact that the humidity meter was located downstream the compressor and the effects described in 3.3.3 prevent a higher humidity. The exact limit is dependent on the (high) pressure and the temperature in the compressor, but this well known effect minimises the humidity range the sensor can be exposed to within this application. This is helpful in term of cross sensitivity, even if the remaining range is the most influencing one for tin dioxide based gas sensors. The results of the three sensors are in very good correlation, all changes go in parallel. This proves that the modulation of baseline resistances is no drift effect, because drift, defined as an undetermined, unsystematic change, would effect every sensor differently.

In addition, it is obvious that the systematic change of the sensor resistances is

strongly correlated with the change of absolute humidity. As expected, the sensor resistance decreases with increasing humidity and this reciprocal relation is observed at nearly every change in **Figure 28**. FID reading and absolute humidity mostly go in parallel but the few exceptions prove the absolute humidity to be more important. This is also the result of a comparison of the correlation coefficients, given in **Table 4**. They are extracted from 43 measurements of **Figure 28** where all devices provided data.

Corr. between:	S 1	S 2	S 3
Abs. hum.	-0.892	-0.850	-0.713
FID reading	0.068	-0.054	-0.310

Table 4: *Correlation coefficients between sensor resistances and absolute humidity (second row) and sensor resistance and FID reading (third row).*

All three sensors correlate with absolute humidity, the correlation with FID reading is negligible for sensors S 1 and S 2. Sensor S 3 shows a moderate correlation with FID reading and the lowest correlation coefficient with humidity. According to this evaluation, sensor S 3 is the most appropriate one for the application of residual oil monitoring.

3.3.3 Behaviour at high humidity

The long term measurements concerning seasonal baseline changes, described in 3.3.2.3, started in autumn 2001 and were continued until spring 2002. In March, the outside temperatures significantly increased the first time within this period. The temperatures, as measured, were unaffected (at least in the beginning), because the system was located inside and had not been directly exposed to ambient conditions. But the increasing outside temperature lead to a higher water content in the atmosphere and the water content was very well

measurable in the system: the intake rate of the compressor provided a complete exchange of the air in the measurement room in less than one hour; it was taken in the compressor and blown through the measurement line. As it can be seen in **Figure 28** the value for absolute humidity was clearly shifted in the second half of march. Not much later more and more measurements suffered from irregular humidity changes, showing peaks, sometimes for minutes but also for hours. The appearance, the size and the shape of these peaks differed in dependency on humidity but also on the mounting position of the capillary. After some time, it was clear that water droplets had been pushed through the capillary and, after coming out at the end of it, had been vaporised by the air coming next.

3.3.3.1 Description of water spikes

The humidity increase was monitored both by humidity meter and MOX sensors, but the shape was strongly differing and the MOX sensor signal was often influenced by other effects.

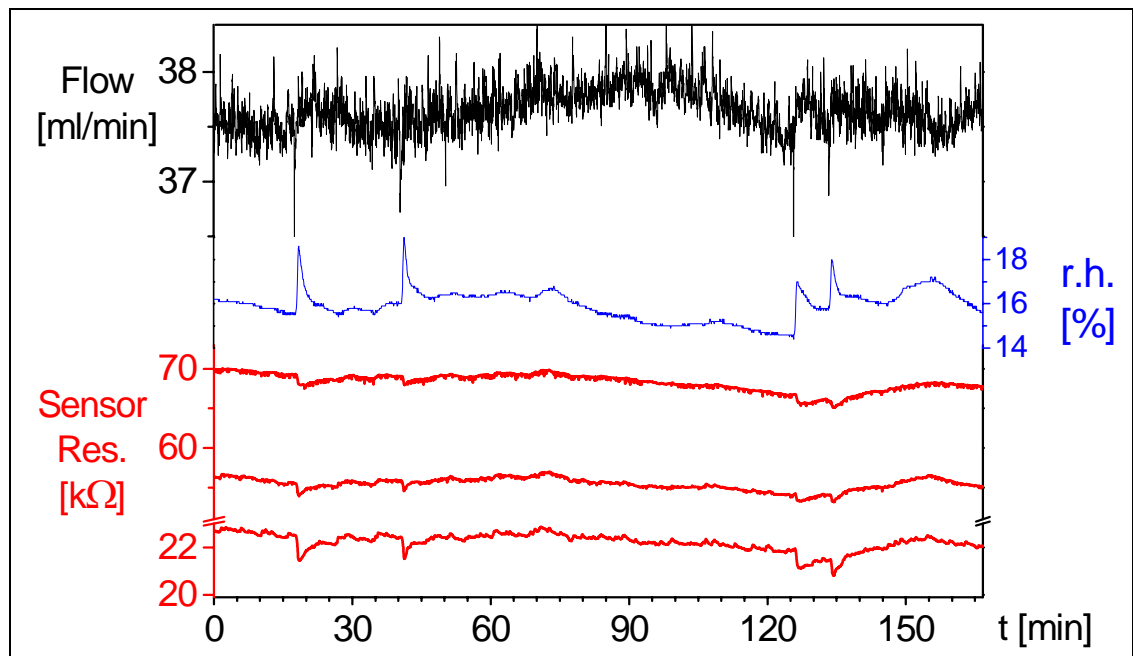


Figure 29: Typical graphs of flow, relative humidity and sensor resistance on a very humid day.

Figure 29 shows very clear peaks of the humidity signal, but the unstable baseline demonstrates that there are also other effects, which complicate the identification of the problem. This is even more valid for the sensor resistance, displayed at the bottom in a linear scale, in order to magnify the response. The result of the flow measurement, shown on the top of **Figure 29**, gives also a subtle indication of what was happening.

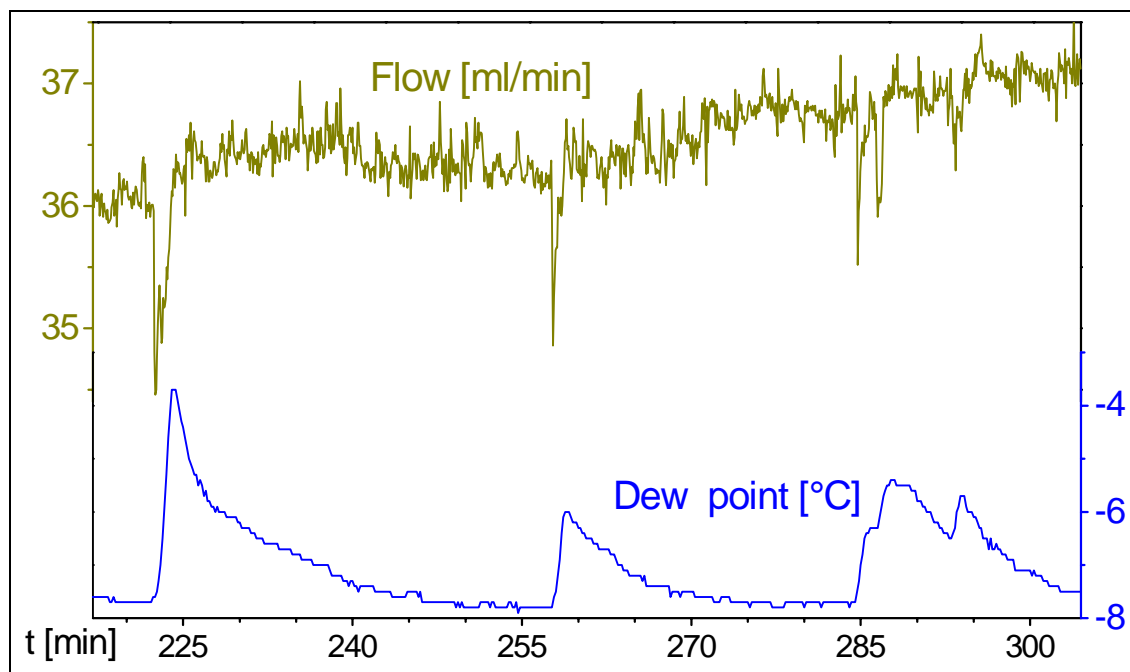


Figure 30: Magnified graphs of flow (smoothed by moving average of three values) and absolute humidity on a very humid day. A discussion is given in the text.

As already stated, the extent and appearance of the effect was strongly dependent on the mounting position of the capillary and the humidity, so, sometimes it was possible to measure isolated peaks on a stable baseline, as shown in **Figure 30** (“water spikes”). The result for the flow, as it is displayed here, was smoothed by moving average of three values. It clearly shows an abrupt decrease of flow, followed by a recovery in the range of 15-30 seconds: the pressure drop of the blocking of the capillary in the beginning of the effect is transferred through the capillary much faster than the droplet itself. The shape of the humidity peak is not that clear: one would expect a rise to an

equilibration value and a stable response until the droplet is completely vaporised because the water reservoir, the droplet at the end of the capillary, will vaporise continuously in the steady air flow until it has vanished; but perhaps surface decrease or evaporation cooling play a role here.

Figure 30 proves that the explanation for water spikes are droplets, which are pushed through the capillary, vaporise and cause responses. Of course, this was also checked by opening the fitting at the end of the capillaries at the beginning of a water spike: in accordance with the explanation given here, mostly liquid water could be found there.

The appearance of liquid water in the high pressure system of a compressor and downstream of it is well known; the draining of this condensate or perspiration water is an important requirement for the construction of systems for the production and handling of pressurised air, because the amount of condensate can be enormous and due to reactions with air pollutants like NO_x or SO_2 the pH-value can go down to four or five. An example of the calculation of the amount of water is given in 3.3.3.2.

3.3.3.2 Thermodynamic explanation

The vapour pressure of (pure) water is, like every other vapour pressure, only dependent on the temperature. It describes the tendency to vaporise and it increases with increasing temperature (This is the reason why in summer the absolute humidity is higher than in winter). The absolute humidity can be quantified by the partial pressure of water. If liquid and gaseous phase coexist in equilibrium, the partial pressure takes the value of its stable maximum, the saturation vapour pressure, which is also temperature dependent. The partial pressure, defined as the pressure in case one single gaseous component would expand alone in the whole volume, represents a concentration per volume. So, if the volume for a constant amount of a gaseous component is decreased (e. g. by compression), the partial pressure increases until it reaches saturation vapour pressure. If compressed even more, condensation starts and the

gaseous component starts to form a liquid phase. In principle, it does not matter whether the gaseous phase solely consists of the respective gaseous component or other gaseous components are present. The latter case is represented, for example, by water vapour in air and the reason for the appearance of liquid water in the compressor is exactly the scenario described above.

Figure 31 gives a simplified overview of the alterations of pressure, temperature, relative and absolute humidity of the air when passing through the compressor and the capillary. The air flow in the schematic is divided in four parts, namely ambient, compressing unit, cooler and capillary, with its different characteristic influences. The figures given in **Figure 31** represent typical empirical values as recorded with the set up shown in **Figure 20** and used for the measurements in 3.3.2. The temperature of 80 °C, after the cooler, is the maximum temperature, as guaranteed by the compressor manufacturer. The qualitative findings have general meaning. The ambient air, as it is taken in the compressor on a humid day, has a pressure of approximately one bar, a certain temperature and a relative humidity of more than 20 %, for example 50 %. The compression in the compressing unit goes in parallel with an inevitable warming due to friction and the (adiabatic) compression itself. The warming and the compression have opposite effects, if regarded separately: the warming increases the saturation vapour pressure, so the relative humidity would decrease. The compression decreases the volume and increases the partial pressure. In case of a compression to seven bar overpressure (corresponding to eight bar total pressure), the partial pressure multiplies roughly by eight and this effect overbalances the increase of the saturation vapour pressure by far. So, the partial pressure reaches saturation vapour pressure, in **Figure 31 c.)** given by the point where relative humidity reaches 100 %. Further compression leads to condensation, shown in **Figure 31 d.)** as a decrease of absolute humidity concerning the gaseous phase. After compression the mixture of air and condensate is cooled, which leads to

further condensation due to the decrease of the saturation vapour pressure.

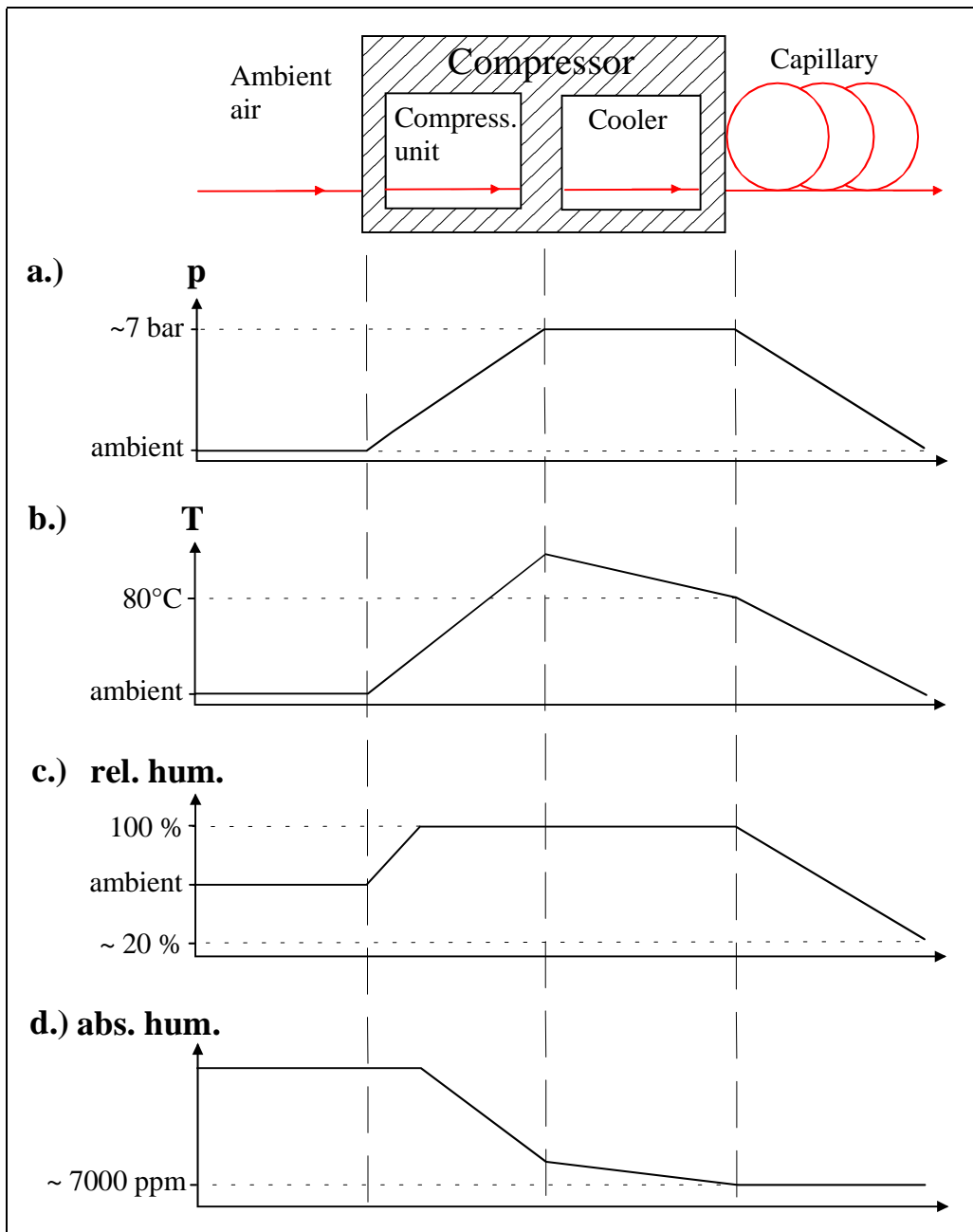


Figure 31: Behaviour of pressure, temperature and humidity of humid ambient air when compressed by a compressor and expanded via capillary (Only the gaseous part is expanded). The numerical values are according to the set up and the conditions described in this chapter; the qualitative information can be applied generally. The absolute humidity here is a concentration per gaseous amount of substance, not per volume.

If the gaseous part is expanded, for example via the capillary, the pressure goes down to ambient pressure and the partial pressure accordingly decreases and it falls far below saturation vapour pressure, so the decrease of saturation vapour pressure due to the decreasing temperature has no effect. The absolute humidity is completely unaffected because the composition of the expanded gas mixture does not change. The relative humidity whereas goes from 100 % (related to 80 °C and 7 bar) to approximately 20 % (related to ambient pressure and ambient temperature, which were also the starting conditions). The water corresponding to the difference of 30 % of the relative humidity is the water that appears in the compressor as a liquid phase.

3.3.3.3 Measures against water spikes

In order to give an idea about the amount of water an example is given:

50 % r. h. (30 °C) correspond to $\sim 15 \text{ g/m}^3$ and

20 % r. h. (30 °C) correspond to $\sim 6 \text{ g/m}^3$.

Consequently, there are 9 g water condensate per cubic meter air; for a flow of $\sim 1 \text{ m}^3/\text{min}$, this means 540 g water condensate in the compressor every hour. In the case of 80 % relative humidity, which still represents a realistic scenario, the amount is doubled to more than one kilogram, corresponding to more than one litre. These figures clearly prove the need for an effective condensate drain, not only for the difficulties concerning an expansion via capillary but also for usual filtering lines and the final device using the pressurised air. Accordingly different solutions for this purpose are on the market. The industrial solutions which are applied are either costly, designed for higher throughput or they also remove the oil aerosols. Our measurements proved that very simple solutions also work. Due to the small volume flow ($\sim 6 \text{ ml/min}$ at the entrance of the capillary in the high pressure region) no turbulences disturb and a simple collecting reservoir (including a drain) directly before the capillary is adequate. Even though the draining causes a small sensor signal and the ensemble has to be separated a little from the main

air stream (in order to be isolated from turbulences) this solution is appropriate: the sensor response to the draining is negligible and the dead volume of the reservoir can be minimised in order to keep on to reasonable response times.

After all measurements and the experience with the different set ups, it even seems probable that it is possible to prevent water spikes only by adequate orientation and location of the capillary entrance.

3.3.4 Results

The long term baseline measurements revealed the following effects and implied the following conclusions, concerning

Cross sensitivity:

- The humidity change is the most important influence of the ambient conditions, on both seasonal and daily basis;
- The humidity change is limited by the thermodynamic parameters in the high pressure system;
- The humidity limitation is responsible for the problem of blocking of the capillary by condensed water inside the system, but the problem can be solved;
- There is no systematic change of background contamination of the ambient air by hydrocarbons as measured by the FID on a seasonal basis;
- The change of ambient temperature on seasonal or daily basis affects the system mainly by the correlated change of ambient humidity. The second effect, the direct warming of the system is not completely clear but the impact is small and probably will be even smaller, because the most usual location for a compressor is in the basement where the effect is strongly attenuated.

Hydrocarbon sensitivity:

- Sometimes there is a systematic change of contamination by hydrocarbons as measured by the FID on a daily basis. It goes in parallel with the ambient temperature and therefore with absolute humidity. It is unclear whether the change of hydrocarbon content is caused by the ambient or by compressor conditions, even if there is more evidence for the latter;
- The hydrocarbon content of the pressurised air shows short term peaks in the range of less than one hour, recorded both by FID and MOX sensors. Sometimes these type of short term peaks are only monitored by one of the devices. As stated in 3.3.2.2, there are reasons to assume that these peaks are caused by hydrocarbons, originating from the compressor.

FID:

- Both FIDs show comparable performance. The exchange of the Testa „2001 T“ by the Testa „1230 Modul“ does not change the results when measuring the baseline contamination.

3.4 Third compressor set up

3.4.1 Set up for dosing of oil & gravimetric referencing

The third set up, as used for the investigations described in 3.4.2 to 3.4.5 was (slightly) modified twice. All three versions were similar to the one used for the baseline measurements as shown in **Figure 20**, differing mainly by the addition of a bypass of the oil separator and the cooler. The resulting schematic is given in **Figure 32**.

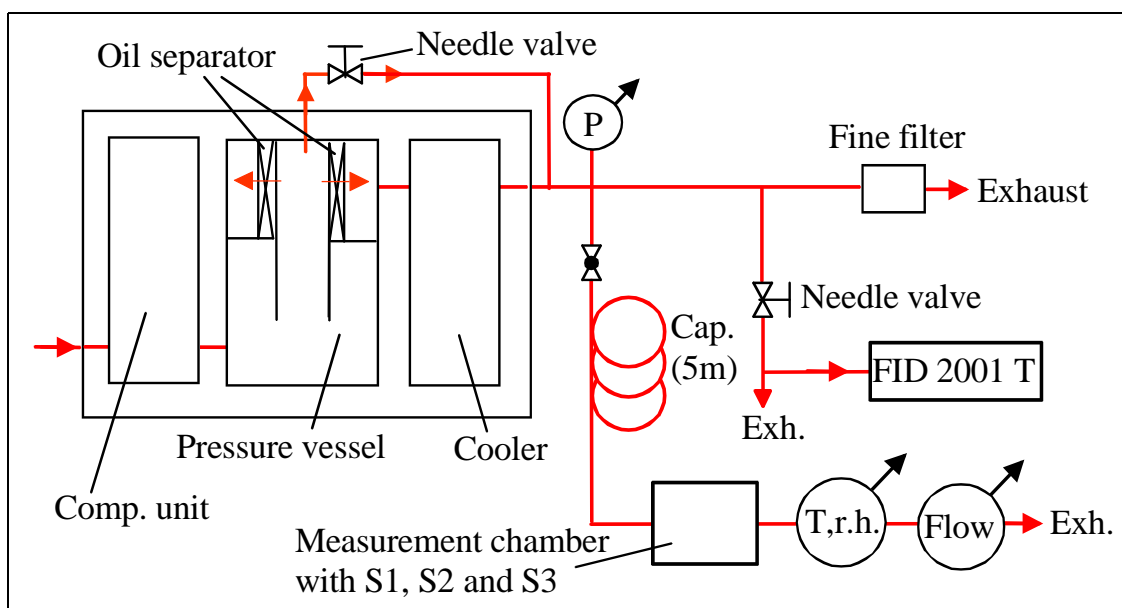


Figure 32: Schematic of the set up as used for the measurements with dosing of highly oil-contaminated air via bypass of the oil separator. The extent of dosing was controlled with a needle valve in the bypass. The tubing lengths are not proportional.

With this set up it was possible to inject air from upstream the oil separator, which was highly contaminated with oil aerosol, into the main air stream directly after the compressor. The extent of dosing could be controlled with a needle valve in the bypass but it was not possible to measure the real ratio of the flows. Accordingly, the dosing was quantified by degrees of rotation or by the number of full rotations applied to open the needle valve. The maximum opening was ~ 9.3 rotations but it should be stressed that probably even in this case the main part of the air passed the oil separator, as the diameter size of the filtered air tubing was $\frac{1}{2}$ " diameter, the double of the diameter of the bypass, and, furthermore, even a completely opened needle valve represents an obstacle for the flow. The sample point for capillary and the FID feeding were located about 1.5 m downstream the injection point, in order to enable an effective mixing.

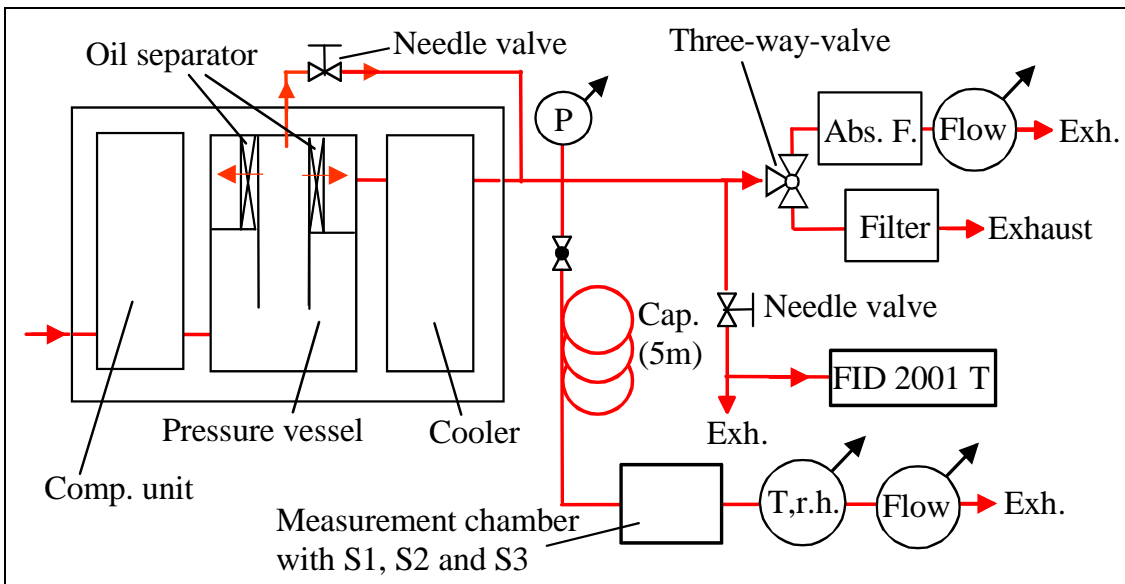


Figure 33: Schematic set up with possibilities for the dosing of highly contaminated air and gravimetric referencing with absolute filters (Abs. F.).

The measurements discussed in 3.4.2 were performed with this set up; afterwards a possibility for the gravimetric referencing with absolute filters was installed. The resulting set up is shown in **Figure 33**: with a three way valve the main air stream can be alternatively directed to the regular fine filter (built in for environmental reasons) or to the absolute filter and the subsequent flow meter. The gravimetric investigation, as already described in 1.2, collects the oil aerosols in an absolute filter. It is necessary to measure the absolute flow through the filter in order to be able to calculate the oil concentration. Due to the high flow rate and the condensed humidity in the air stream, a very robust device was chosen, namely a Bernoulli nozzle with a hydrostatical differential measurement of the pressure drop. The pressure drop can be converted into flow, V_F , with a calibration curve given by [Gil99], together with the time of exposure, T , and the difference in filter weight before and after exposure, Δm . This allows to calculate the aerosol contamination, c_{aer} , according to

$$c_{\text{aer}} = \frac{\Delta m}{V_F T}$$

The measurements revealed a discrepancy between the FID readout (in this case the Testa FID „2001 T“) and the gravimetric reference. In a next iteration, the Testa FID „1230 Modul“ (low intake rate allowing capillary expansion) was installed. In order to ensure identical sample gas, a common feeding for both FID and the sensor chamber was realised by two capillaries in parallel with subsequent mixing. This part of the set up is already shown in **Figure 21**, not shown there is the additional line for the absolute filter, which is shown in **Figure 33**.

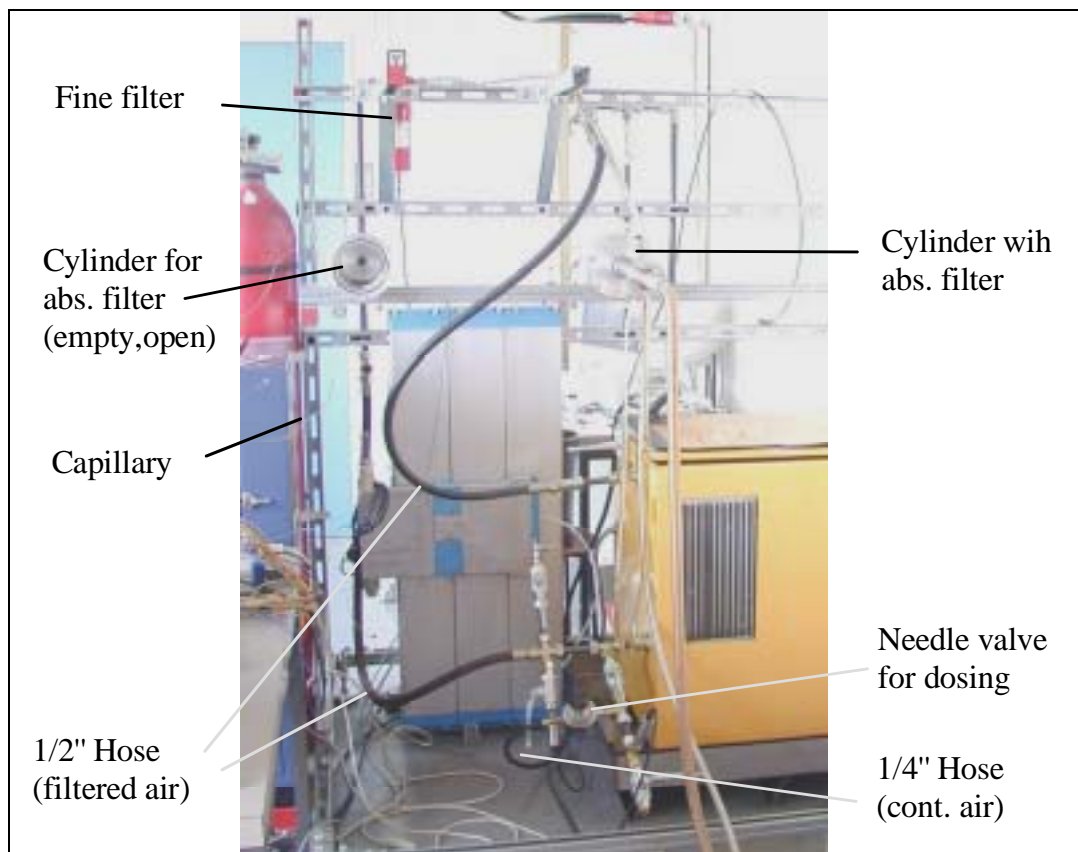


Figure 34: Photograph of the set up with a possibility for dosing of highly contaminated air and gravimetric referencing.

This set up was also used for the parallel investigation of residual oil content with FID, MOX sensors and the gravimetric method, but the discrepancy remained. For this reason, the FID measurements were abandoned, except for

the investigation of the baseline of the hydrocarbon content, where they were continued in order to obtain a complete data set. So, the set up with the Testa „1230 Modul“ did not provide new, results and therefore only one of the two set ups with parallel FID measurements and gravimetric referencing is given as a schematic in **Figure 33**, which shows the set up with the Testa „2001 T“.

In order to give an impression of the dimensions and the arrangement, **Figure 34** shows the compressor (upper part , right), the hoses, the tubing and the containers for fine and absolute filters.

3.4.2 Measurements with dosing of oil

The measurements with dosing of oil were performed in parallel to the second half of the baseline measurements and started with small dosings. **Figure 35** shows the measurement with the smallest dosing that was applied within the investigations presented in this work. The periods of dosing are marked with striped rectangles because the responses do not give a clear indication in case of 100 ° and 200 ° opening of the valve (left side of **Figure 35**). The scale of the sensor resistance is linear in order to point out the sensor response. The FID does not show a response to an opening of 100 ° or 200 ° and no change of humidity is recorded. This already proves the high sensitivity of the MOX sensors, and again, like already proven in 3.2.3, sensor S 2 shows a high response and the highest sensor signal towards an increased oil content.

The subsequent peak, also visible in the FID signal, originates from a short (< two minutes) shut off of the compressor. This reproducible effect was already discussed in 3.3.2.1.

After some time needed to reach equilibrium, the dosing was increased to 720 °, (two full rotations) and applied three times with intermediate recovery. The sensor responses are systematic and reproducible, in contrast to the FID signal. The FID response varies from 0-0.1 ppm readout, but it has to be stressed, that the three times dosing of two rotations did very probably not affect in the same way all three times. This is also indicated by the MOX

sensors, not only by the different maximum responses, but also in the clearly differing shapes of the three peaks. The coherence between the three sensors indicate that the difference is in the sample they are exposed to and that the different shapes obtained by the repetitions of the dosing are no sensor artefacts. The pressure in the system is not displayed in **Figure 35**, due to incomplete data, but as far as it was recorded it does not show a change, except, of course, for the shut off of the compressor.

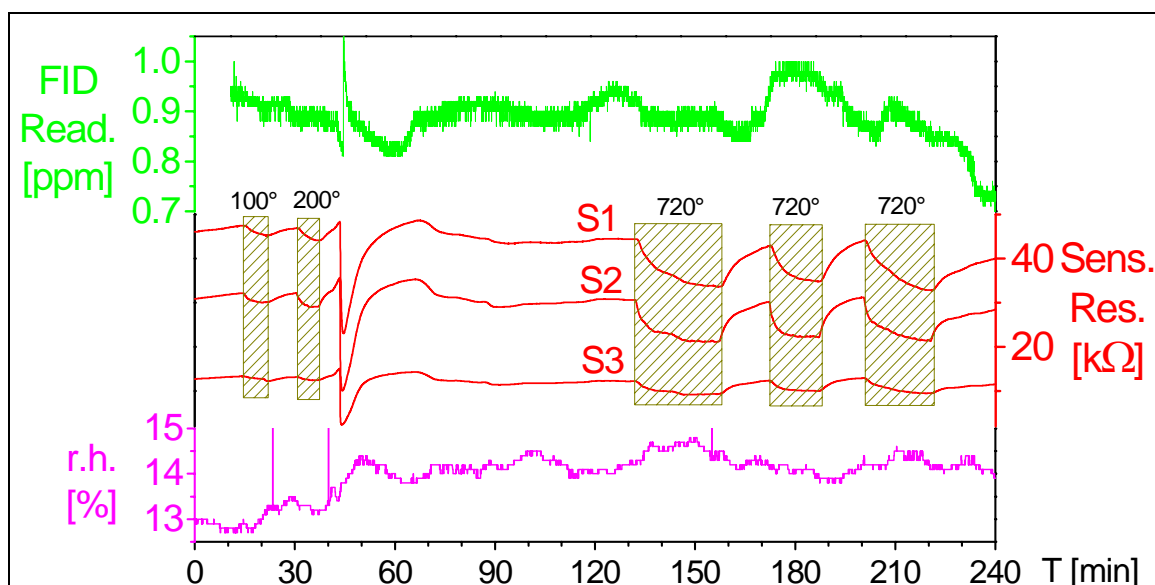


Figure 35: *Graphs of the first measurement with dosing of highly contaminated air via bypass. The peak between ~40 and 50 minutes resulted from a short shut off (< two minutes) of the compressor. In this diagram, the opening of the needle valve is indicated in degrees.*

It is not clear why the FID did not show a stable baseline, but these effects were already known from the baseline measurements and are reported in 3.3.2.2. The dosing itself can be excluded to have such a direct effect, as the measurement one day later, reported in **Figure 36**, does not show this problem. **Figure 36** shows the graphs resulting from the successive dosing of two, three, four and five full rotations of the needle valve. There, the peak shapes of the different dosings are more comparable and the FID does show a

systematic and reproducible response, which allows a numerical evaluation.

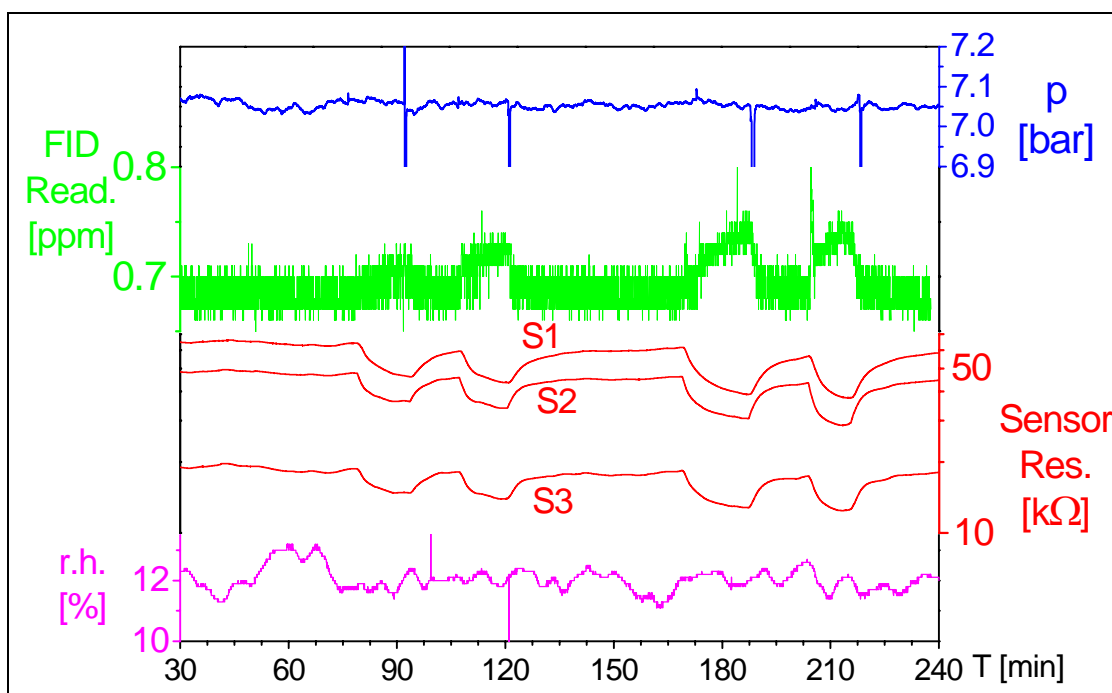


Figure 36: Graphs of a measurement with successive dosing of two, three, four and five rotations of the needle valve and intermediate baseline recovery.

It can be seen that the pressure systematically shows a small upward spike, when starting the dosing, and a bigger spike downward, when the dosing stops. This artefact of dosing could be regularly observed, but it did not lead to any other effects.

As expected, humidity is not influenced by the dosing, which was one motivation for the investigations presented in this chapter: the sensor responses can be correlated only to the change of the content of hydrocarbons, originating from changing oil aerosol content. The unsystematic alterations in the range of two percent relative humidity affect the sensor resistance slightly but they do not disturb the response to oil .

The presentation of measurements with successive dosing of oil is completed by **Figure 37**, giving the graphs for the dosing of five (twice), seven, nine and 9.3 rotations of the needle valve. The latter represents the maximum dosing

possible with this set up.

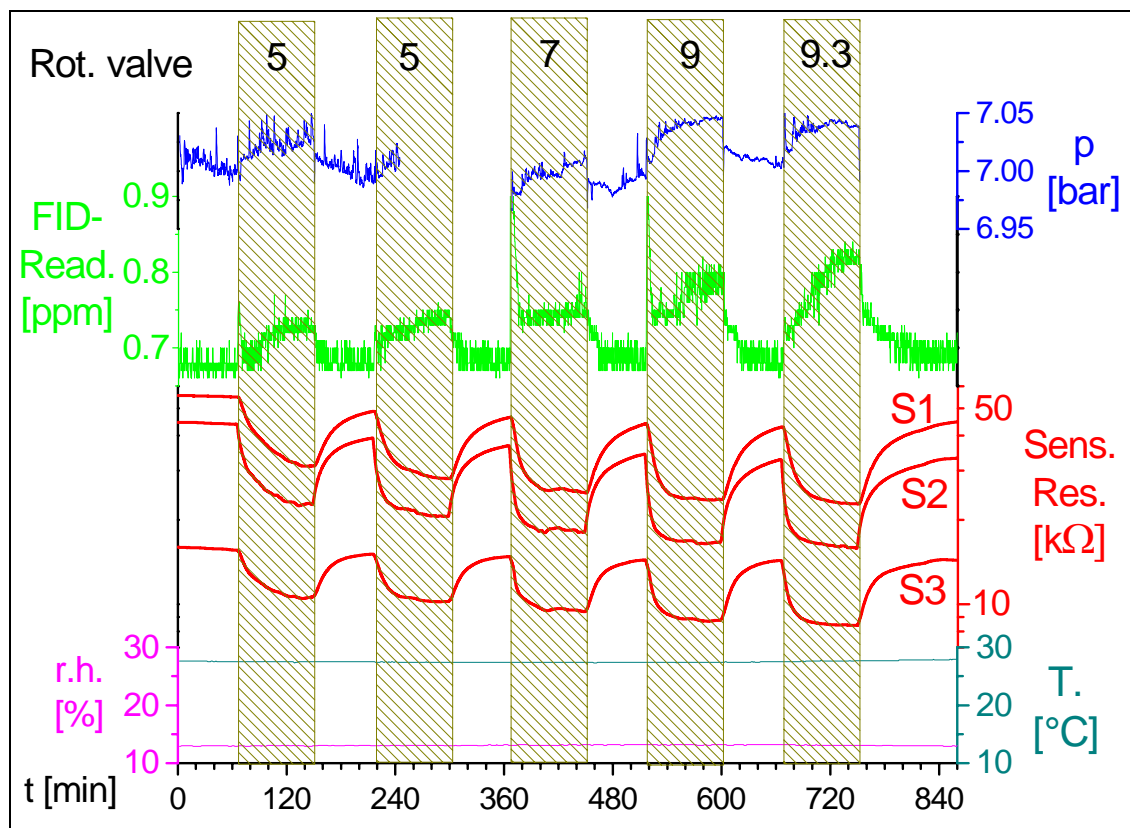


Figure 37: Graphs of a measurement with increasing dosings up to the maximum exposure to oil aerosols with the set up (9.3 rotations of the needle valve). A discussion is given in the text.

The pressure graph also shows spikes like in **Figure 36** (hidden by the rectangles indicating the periods of exposure); besides that, an additional upward shift due to dosing can be observed, increasing with the dosing. The bypass of the oil separator is also a bypass in terms of pressure reduction, due to the flow obstacle represented by the oil separator.

Again, both the FID and the MOX sensors show a systematic and reproducible response, increasing in parallel with the extent of dosing, and, again, the MOX sensor S 2 shows the highest sensitivity. The temperature and humidity of the sampled air stay constant and the MOX sensor response can be only correlated with the change of hydrocarbon content.

Altogether nearly 30 dosings have been realised with the FID as a reference. This was done in order to obtain a kind of calibration curve. The situation was complicated by the cross sensitivity to water because a lot of measurements with dosing of oil suffered from strong interferences with changes of water content. **Figure 38** gives an example of two typical problems:

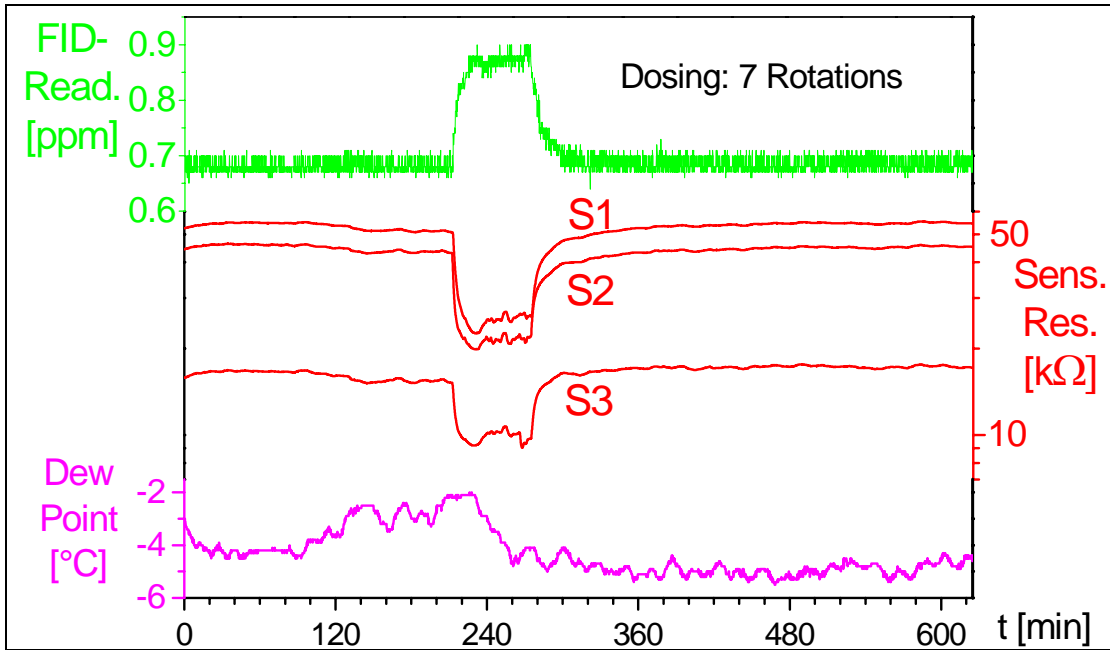


Figure 38: Graphs of a measurement with strong humidity interference. The sensor response to the dosing is superposed by a humidity response.

- The sensor resistance is continuously changing as a response to the continuously changing water content. This effect is stronger when the oil content of the sample is higher. So, the sensor resistance, especially for oil exposure has to be averaged or fitted. **Figure 38** gives an impression of the extent of humidity interference and the difficulties to define a representative time window for averaging the sensor resistance.
- The absolute humidity significantly decreases while exposure to high oil content. This causes a notable sensor response, which overlaps over the response to oil. If the subsequent recovery (of the oil signal) completely

happens under stable humidity it is possible to work with this baseline value, unfortunately this was not the most common case.

In spite of these problems, 24 out of 28 measurements with dosing were evaluated and could be used for the investigation of the correlation between the sensor signal as one parameter and the FID response or the degree of opening of the needle valve as the second. **Figure 39 a.) – c.)** show the correlation of the sensor signals from sensors S 1 – S 3 and the opening of the valve, **Figure 39 d.)** show the correlation of S 1 and the FID response. The value displayed on the y-axis is the sensor signals minus 1: reducing analytes decrease the sensor resistance and therefore the sensor signal (defined as R_0/R_{Exp}) is always bigger or equal to one, so no dosing (zero rotation on the x-axis) causes a sensor signal of one and in order to get a linear fit going through origin the scaling on the y-axis was chosen to be signal minus one.

As it can be seen, the FID response, defined as the difference of the FID readout with and without exposure, does not show a reasonable correlation with the sensor signal of S 1. This is the same for S 2 and S 3 (not shown). The correlation between rotations of opening of the valve and FID response (not shown) is a little better, because the different sample feeding lines of MOX sensor and FID do not contribute to the irreproducible and disturbing effects. Anyhow, the deviation is still very high due to a rather low day to day reproducibility. This proves that the poor correlation between the responses from MOX sensors and FID when exposed to higher oil content mainly originates from the FID, which is not very appropriate for this application. The small FID response (**Figure 39 d.)** x-axis) additionally proves a lack of sensitivity towards the target analytes.

It is obvious that the correlation between the sensor signals and the opening of the valve is much better. On the other hand, the scattering of the correlation with the extent of opening of the valve (**Figure 39 a.) – c.)**) is also high, but in opposition to the FID response, here the tendency is clear and a proportionality is unambiguous.

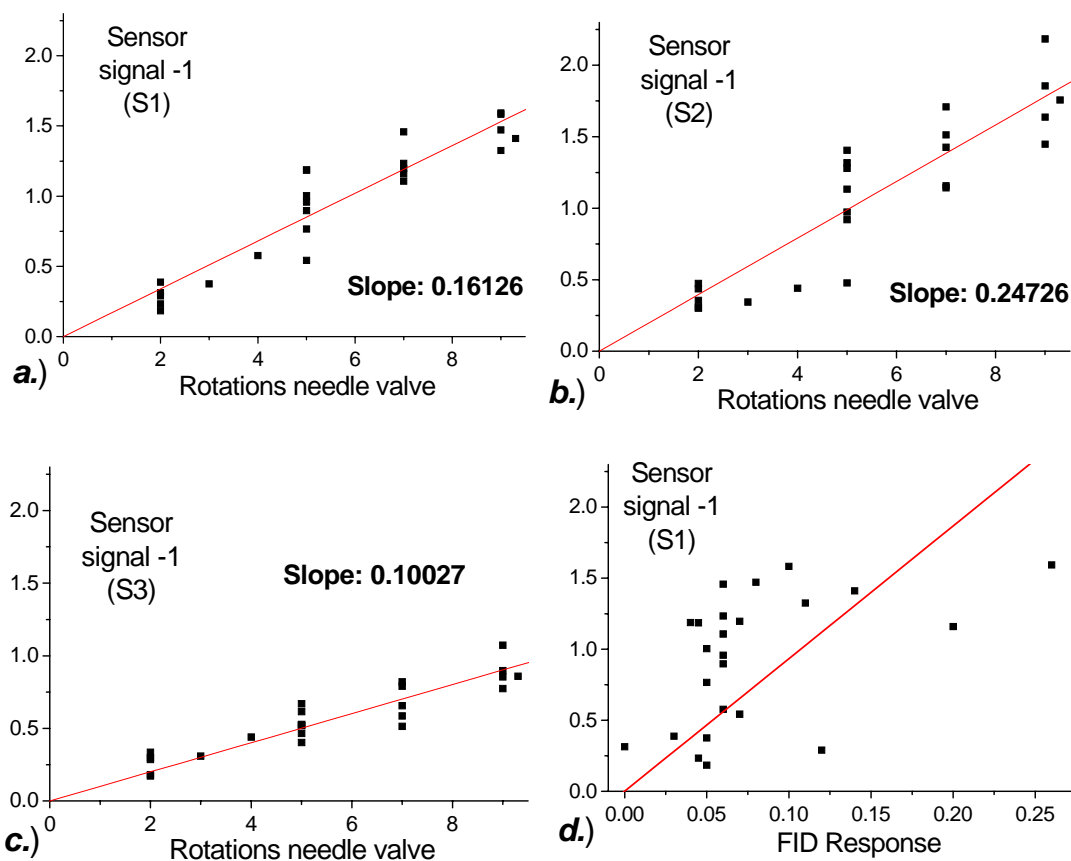


Figure 39: Correlation between the sensor signals and **a.) – c.):** rotations of the needle valve, **d.):** FID response.

The linear fit confirms the interpretation of the measurements presented in 3.2.3 and 3.3.4 concerning the sensitivity of the three MOX sensors: sensor S 2 shows the highest responses, followed by S 1 and S 3. Even if the scaling on the x-axis does not allow to give figures in terms of a concentration based sensitivity, it enables a quantitative comparison between the three sensors.

One more observation, made while performing the measurements with dosing, has to be mentioned: from time to time it was necessary to open the fitting at the end of the capillary and sometimes a very small amount of liquid oil could be observed there. It was much less than a droplet, hardly visible, but it clearly could be felt when touched with the fingertips. It is known that often wallflow appears in systems for pressurised air, especially in regions with increased oil

aerosol content. For the set up discussed in this thesis this was also the case, as an oil film could be observed when dismounting and remounting the system. Some exposures to high oil aerosol content lasted very long and therefore, it was not surprising to finally find the wallflow also at the end of the capillary. Surprisingly, these residuals did not disturb the measurements, which indicates that they do not vaporise and saturate the air in any case, with or without dosing. As a practical solution to guarantee a successful long-lasting application of a residual oil indicator on the basis of the concept presented in this work, a small fleece (5 xc 5 mm) of felt or glass fiber was found appropriate to adsorb enough oil to guarantee a two years lifetime.

3.4.3 Results of measurements with dosing of oil

The measurements with dosing of highly contaminated air via bypass of the oil separator enabled the change of oil aerosol content independent from all other parameters, especially independent from water content. By this, it should permit to investigate the response of the MOX sensors to an increased oil aerosol content vaporised by capillary expansion without any cross sensitivities.

The measurements provided the following results:

- The set up performed as intended. The addition of air from the bypass solely increases the oil aerosol content, the increase is recorded both by the FID and the MOX sensors. Humidity stays constant, the change of pressure, observed at high dosings, and the change of flow as a consequence is negligible.
- Air with increased oil aerosol content, expanded via the capillary, reproducibly leads to responses of the MOX sensors, no poisoning is observed and no oil film appears in the measurement chambers. The only liquid oil downstream the capillary is a small amount ($\ll 1 \mu\text{l}$) directly at the end of the capillary, resulting from wallflow. This does not disturb the measurement, as it was empirically proven.

- Tin dioxide based MOX sensors show a notable response when the concentration of oil aerosol increases. The sensor S 2 shows the highest response, the sensor signals of S 1 and S 3 are 65 %, respectively 40 % of the signal of S 1.
- The magnitude of the responses and the signals of the MOX sensors are clearly correlated with the degree of opening of the needle valve. The data allows a linear fit, which was not foreseeable for different reasons: the relation flow ratio / rotations of the valve was unclear, the extent of vaporisation may be limited due to saturation,
- The reproducibility of the relation MOX sensor response with the dosing is moderate. It is very probable that several reasons contribute to this inaccuracy.
- The FID is not an appropriate (quantitative) reference technique for the content of oil aerosols vaporised by capillary expansion. It reproducibly shows a response to a notably increased oil content, but the effect is not reproducible.
- The dosing of highly contaminated air does not lead to continuous long term contamination of the system. The recovery times are long, but there was no systematic baseline change even after heavy exposure. This does not concern the discontinuous effects on the gravimetric reference method discussed in the following two chapters 3.4.4 and 3.4.5.

3.4.4 Measurements with gravimetric referencing

During the investigations it became more and more clear, that it would be necessary to measure the oil aerosol content with the gravimetric method by using absolute filters. The FID did not provide reliable data and even if the FID would have done so, it would had been essential to calibrate the FID readout (and the sensor signals) according to concentration specifications

investigated with an accepted method. In the field of residual oil content, which uses mass of oil per volume of air in mg/m^3 (utilised in the specification of quality of pressurised air given in DIN ISO 8573-1), the oldest and still the most common method of its investigation is the gravimetric one and it is clear that a new concept has to meet this current benchmark.

The method is described in 1.2, the set up is shown and explained in 3.4.1. It was also mentioned that the measurements with gravimetric reference took a long time. For the gravimetric reference of the baseline contamination this was due to the long time of exposure to the sampled air (five - six hours): the contamination is low, so a lot of air has to be filtered to achieve a reliable increase of weight of the filter. For the measurements with dosing, the time need was due to the concept: the previous measurements with dosing showed that it took some time until the responses of MOX sensors and FID reached a stable value and it was clear that at least a part of this inertia is due to the system and would also effect the gravimetric measurement. So, the air stream was not switched to the absolute filter before the MOX sensor resistance had reached a plateau, in order to obtain a gravimetric value that can be correlated to a stable numerical value of sensor response; the gravimetric result represents the mean over the whole time of exposure and therefore it can only be correlated with an equilibrium sensor response. So, due to the long exposure times it was not possible to gravimetrically measure the baseline value before a gravimetrically referenced dosing. In general, no more than one gravimetric measurement was performed in a day.

The first measurement with dosing and gravimetric investigation was performed with nine rotations of the valve. The oil aerosol contamination was gravimetrically determined to be $139 \text{ mg}/\text{m}^3$; the FID response due to dosing was 0.25 ppm, which means $0.47 \text{ mg}/\text{m}^3$, according to the calculation given in 2.3.2. It was expected to have a certain deviation but a factor of roughly 300 indicates a general problem. After a few more measurements giving similar results, the FID measurements for calibration purpose had been abandoned. A

detailed discussion concerning possible reasons for this discrepancy is given in 2.3.3.

It was not possible to investigate the reason for this, as it was not the aim of this work, but it was clear that a correlation of the sensor signals with the parameter of interest was only possible with a parallel gravimetric investigation. Especially the sensor response to an oil aerosol content of 30 mg/m^3 was important, because this value represents the limit of acceptance for the performance of an oil separator.

A typical result, concerning the transient devices, is shown in **Figure 40**.

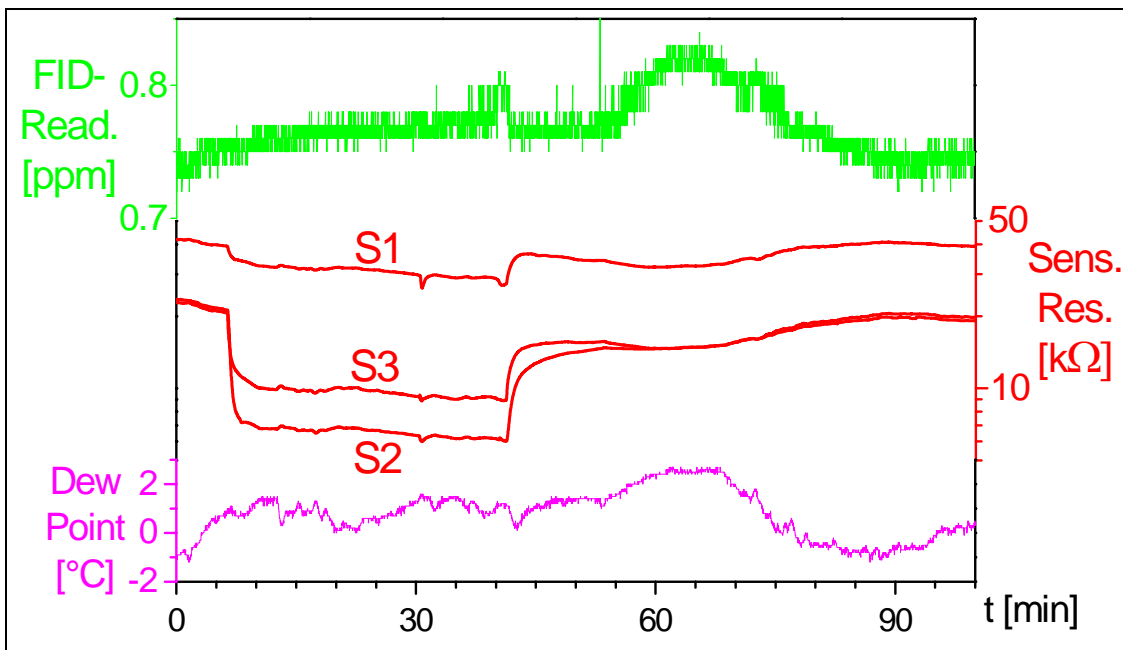


Figure 40: Typical graphs of a measurement with dosing (two rotations of the valve) and gravimetric investigation of the oil aerosol content.

The sensor response to the opening of two rotations of the needle valve is clearly visible, 25 minutes later the main part of the air stream was directed from the fine filter to the absolute filter for the gravimetric investigation. This regularly caused a small spike of the MOX sensors, as it can be seen in **Figure 40**. The size of this spike differed and sometimes it was also present in the FID or humidity signal. Switching the whole air stream back to the fine filter also caused a spike but often this one was covered by the response to the end

of the dosing.

The pressure inside the system was kept constant throughout the whole measurement by tuning the volume flows adequately.

Table 5 lists the results of the measurements with gravimetric reference. The lowest five rows, with dosing of zero rotations, represent baseline measurements. It is clear that there is no sensor response on this and therefore the sensor signal is one, due to the definition R_0/R_{Exp} . The respective gravimetrically investigated oil aerosol content differs between 0.3 and 4.3 mg/m³. The top value of 4.3 was recorded directly one day after the measurement with dosing of nine rotations (correlated to 139 mg/m³ !); the baseline measurement started 20 hours after the end of exposure. This indicates that the contamination of the system with liquid oil lasts longer than this, as this value represents a clear outlier, all other baseline values are lower than 50 % of the baseline value after this extreme exposure. It has to be mentioned that the MOX sensor baseline before and after the heavy exposure, as well as on the next day, without dosing, does not differ much and furthermore the MOX sensor recovery after the heavy exposure is complete. This proves that the memory effect, causing the high gravimetric value here and a general problem concerning reproducibility, as reported later, is related to liquid oil and, probably, especially to wallflow. The oil aerosol, expanded by the capillary mainly causes the sensor response, wallflow is probably contributing less, which is in contrast to what happens for the absolute filter method and may explain the differences of the impact of the memory effect.

The other baseline values are in accordance to the specification of a residual oil content of less than 3 mg/m³ downstream a new oil separator, even if the relative deviation is still high. This random deviation also indicates an unsystematic memory effect based on liquid oil in the system: the air was doubtlessly exchanged and the performance of the oil separator should not change that fast and in both directions. The MOX sensors do not report this deviation, which also indicates that the origin of this memory effect is liquid

oil, very probably wallflow, and not oil aerosol.

Degree of dosing [rot. valve]	Oil aerosol content (gr. inv.) [mg/m ³]	Sensor signal S 1	Sensor signal S 2	Sensor signal S 3
9	139.2	8.2	19.9	3.1
2	112.7	2.3	3.6	1.4
1	74.7	3.6	9.2	2.3
1	42.6	4.1	5.4	2.2
1	38.4	1.5	1.4	1.1
1	35.3	1.5	2.0	1.2
1	23.4	1.5	3.4	1.0
0	4.3	1.0	1.0	1.0
0	1.9	1.0	1.0	1.0
0	1.3	1.0	1.0	1.0
0	0.7	1.0	1.0	1.0
0	0.3	1.0	1.0	1.0

Table 5: Numerical results of the gravimetric investigations. Without dosing no sensor response was recorded and so the sensor signal is one due to the definition of R_0/R_{exp} .

It was already stated that the whole system of tubing, hoses, filters, valves and sample feeding lines was rather large and provided dead volumes and blind holes that can function as a reservoir and, afterwards resend liquid oil in the air stream. It seems more reasonable to blame wallflow for this effect, because aerosols in the gaseous phase need much more space, are more mobile and probably will not stay that long in the system.

The results for the dosing of one rotation show also big deviations for both the gravimetric method and for the sensor signals. The measurements with more than one rotation were not repeated as it became clear that this is far beyond the range of interest. In **Table 5**, it is easy to see that there is no clear

correlation between the sensor signals and the numbers of rotations, so no evaluation in this respect is given here.

A visualisation of the correlations between the sensor signals and the gravimetrically investigated aerosol content is given in **Figure 41**. On the ordinate the sensor signal minus one is displayed in order to enable a linear fit with zero crossing. Again, sensor S 2 shows the largest response, followed by S 1 and S 3. It is also visible that the deviation is high, but the patterns of some deviations are similar, e. g. the measurement point with $\sim 112 \text{ mg/m}^3$ is an extreme outlier at the lower limit in terms of sensor response for all three sensors. This is a strong hint that rather the gravimetric investigation is an outlier at the upper limit, again probably not caused by oil aerosols, but by wallflow or memory effects.

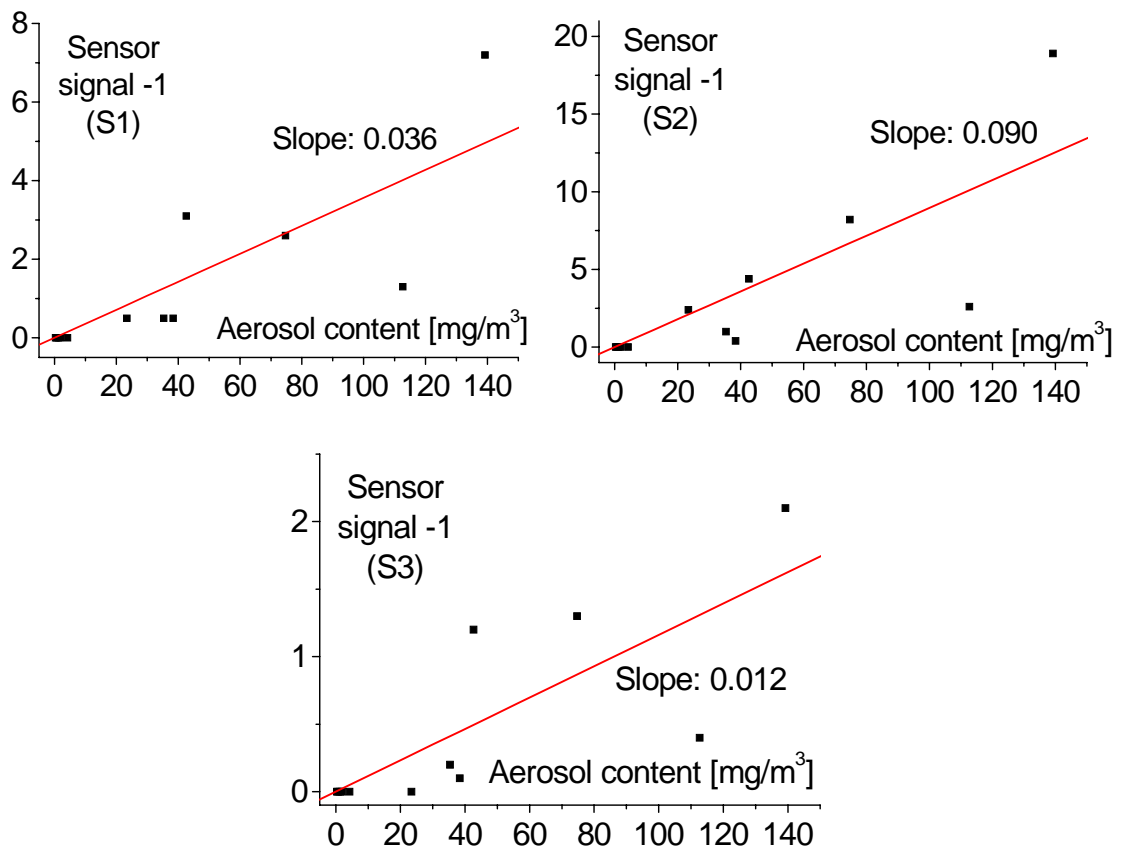


Figure 41: Correlation of gravimetrically investigated aerosol content and sensor signals minus one. A linear fit with zero crossing was applied.

The reason for the deviation (memory effect) is mentioned above in the presentation of the gravimetric referencing with dosing, but here the reproducibility problem of the dosing is an additional effect of unknown impact. Especially the memory effect of the system leaves space for optimisation of the set up and will be discussed in chapter 4.3.

The parameter underlying the ordinates value of **Figure 41**, the sensor signal (R_0/R_{Exp}), is a relative parameter which is affected by several factors. This means, it is also affected by a change of the baseline value R_0 (e. g. due to extreme humidity values) in the case that the absolute sensor response is constant. Furthermore, the absolute sensor response can also be different at different humidities; both explanations can be excluded in the case of the measurement with 112.7 mg/m^3 , as this is the measurement shown in **Figure 40** with a dew point between -2 and $2 \text{ }^\circ\text{C}$, which is a common value. Consequently, it is most probable that this data point represents an outlier of the gravimetric reference.

In contrast to **Figure 41**, the ordinates in **Figure 42** display absolute values; for reasons of clarity the sensor conductivity is displayed and not the resistance, as usual. The first difference is striking: the slope of the graph of sensor S 3 is close to zero and negative, the deviation is significantly higher than in case of S 1 and S 2. This proves that the influence of other parameters besides the gravimetrically investigated aerosol content, as displayed on the x-axis, is more important for the sensor resistance of S 3 than the oil content. This result is in accordance to the correlation factors for S 3, given in **Table 4**: S 3 has the lowest correlation to the FID reading and the best correlation to humidity when compared to S 1 and S 2.

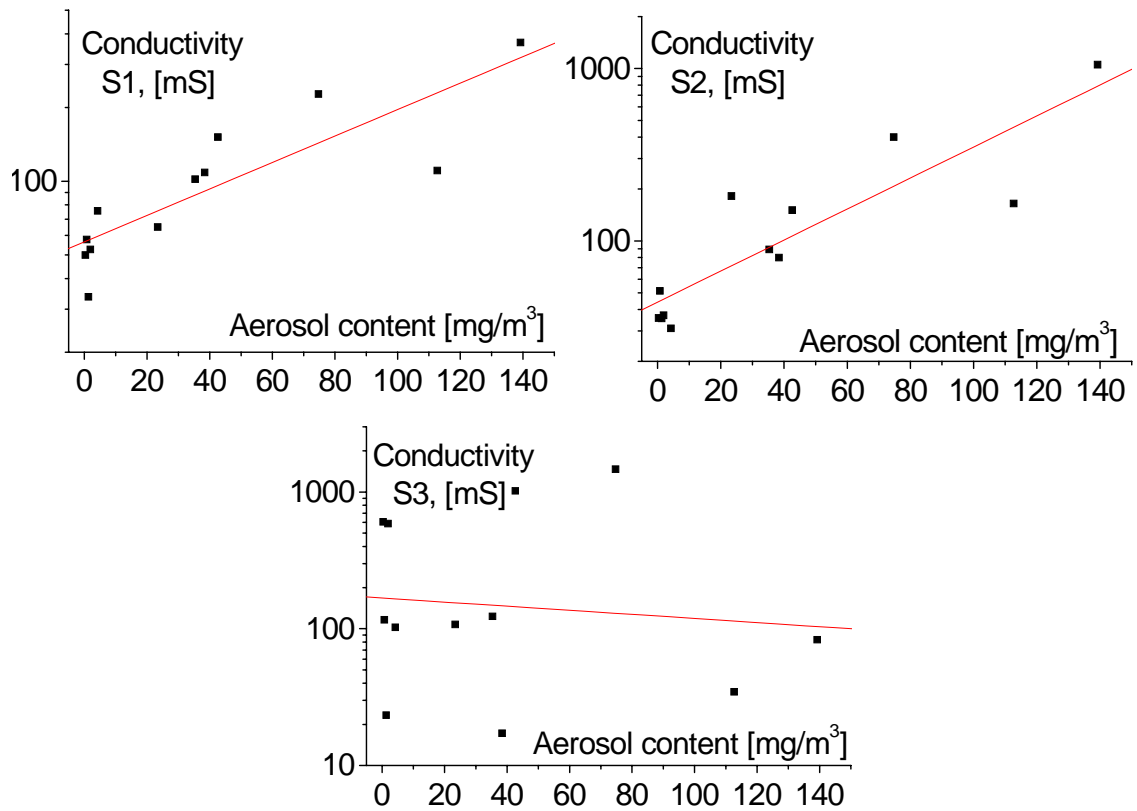


Figure 42: Correlation of gravimetrically investigated aerosol content and sensor conductivity (in mS). The respective trends are visualised by a linear fit.

Of course, the sensor results (y-axis in **Figure 42**) without dosing ($< 10 \text{ mg/m}^3$) differ, in contrast to **Figure 41**. These variations represent changes of baseline values, as discussed in 3.3.2, and they have to be regarded separately from the sensor responses to increased oil content. While **Figure 41** reports the signals corresponding to oil vapours and characterises the ability of the respective sensor to deliver a signal towards increased oil content, **Figure 42** takes also the selectivity into account: the sensor response must not be masked by interferences in order to really detect increased oil contents, for example, by means of a simple threshold value of sensor resistance. It is easy to see that S 3 is not appropriate for this purpose because the oil content does not significantly affect the sensor resistance. S 1 would have failed in one case, where the resistance with dosing was lower than without. S 2 shows a gap between all (gravimetrically referenced) measurements with and without

dosing. This property is displayed more clearly in **Figure 43**. It linearly shows sensor resistances for the gravimetrically referenced measurements with and without dosing and the baseline resistances before dosing (in the graph *n. r.*: not referenced due to time reasons). The arrows in the graph show the change of sensor resistance due to dosing, but more important is the fact that there is a clear gap of nearly ten k Ω between all measurements with dosing and all measurements without dosing.

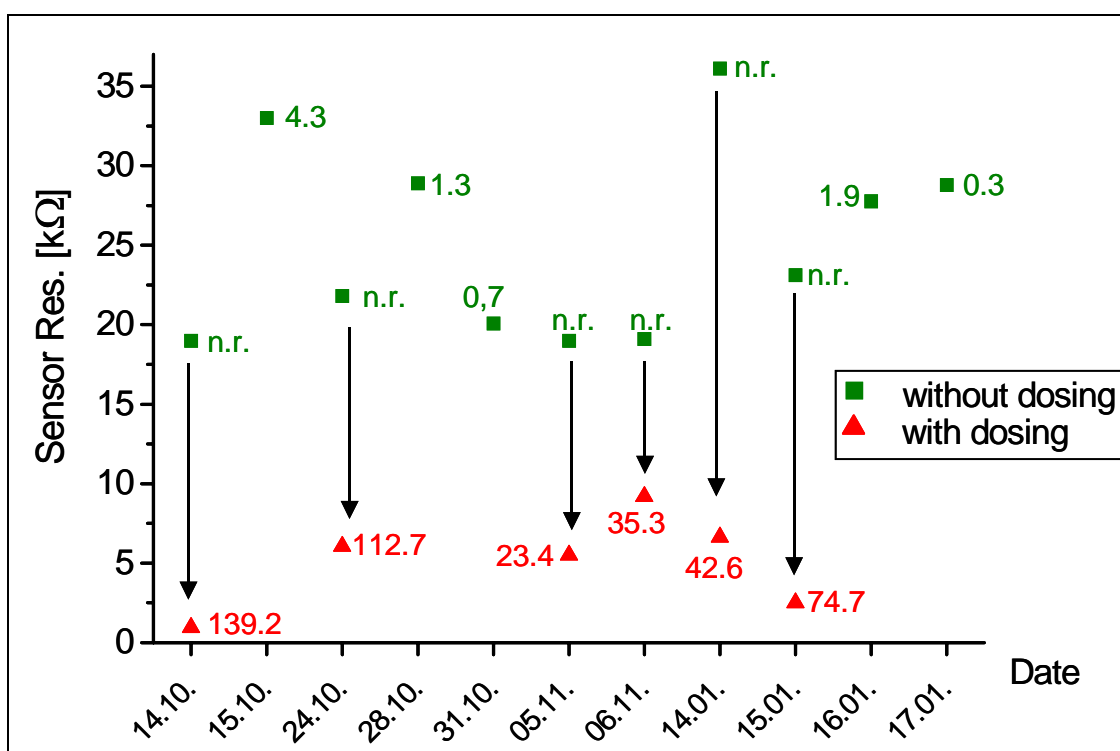


Figure 43: Visualisation of the absolute sensor response of S 2 due to dosing and gravimetrically referenced baseline resistances. The baseline before dosing was not gravimetrically referenced (*n. r.* in the graph).

3.4.5 Results of gravimetric referencing

The measurements with gravimetric referencing and / or with dosing of highly contaminated air provided the following results and preliminary conclusions:

- The FID is no appropriate reference analytics for this application (low concentrations of oil vapours produced by the expansion of oil aerosols in high pressurised air by a capillary). The FID results differ from the measurements performed with accepted methods by a factor of up to 300, which is too high to be explained with an extraordinary response factor.
- The measurement of oil aerosol content with capillary expansion and MOX sensors on the one hand and with the established method with absolute filters on the other hand do not provide fully coherent results, but both methods in accordance provide results that enable a clear discrimination between cases with dosing of oil and without. In case of the MOX sensor S 2 the discrimination is made possible by a significant gap of nearly ten k Ω concerning the absolute resistance. For S 1 and S 3 no discrimination based alone on absolute resistance is possible.
- The dosing of oil reproducibly leads to a sensor response. The resulting sensor signal (R_0/R_{Exp}) is moderately correlated with the parallel reference measurements performed by using absolute filters.
- The sensor conductance, respectively the resistance, correlates with the parallel reference measurements, both for measurements with and without dosing.
- The dosing of oil from upstream the oil separator to the main air stream is not reproducible when one speaks about the increase of oil the content, as measured with MOX sensors or with the established method with absolute filters. This is very probably due to memory effects due to the large set up, as outlined in **Figure 33**.
- The general lack of exact reproducibility, observed both with and without dosing, is very probably caused by memory effects, which are based on the remaining liquid oil in the system, which could be observed. MOX sensors and absolute filters differently respond to this irreproducibility. This can be explained by the different working principles of the devices.

4 Conclusion

4.1 Proof of Feasibility

As it was stated in 1.3, the proof of feasibility of the new concept to monitor residual oil aerosol content in pressurised air, as introduced within this work, can be divided in three requirements that have been met, in order to prove the overall concept:

- Sufficient vaporisation
- Sensitive gas sensor
- Selective gas sensor (Cross sensitivity)

It was aimed to prove every point independently from each other, but the unexpected failure of the FID method severely complicated this and necessitated some indirect proofs: if there is no alternative device (except the MOX sensors) for the measurement of gaseous hydrocarbons, produced by the expansion process, it is not possible to prove the first point without relying on the second. On the other hand; if there is no online parallel referencing, it is not possible to directly prove the sensitivity of the MOX sensor towards the vaporised hydrocarbons, because the response can be caused by other parameters. It only was possible to indirectly prove this by exclusion of other possible parameters. Nevertheless, it was possible to prove that all three requirements are fulfilled, even if, in some cases this had to be done on the basis of presumptive evidences. In the following one tries to discuss the three points as separately as possible.

4.1.1 Vaporisation via capillary expansion

The expansion of the pressurised air, contaminated with oil aerosol, is done in order to vaporise the aerosols and to thereby obtain oil vapours. The expansion is carried out in a capillary to guarantee a slow, controlled, isothermal and therefore reproducible and efficient process. It is clear that it is

not possible to vaporise all components of the oil, but the extent of vaporisation has to meet two requirements:

- The residual aerosols must not poison the sensor
 - ➔ In the two years of investigations the identical three sensors could be used, without any observable change of properties and performance
 - ➔ The measurement chamber, which also was in use for two years, did not show any oil aerosol deposition or any comparable contamination
- The process has to produce sufficient oil vapour to be detected by a gas sensor.
 - ➔ The change of oil aerosol content upstream the capillary, reproducibly leads to a response of the MOX sensors

4.1.2 Sensor sensitivity

All of the three MOX gas sensors, investigated in this work, show a response when exposed to oil vapours produced either by a gas mixing system or by capillary expansion of air contaminated with oil aerosols. This is in accordance with the well known hydrocarbon sensitivity of semiconducting metal oxide based gas sensors in general and of tin dioxide based palladium doped thick film sensors especially. As expected, the sensitivity is strongly dependent on the composition and the preparation route of the sensing layer, the best performance in all investigated properties shows sensor S 2, characterised by 2 % palladium doping introduced by gel impregnation.

4.1.3 Cross sensitivities in real life measurements

Nearly all measurements were performed with ambient air as a carrier gas. Humidity turned out to be the only component showing a significant influence on the sensor baseline. The change of sensor baseline resistance is mainly

correlated with absolute humidity. The range of absolute humidity has a pressure dependent upper limit due to processes in the compressor, but the remaining range is the most critical for MOX sensors.

The decrease of resistance due to humidity is up to 65 % of the maximum baseline value, which touches the range of resistance change caused by increased oil aerosol content of $\sim 30 \text{ mg/m}^3$. This means that it is possible to trigger false alarms at less than the threshold oil contents of for high humidities. The implementation of a humidity sensor and a correlation of both results will substantially improve the accuracy of the system.

4.2 Other findings

Within the investigations two findings were made that are not directly related to the proof of concept as given in this work. Both of them were unexpected and represented setbacks for the investigation. Every continuation of it, should address these concerns, which are, therefore, explicitly given here.

4.2.1 Measurement of oil vapours with FID

Both FIDs in use are not appropriate for the measurement of oil vapours in the application (and the processing) described in this work. This widened the analytical gap this work had to cope with and, still, the reason is not completely clear. It is not known whether other types of FIDs also suffer from this handicap to the same extent, but this is probable, as, according to current assumptions, it is correlated with the temperatures inside the FID.

4.2.2 Real life set up with compressor

Oil wallflow is a known effect in the business of compressed air processing, but the extent is in dispute, even among industrial professionals. But at least in case of an aged oil separator (or a simulation of it) it is clear that a part of the oil aerosols is deposited on the surfaces and forms wallflow. The wallflow extends to the whole system up to the next working filter. As a liquid, it is

moved by air turbulences in this region and can accumulate in blind holes (or other appropriate spaces) and reappears later on in the line. In addition, there is often condensed water in the high pressure system, that can drive out the oil. Furthermore, the oil can form foam-like mixtures with water, which were also observed. These unsystematic effects become larger for larger system and it turned out to be a severe problem concerning the reproducibility of the measurements, especially for the gravimetric investigations.

4.3 Outlook

4.3.1 Proposed steps of further development and investigation

After the successful proof of the general concept some optimisation steps are needed:

- It will be necessary to combine the MOX sensors with a humidity sensor and to correlate its readout with the sensor resistance, in order to obtain a higher accuracy of the threshold value.
- A more sophisticated data evaluation, taking the slope of the sensor resistance into account will enable a faster reaction in case of filter breakthrough.

Another completely unexpected observation was made at the end of the measurements and should not be left out: if the stainless steel capillary is exchanged by a copper capillary the sensor responses dramatically decrease. All other parameters except the capillary material have been kept constant, so the material seems to play a more active role than expected.

4.3.2 Will the residual oil indicator be established?

The investigations presented in this work were performed within a publicly funded project and aimed to prove the concept. This was successfully done

and, furthermore, it was possible to develop prototypes as shown in **Figure 44**. The device includes a five meter capillary and a MOX sensor, mounted on a PCB that also provides temperature control, sensor readout and A/D converting, so it is fully digitally controlled. Some modifications are necessary to reach the performance of the sensor set up, utilised for the measurements of this work, but the crucial points are known.

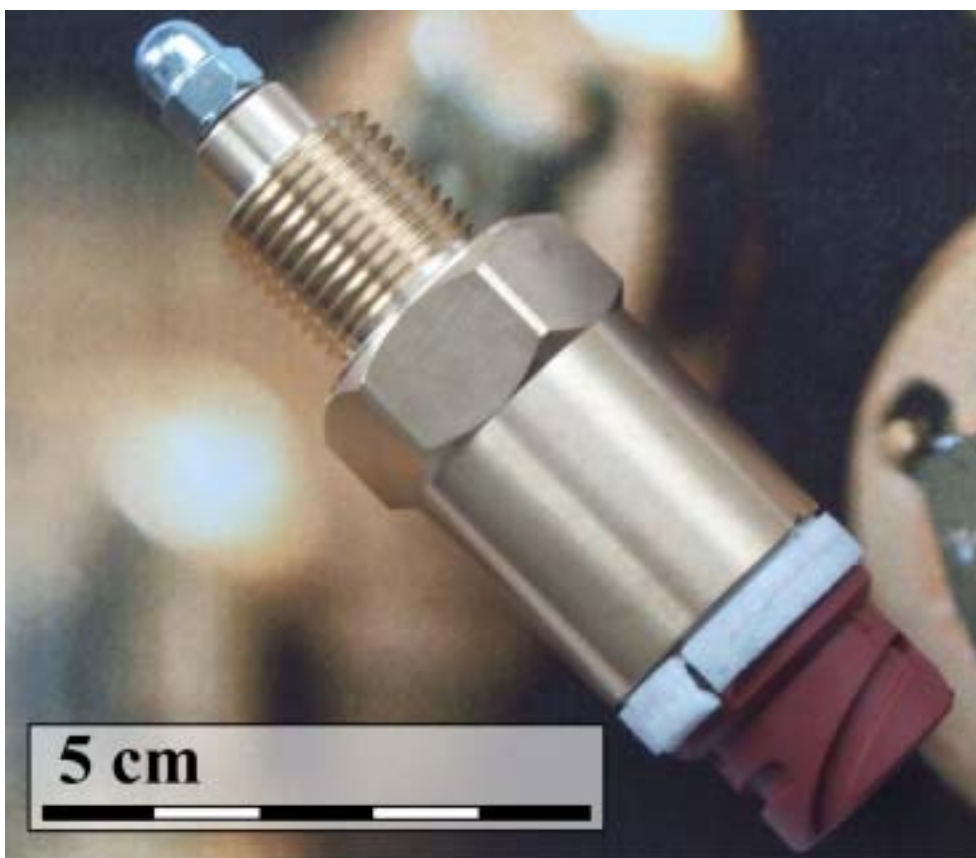


Figure 44: Prototype of the residual oil indicator housing a five meter capillary, one MOX sensor and a PCB with readout, temperature regulation of the sensor heating and an A/D converter for complete digital control.

By the end of this work, all investigations concerning the residual oil analyser are finished. Any development beyond this, for example in the direction of a commercial application, cannot be undertaken within the academic frame, that covered the investigations so far. By publishing this work, the author presents to the public a comprehensive survey of the experiments, that were performed,

and of the knowledge that has been gained in this field. The feasibility is proven and the next steps will be to evaluate the influence of different locations and working conditions of the compressor at the point of application and to transform the academic know-how into a industrial producible device.

5 References

- [Aga80] Agarwal: *Sem: Condensation Particle Counter. J. Aerosol Sci.* 1980, 11, 343-357,
- [Atk01] P. W. Atkins: *Physikalische Chemie, Wiley-VCH 2001, 910,*
- [Bar00] N. Barsan: *Oral communication,*
- [Bre97] D. Breuer: *Messen und Beurteilen von Kühlschmierstoffen. Sicherheitsingenieur.* 1997, 1, 18-23,
- [Cam01] K. Cammann, *Instrumentelle analytische Chemie, Verfahren, Anwendungen und Qualitätssicherung, Spektrum, Akad. Verl., Heidelberg, Berlin 2001., ISBN 3-8274-0057-0, 6-95,*
- [Emi01] *In situ diffuse reflectance infrared spectroscopy study of CO adsorption on SnO₂, S. Emiroglu, N. Barsan, U. Weimar, V. Hoffmann, Thin Solid Films, 391 (2001) 176-185,*
- [Dah01] D. Dahmann et al: *Intercomparison of mobility particle sizer (MPS). Gefahrstoffe-Reinhaltung der Luft 61. 2001, 423-428,*
- [Fis83] Fissan et al. : *Differential Particle Sizer System. J. Aerosol Sci..* 1983, 14, 345-357,
- [Goe96] W. Goepel, C. Ziegler: *Einfuehrung in die Materialwissenschaften: Physikalisch-chemische Grundlagen und Anwendungen, B. G. Teubner Verlagsgesellschaft, Stuttgart, 1996, 129-131,*
- [Gil00] E. Gillenberg: *Oral communication,*
- [Gil99] E. Gillenberg: *Personal communication of internal results,*

- [Har03] S. Harbeck, A. Szatvanyi, N. Barsan, U. Weimar and V. Hoffman: DRIFT studies of thick film un-doped and Pd-doped SnO₂ sensors: temperature changes effect and CO detection mechanism in the presence of water vapour, *Thin solid films*436 (2003), 76-83,
- [Hei88] G. Heiland and D. Kohl in T Seiyamali (ed.), *Chemical Sensor Technology*, Vol. 1, Kodansha, Tokyo (1988) 1-35,
- [Kae96] *Kaeser Kompressoren GmbH: Sicherheitsdatenblätter Kaeser Sigma fluid Plus*, 1996,
- [Kap02] J. Kappler, P. Siciliano, N. Barsan and U. Weimar: CH₄ detection with SnO₂ sensors in the presence of humidity and dry-air by means of DC and AC measurement, *Conf. Proc. IMCS, Boston (USA)*, 2002, 310-311,
- [Kap01] J. Kappler: *Characterisation of high performance SnO₂ gas sensors for CO detection by in situ techniques*, Dissertation, University of Tuebingen, 2001,
- [Kuc84] H. Kuchling: *Taschenbuch der Physik*, Verlag Harry Deutsch, Thun und Frankfurt / Main, 1984, ISBN 3 87144 097 3, 163,
- [Lev01] D. M. Levermore, M. Josowicz, W. R. Rees Jr., J. Janata: *Headspace analysis of engine oils by gas chromatography/mass spectroscopy*, *Anal. Chem.* 2001, 73, 1361-1365,
- [Man00] *Mann+Hummel, Internal communication*, 2000,
- [Man03] www.mann-hummel.com/industrialfilters,
- [Mue01] Marion Mueller, *Polare Stratosphaerenwolken und mesoskalige Dynamik am Polarwirbelrand*, Dissertation FU Berlin 2001, 32,
- [Mob99] *Mobil Schmierstoff GmbH: Industrie Report Synthetische Schmierstoffe*, Ehrenberg Werbung, Hamburg 1999, 6,

- [Nob96] C. A. Noble, K. A. Prather: *Real-time measurements of correlated size and composition profiles of individual atmospheric aerosol particles. Env. Sci. and Tech.* 1996, 30, 2667-2680,
- [Ott00] M. Otto, *Analytische Chemie, 2nd Edition, Wiley-VCH, Weinheim, 2000, ISBN 3-527-29840-1, 175,*
- [Roe95] *CD Roempp Chemie Lexikon, 9. Edition, Georg Thieme Verlag Stuttgart, 1995, ISBN 3 13 100489 4,*
- [Sch02] W. Schmid, N. Barsan, U. Weimar: *Sensing of hydrocarbons with tin oxide sensors: Possible reaction path as revealed by consumption measurements, Sensors and actuators B, 89, 2003, 232-236,*
- [Tes00] *Testa: Bedienungsanleitung FID „1230 Modul“,*
- [Ulr03] *Bernhard Ulrich, Testa GmbH: Personal communication,*
- [Wei02] U. Weimar: *Gas Sensing with Tin Oxide: Elementary Steps and Signal Transduction, Habilitation Thesis, University of Tuebingen, 2002,*
- [Wil99] D. E. Williams: *Semiconducting oxides as gas-sensitive resistors, Sensors and Actuators B, 57, 1999, 1-16,*
- [Woe01] J. Woellenstein et al.: *Preparation, morphology and gas-sensing behaviour of $Cr_{2-x}Ti_xO_{3+z}$ films on silicon substrate, Booklet of abstracts Matchems 2001, Brescia, 60-61,*
- [Zei03] W. Zeitz, *Kaeser Kompressoren GmbH; personal communication,*

6 Publications

Parts of this work have been previously published or presented.

- Wolf Schmid, Nikos Papamichail, Nicolae Barsan, and Udo Weimar: *Measurement of catalytic combustion of hydrocarbons by tin oxide gas sensors with mass spectrometry*, Conf. Proc. IMCS 2000, Basel (Switzerland) (7/2000), 2000, 109-112.
- R. E. Baby, M. D. Cabezas, V. Labud, N. Papamichail, N. E. Walsøe de Reca: *Evolution of the thermophilic period in composts of biosolids analysed with an electronic nose*, Conf. Proc. Ibersensor 2000, Buenos Aires (Argentina), 2000.
- N. Papamichail, U. Weimar: *Discrimination of different Mixtures of Volatile Organic Analytes by Mass Spectroscopy and Sensor Arrays in Parallel*, Sensoren im Fokus neuer Anwendungen, Conf. Proc. 5. Dresdner-Sensor-Symposium, 2001, Dresden, 3-935712-71-5, 116-119.
- N. Papamichail, N. Barsan, U. Weimar: *Gas sensing of lubricant oil vapours with SnO₂-based thick film sensors in real life conditions*, Conf. Proc. EUROSENSORS XVI, 2002, Prague (Czech Republic), 453-454.
- N. Papamichail, U. Weimar: *The Discrimination of Constitutional Isomers with different Types of chemical Gas Sensors*, N. Papamichail, U. Weimar, Conf. Proc. 9th International symposium on Olfaction and Electronic Nose ISOEN, Rome, 2002, Rome (Italy), 91-92.
- A. Perera, N. Papamichail, N. Barsan, U. Weimar, S. Marco: *Event Detection by Recursive Dynamic Principal Component Analysis and Gas Sensor Arrays under drift conditions*, IEEE Sensors Conference, October 2003, Toronto (Canada), (in press).
- Nikos Papamichail, Nicolae Barsan, Udo Weimar: *Monitoring of oil aerosol contamination in pressurised air with SnO₂-based thick film sensors in real life conditions*, Conf. Proc. 10th International symposium on Olfaction and Electronic Nose ISOEN, Riga (Latvia), 2003, 141-144.

- U. Weimar, N. Barsan, N. Papamichail: *Verfahren zur Detektion von flüssigen Komponenten in einem Aerosolstrom*, Offenlegungsschrift DE 101 62 278 A1 Deutsches Patent- und Markenamt, 2003.
- Nikos Papamichail: *Kostengünstiges online-monitoring des Restölgehaltes in Druckluft*, Drucklufttechnik 7-8/2003, Vereinigte Fachverlage, Mainz 2003, 52-54.

7 Acknowledgements

First of all, I want to thank Prof. Dr. Dr. hc W. Göpel (†) for providing the opportunity to pursue my Ph.D. in his workgroup and to profit from the interdisciplinary approach and the excellent instrumentation.

I wish to thank Prof. Dr. G. Gauglitz, who strongly supported the continuation of all the activities in the IPC gas sensor group after the tragic accidental death of Prof. Göpel, for his readiness to co-examine the doctoral exam and this thesis.

A very comprehensive thank goes to Dr. Udo Weimar. He gave me instructive insight in making and managing science and supported me wherever he could in a generous, and if necessary, in a very unbureaucratic way. He made it possible for me to take part in international conferences and meetings and to gain experience also in not strictly academic skills.

A very special thank to Dr. Nicolae Bârsan, not only for the scientific supervision of the work, but also for his openness and his humour, which provided the joyful possibility to practise and improve my English beyond the scientific scope.

I thank Eric Gillenberg and Wolfgang Heikamp from Mann+Hummel for the compressor set up and the cooperation within the CMOSSens project.

I want to thank Martin Schaller and Rainer Dudzik from Seuffer for the quick and effective interplay between IPC and Seuffer, which finally resulted in the prototypes.

I wish to thank AppliedSensor / Advanced Sensing Devices and especially Dr. Andreas Krauss and Dr. Jürgen Kappler for the extremely pleasant and fruitful cooperation within the CMOSSens project, which made the project meetings the more enjoyable the later the day grew... .

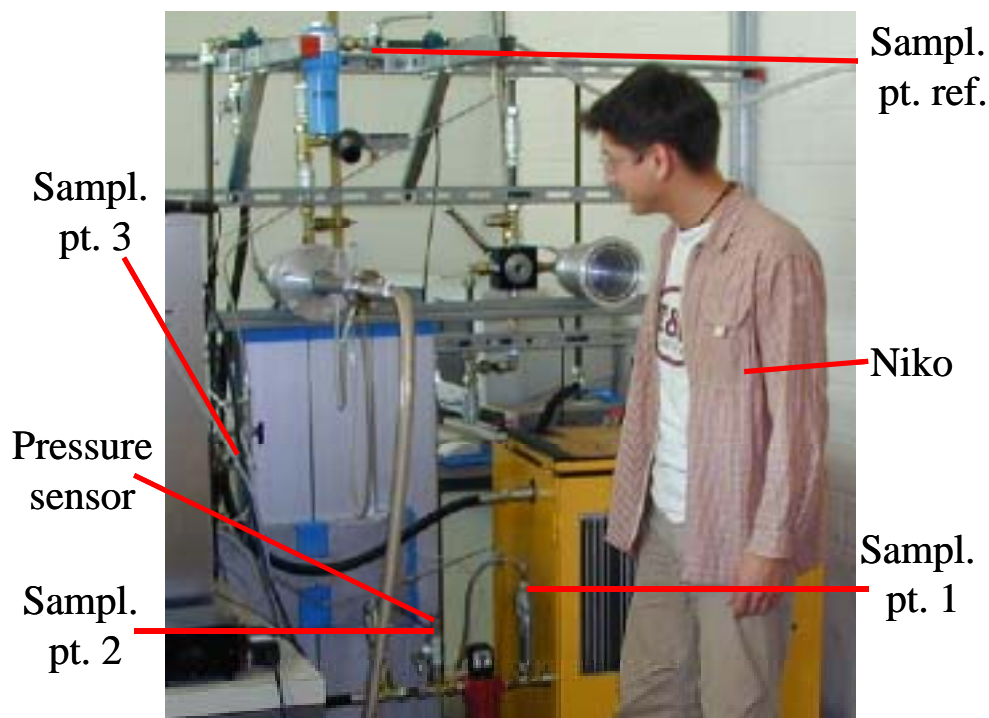
I thank my office mates, Mika Harbeck, Mathias Nagel, Michael Wandel and especially Wolf Schmid for their tolerance towards an untypical chemist, for

the discussions about everything that can be discussed and more, and for their patience in explaining “details” of how to tame bits and bytes to a computational amateur. And for telling so many people that I was in the B-building... .

I want to thank the whole gas sensor group for the open and companionate atmosphere full of good mood and laughs, it seems you enjoy working here just as I did and still do. There are too many to mention, present and former students as well as permanent stuff, I exemplary want to thank Ute Harbusch, who always seems to be ready to answer the next stumbling block on the way to administrative orderliness with a smile.

I thank my family for giving me the possibility to do what I have done and especially for their patience in the last six months (Ja, sie ist jetzt endgültig fertig!). Sometimes they were more nervous than I was.

At the end I want to thank my people at *Schellingstrasse* and Christian for keeping my feet on the green when my head was full of pressurised air, contaminated with different dosings of residuaaaaaa... .



Liste der Akademischen Lehrer

Meine akademischen Lehrer waren:

K. Albert, E. Bayer, D. Christen, H. Eckstein, G. Gauglitz, W. Göpel, G. Häfelinger, H. P. Hagenmaier, M. Hanack, V. Hoffmann, W. Jäger, G. Jung, W. Koch, B. Koppenhöfer, D. Krug, N. Kuhn, E. Lindner, U. Nagel, P. Nakel, H. Oberhammer, D. Oelkrug, H. Pauschmann, G. Pausewang, F. Pommer, A. Rieker, V. Schurig, E. Schweda, F. F. Seelig, G. Staudt, H. Stegmann, J. Strähle, W. Voelter, K.-P. Zeller, C. Ziegler

Lebenslauf

Persönliche Daten

Nikos Papamichail, geb. am 4. Juli 1969 in Erfurt, ledig,

Staatsangehörigkeit: deutsch

Schulbildung

Aug. 1976 – Juni 1980 Vogt-Hess-Grund-und-Hauptschule Herrenberg

Aug. 1980 – Juni 1989 Andreae-Gymnasium Herrenberg

Juni 1989 Allgemeine Hochschulreife

Zivildienst

Jan. 1990 – März 1991 Marienheim Stuttgart

Studium

Okt. 1991 – Sep. 1998 Chemiestudium an der Eberhard-Karls-Universität Tübingen

April / Mai 1998 Diplomhauptprüfungen

Juli 1998 – Jan. 1999 Anfertigung der Diplomarbeit unter Anleitung von Prof. W. Göpel; Titel: „*Gasanalysen mit elektronischen Nasen und chemischer Analytik; Orientierende Untersuchungen*“

Promotion

Jan. 1999 – Dez. 2003 Wissenschaftlicher Mitarbeiter am Institut für Physikalische und Theoretische Chemie und Anfertigung der Dissertation unter Anleitung von Privatdozent Dr. U. Weimar mit dem Titel: „*Online monitoring of residual oil in pressurised air with SnO₂-based gas sensors*“